Design of a permanent magnet radial flux concentrated coil generator for a range extender application

Public version

Text:	**MSc. Thesis Report**
Author:	**Ing. T.D. Strous**
Date:	**August 2010**
Thesis committee:	**Dr. Ir. H. Polinder**
	Prof. Dr. J.A. Ferreira
	Prof. Ir. L. van der Sluis
	Ing. D.J. Toeters

EEC
Electrical Energy Conversion
Delft University of Technology

ABSTRACT

Peec-Power B.V. is developing a high power range extender for the automotive sector. In this range extender combustion engine and generator are integrated. This thesis deals with the development of the integrated generator.

Generator construction types are discussed. This includes the machine excitation, construction types, winding arrangements, rotor constructions, and the use of different permanent magnet materials.

Analytical models are developed for permanent magnet radial flux concentrated coil machines. The derived models are validated with the use of finite element method (FEM) models. Using the analytical models an optimizing routine is developed for finding optimal machine geometries according a given set of design criteria.

A generator with concentrated coil fractional pitch windings with a multiple of 9 coils around 9 teeth and 8 magnet poles is developed. Also a generator with concentrated coil fractional pitch windings with a multiple of 3 coils around 3 teeth with 2 magnet poles is developed. Also two different rotors are developed for the generators. One with surface mounted permanent magnets and one with V-shape inset mounted permanent magnets.

With use of the developed analytical models and FEM models, calculations are performed on both generator designs. Calculations include the magnetic parameters, including the flux density distribution at different places in the machine. Calculations also include the electric parameters, including the no-load voltage due to the permanent magnets, resistance and inductance components and output characteristics. Calculations on the machines starting behavior have been performed, including the non linear effects of the steel. Generator losses are modeled, including copper losses, stator iron losses and magnet losses due to the space harmonic content of the armature magnetic field.

The developed machines are in production and will soon be ready to be tested in the lab.

LIST OF USED SYMBOLS

A_{cu}	[m^2]	conductor area
A_s	[m^2]	slot area
B_{ar}	[T]	a.r. flux density in air gap and rotor
$B_{ar,ry}$	[T]	rotor yoke flux density due to a.r.
$B_{ar,sy}$	[T]	stator yoke flux density due to a.r.
$B_{ar,tooth}$	[T]	tooth flux density due to a.r.
$B_{ar,magnet}$	[T]	magnet a.r. flux density
$B_{ar,max}$	[T]	magnet a.r. flux dens. during fault
B_r	[T]	remnant flux density
$B_{m,min}$	[T]	min. allowed magnet flux dens.
B_m	[T]	magnet flux density
B_g	[T]	air gap flux density
B_{ry}	[T]	PM flux density in rotor yoke
B_{sy}	[T]	PM flux density in stator yoke
$B_{sy,tot}$	[T]	total flux density in stator yoke
B_{tooth}	[T]	PM flux density in tooth
$B_{tooth,tot}$	[T]	total flux density in stator teeth
C_{steel}	[€/kg]	cost price of steel
C_{magnet}	[€/kg]	cost price of magnet
C_{copper}	[€/kg]	cost price of copper
d_1	[m]	stator teeth shoe top length
d_2	[m]	stator teeth shoe skew length
d_3	[m]	stator teeth length without shoe tooth
E_{ph}	[V]	RMS 1-phase voltage
E_{ll}	[V]	RMS no load line-line voltage
F_{gen}	[N]	generated force
f_e	[Hz]	electrical frequency
g	[m]	air gap length
g_{eff}	[m]	effective air gap length
H_c	[A/m]	coercive field strength
H_m	[A/m]	magnet field strength
I_{ph}	[A]	RMS phase current
I_s	[A]	slot current
I_{scc}	[A]	maximum short circuit current
I_{start}	[A]	start current
J_{nom}	[A/m^2]	Nominal current density
k_c		air gap correction factor
k_{ml}		leakage factor
k_{fill}		slot fill factor
k_{stk}		lamination stacking factor
k_{cu}	[/°C]	temperature coefficient of copper
k_w		winding factor
k_p		pitch factor
k_d		distribution factor
k_s		skew factor
L_{max}	[H]	maximum allowed inductance
L_s	[H]	phase self inductance
L_{sm}	[H]	main component of L_s
$L_{s\sigma}$	[H]	Leakage component of L_s
$L_{\sigma,gap}$	[H]	air gap leakage inductance
$L_{\sigma,slot}$	[H]	slot leakage inductance
$L_{\sigma,end}$	[H]	end turn leakage inductance
l_m	[m]	magnet length
l_{stk}	[m]	stack length (and effective machine length)
M_{ab}	[H]	mutual inductance
MMF	[A-t]	magneto motive force
m_{cu}	[kg]	mass of copper
m_m	[kg]	mass of magnets
m_s	[kg]	mass of steel
N_m		number of magnets
N_{ph}		number of phases
N_s		number of slots
n_c		number of turns per coil
n_m	[RPM]	mechanical rotational speed
P_e	[W]	Electric power
P_{in}	[W]	Input power
P_{mech}	[W]	Mechanical power
$P_{loss,cu}$	[W]	Copper losses
$P_{loss,Fe}$	[W]	Iron losses
$P_{loss,m}$	[W]	un-laminated magnet losses
$P_{loss,ml}$	[W]	laminated magnet losses
P_{out}	[W]	Output power
p		number of pole pairs
p_λ		number of pole pairs that fit in λ_1
p_{cu}	[€]	price of copper
$p_{Fe,spec}$	[W/kg]	specific iron losses
p_m	[€]	price of magnets
$p_{m,spec}$	[W/kg]	specific magnet losses
$p_{ml,spec}$	[W/kg]	specific laminated magnet losses
p_s	[€]	price of steel
R_{dc}	[Ω]	DC component of phase resistivity
$R_{m,m}$	[A/Wb]	reluctance of the magnet
$R_{m,g}$	[A/Wb]	reluctance of the airgap
$R_{m,l}$	[A/Wb]	leakage reluctance
$R_{m,t}$	[A/Wb]	reluctance of a stator tooth
$R_{m,y}$	[A/Wb]	reluctance of the stator yoke
$R_{m,\sigma}$	[A/Wb]	a.r. leakage reluctance
$R_{m,\sigma(slot)}$	[A/Wb]	slot leakage reluctance
$R_{m,\sigma(gap)}$	[A/Wb]	air gap leakage reluctance
R_{ph}	[Ω]	phase resistivity
r_{ri}	[m]	rotor inner radius
r_{rb}	[m]	rotor yoke outer radius
r_{ro}	[m]	rotor outer radius
r_{si}	[m]	stator inner radius
r_{sb}	[m]	stator yoke inner radius
r_{so}	[m]	stator outer radius
T_{emp}	[°C]	steady state working temperature
$T_{air,gap}$	[Nm]	magnetic torque
T_{gen}	[Nm]	generated torque
T_{start}	[Nm]	starting torque
T_{nom}	[Nm]	nominal mechanical torque
$T_{k,Br}$	[%/°C]	temp. coef. for flux density
$T_{k,Hc}$	[%/°C]	temp. coef. for field strength
U_t	[V]	terminal phase RMS voltage

U_{ll}	[V]	terminal line-line RMS voltage
U_{dc}	[V]	rectified DC voltage
$V_{s,sy}$	[m^3]	steel volume of stator yoke
$V_{s,teeth}$	[m^3]	steel volume of stator teeth
$V_{s,ry}$	[m^3]	steel volume of rotor yoke
V_m	[m^3]	volume of magnets
V_{cu}	[m^3]	volume of copper
W_m	[J]	magnetic energy
w_t	[m]	teeth top width
w_{ti}	[m]	teeth inner width
w_{tb}	[m]	teeth outer width
w_s	[m]	slot top width
w_{si}	[m]	slot inner width
w_{sb}	[m]	slot outer width
w_{ry}	[m]	rotor yoke width
w_{sy}	[m]	stator yoke width
α_c		flux concentration factor
α_s		slot fraction
α_m		magnet fraction
δ	[rad]	phase angle between E and U
δ_{skin}	[m]	skin depth
λ	[Wb-t]	flux linkage
λ_1	[m]	fundamental wave length
θ	[rad]	electric rotor position angle
θ_m	[rad]	magnet angle

θ_p	[rad]	pole angle
θ_s	[rad]	slot angle
θ_{st}	[rad]	electric stator position angle
ρ_{cu}	[Ω.m]	resistivity of copper
ρ_m	[Ω.m]	resistivity of magnets
ρ_{steel}	[kg/m^3]	mass density of steel
ρ_{magnet}	[kg/m^3]	mass density of magnet
ρ_{copper}	[kg/m^3]	mass density of copper
τ_c	[m]	coil pitch
τ_p	[m]	pole pitch
τ_m	[m]	magnet pitch
τ_s	[m]	slot pitch
η		rendement
μ_0		permeability of air 4.π.10^(-7)
μ_{rec}		recoil permeability of the magnet
$\mu_{r,steel}$		relative permeability of steel
η	[%]	efficiency
φ	[rad]	output voltage phase angle
ψ	[rad]	induced voltage phase angle
ω_m	[rad/s]	mechanical rotational speed
ω_e	[rad/s]	electrical rotational speed
ω_r	[rad/s]	speed of space harmonics seen by the rotor
Φ_r	[Wb]	remanent flux
Φ_g	[Wb]	effective air gap flux
Φ_m	[Wb]	magnet flux
Φ_l	[Wb]	leakage flux

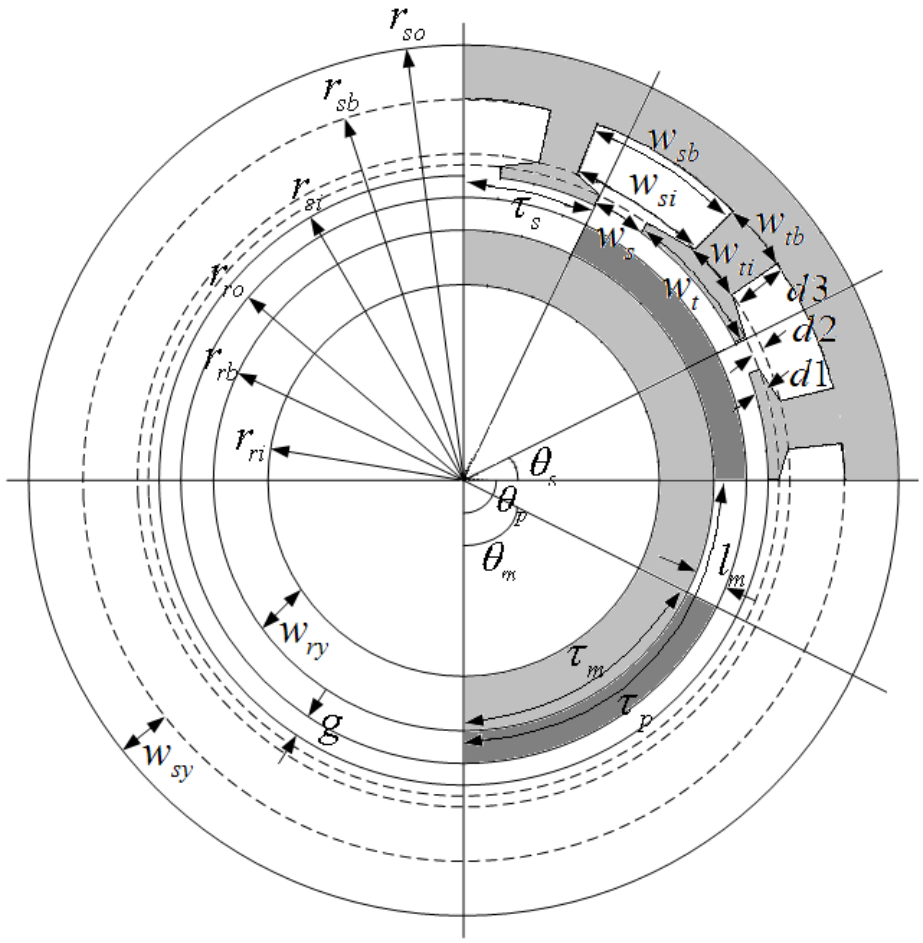

PREFACE

A good generator design is dependant of good modeling work. Therefore I have spent much of my time, during the last months, on generator modeling. During the development of the generator models I frequently got new ideas and insight, which forced me to adapt my models and make them more accurate. I discovered that modeling is an endless business. It is always possible to make a model more accurate, but also more complex at the same time. At some point I had to stop modeling and use my models to generate the designs. I learned that modeling is only an attempt to describe nature and use these descriptions to predict the future. Since models only approximate reality there is always the question of how precise a model must be. A trade off between accuracy and complexity must be made.

First of all I want to thank my daily supervisor, Henk Polinder, associate professor at TU Delft, for all these things I have learned. He showed me the way in the world of generators and was always there to provide guidance when it was needed. I also want to thank Dirk Toeters, director of the Peec-Power B.V. company, for providing me the opportunity and freedom to develop a generator for their range extender prototype. His confidence in my work was a big support. Further I want to thank all other people who supported me in any way during the last moths, without their help and support I would not have reached this far.

TABLE OF CONTENTS

Chapter 1: Introduction

1.1. Background

Mankind has always been inspired to develop methods for faster mobility. The ambitious attempts to fulfill this aspiration have lead to the development of the automotive industry. The first developments of combustion engines for automobiles started in the 1860s and 1870s, mainly in France and Germany. Together with the development of the combustion engine, came the development of the steam powered engine and electric engine. But the limitations of electric energy storage for electric vehicles proved competitively fatal. By the time Ford started to produce the first T-Ford in 1908 the era of the internal combustion engine (ICE) vehicles was born. Cars replaced horses as the main manner of transportation. It looked like an enormous improvement of the city environment. According to historians, in the 1920s tuberculosis rates had decreased [Sah 01].

Nowadays the health conditions of millions of people, living in the big cities, are threatened by vehicle emissions and increasing atmospheric carbon dioxide densities jeopardizes life at whole the planet. Due to political pressure and the people's will to improve the environment, once again, the development of vehicle propulsion by alternative energy sources has started. The EV now seems to be the most promising and feasible medium term alternative. All the major manufacturers have developed their prototypes. Although technology has advanced over the last 100 years, EV's still having their limitations compared to ICE vehicles. This prevents the breakthrough of the EV into the streets. The limitations of currently developed EV's include:

- Limited driving range
- Large recharge times of electric batteries
- High cost prices
- The lack of a reliable infrastructure for EV's

While technology is advancing, hybrid electric vehicles (HEV's) are the temporarily solution in the transition period from ICE vehicles to EV's. A HEV basically is an electric car supplemented with a small or medium sized combustion engine. The HEV design can mainly be divided in two groups: series-hybrid designs and parallel-hybrid designs. A parallel-HEV uses both an ICE and an electric machine to power a drive shaft. The electric machine can work both to power the drive shaft or it can work as a generator. Since both electric machine and ICE work together a smaller ICE can be used. Nowadays many car manufacturers have already implemented this technology into their cars. A series-HEV on the other hand, uses an ICE to drive a generator, which charges an electric energy storage device. The vehicle is then driven with the use of an electric motor. It is in the development of this technology, that the company Peec-Power B.V. sees the best technological advancement of vehicles in the near future.

1.2. Problem definition

Peec-Power B.V. is developing a high power range extender (HPRE) which is most suitable for series-hybrid applications. According to their vision the main disadvantages of the currently available EV's can be overcome by integrating range extenders in short range EV's. The use of range extenders limits the needed battery capacity to cover only short distances that people drive 90% of the days [PP 10]. This is shown in figure 1.1.

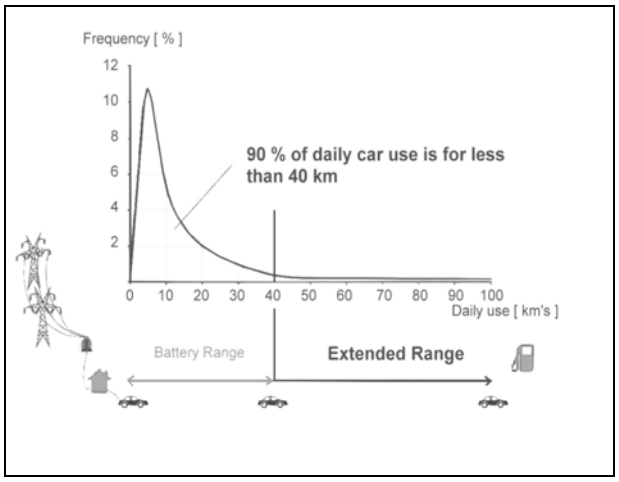

Figuur1.1: Frequency of driving distances

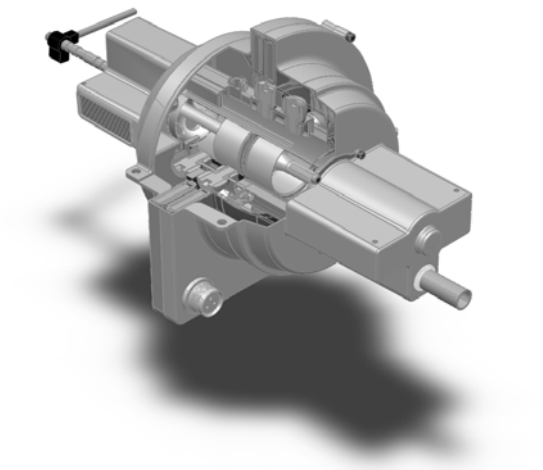

Figure1.2: High Power Range Extender

When range extenders are applied in EV's, people basically drive electrical 90% of the time, but they don't lose the freedom of a conventional ICE vehicle. For the larger distances the range extender supplies the required electric energy to continue traveling, after the batteries have reached a certain pre-programmed limit. The range extender reduces the battery cost dilemma to manageable proportions and provides an unlimited driving range. Moreover gasoline consumption can decrease with 95%, compared to conventional ICE driven cars.

The HPRE (figure 1.2) developed by Peec-Power, uses two symmetrical opposed pistons to transfer the combustion energy, in a unique and patented way, to the rotating generator. In this way an expensive and inefficient crankshaft construction is eliminated. The result is a more efficient energy conversion and a small integrated unit. This unit can be built with fewer components, compared to comparable auxiliary power units.

The main objective of this thesis is to develop the integrated generator for the Peec-Power HPRE prototype series. In order to accomplish the main objective the following objectives have to be accomplished:

- Determine the best machine construction type for the generator of the prototype HPRE.
- Develop a generator calculation model.
- Determine the optimal generator design parameters according a set of design criteria.

Since the HPRE is mainly developed for the automotive sector the generator has to be designed according to the following design criteria:

1. Optimizing to cost
2. Optimizing to weight
3. Optimizing to efficiency

Another design criterion is the use of the generator as starter motor for the combustion engine. The next subchapter describes the different phases a generator designer has to go through, to come to a suitable generator design according to the design criteria.

1.3. Thesis layout

When designing a generator many unknown parameters are involved. In order to make a design it is necessary to fix some of them and determine the remaining parameters as part of the design process. The layout of this thesis is such that it represents the different phases of the electrical machine design process:

- Determine the design criteria.
- Determine a machine construction type.
- Develop a calculation model for the chosen machine construction.
- Develop an optimizing routine to optimize a design for the set of given criteria.
- Fix all machine parameters.

Determine the design criteria:
The design criteria consist of fixed electric, magnetic and geometric parameters, but also of criteria stating the design optimizing requirements. The stated design criteria, given in chapter 1.2, will be used for finding the optimal generator geometric parameters.

Determine a machine construction type:
Many different constructing types for rotating electrical machines exist. Searching for an optimal generator design, by using calculation models for every existing machine type, is very time consuming and beyond the scope of this thesis. Instead, a qualitative discussion of existing generator constructions is made in Chapter 2. In this way, the best suitable construction types, for the HPRE, are chosen according the given design criteria.

Develop a calculation model for the chosen machine construction:
For the chosen electrical machine constructions, models are made and equations are set up to do calculations on these types of constructions. This is done analytically in chapter 3. Chapter 5 then deals with generator modeling using FEM. These FEM models are used as feedback for the analytical models and they are used as validation of the analytical generator designs.

Generate an optimizing routine
The analytical generator models of Chapter 3 are used in Chapter 4 to develop an optimizing routine to find the optimal machine geometrics. Using the optimal geometrics generator designs are developed for the prototype HPRE. These generator designs are then used in Chapter 5 to develop the FEM models.

Fixing all parameters
Chapter 6 presents the calculation results of the parameters and output performance for the optimized generator designs. A comparison between the analytical results and the FEM modeling results is given. From the developed generator designs, prototypes will be produced, as described in chapter 7.

Chapter 2: Electric machine constructions

This chapter presents an overview of existing electrical machine construction types. Different aspects of a construction type that are discussed are:

- The machine excitation.
- The machine construction.
- The machine coil winding arrangement.

The chapter ends with the selection of the best suitable machine construction types for the generator of the prototype HPRE. The chosen construction types will further be used to develop analytical calculation models.

2.1. Machine excitation types

First the machine excitation will be discussed. An electrical machine needs a magnetic field in order to convert mechanical energy into electrical energy and vice versa. Several electrical machine types exist to excite a magnetic field in an electrical machine.

The induction machine (IM):
An induction machine supplies the energy for the rotor excitation field through the stator windings into the rotor. The stator windings must carry both the active power, required for the electro mechanical conversion and the reactive power, required by the rotor for its excitation. This provides an increase in stator copper losses compared to machine types with separate excited excitation fields. Because of this, the IM requires larger copper conductor cross-sections and slot space in the stator.

Synchronous machine (SM):
The synchronous machine uses separately excited windings in the rotor in order to excite the magnetic field in the rotor. Separate excited windings give the possibility to change the output voltage by adjusting the excitation of the magnetic field of the rotor. Since the stator windings do not have to carry the power to excite the rotor magnetic field, a reduction in mass of the active materials, over the IM, is possible. This has been confirmed in the work of [Dub 04], [Had 99]. Another advantage over the IM is that smaller power handling equipment, like converters, can be used to control the SM.

Permanent magnet synchronous machine (PMSM):
When the separate excitation of the synchronous machine is done by permanent magnets (PM's) instead of windings, the machine is called a permanent magnet synchronous machine. No power is lost to excite the rotor magnetic field through windings and efficiency will increase compared to the SM. Also a weight reduction can be made over the SM, since the rotor construction of the PMSM is smaller than the rotor construction of a SM made with excitation windings. The cost reduction of a PMSM over a SM will not be proportional with the reduction in mass, since PM material is much more expensive than copper and steel used in SM rotor constructions. However the total costs for a PMSM are lower than for a SM. This is discussed in [Dub 04].

Switched reluctance machine (SRM):
In a switched reluctance machine only the stator windings are excited and produce a magnetic field. The rotor is constructed in such a manner that by moving it, the rotor causes a change of stored magnetic energy in the machine. By sequentially exciting the stator coils, torque can be produced, or electricity can be generated.
The benefits of the SRM lie in a simple, low cost and rigid construction. But as with an IM the SRM draws its excitation magnetic field from the power source, therefore larger converters are needed to operate a SRM. For equal efficiencies the SRM construction appears to be more compact and slightly lighter than the IM construction according to [Dub 04], [Har 89].

Based on this literature survey on machine excitation types, a PMSM is chosen to be constructed for the HPRE application. This form of excitation in the generator is preferable because low cost, light weight and efficient generator designs can be expected.

2.2. Machine construction types

A permanent magnet synchronous machine can be constructed in different ways. Two design characteristics of a construction type are:

- The orientation of the magnetic flux within the machine.
- The type of rotor construction with permanent magnets.

The magnetic flux orientation:
The magnetic field can be given a radial direction by placing the stator around the rotor. A machine construction like this is called a radial flux machine. This is shown in figure 2.1 (a). By placing stator and rotor such that the air gap is perpendicular to the rotational axis, the magnetic flux crosses the air gap in axial direction, in this way an axial flux machine is constructed. This is shown in figure 2.1 (b). An axial topology often appears in applications where the machines axial dimension is more limited than the radial dimensions. By increasing the machine radius the air gap area of the radial flux machine will increase linear whereas the air gap area of the axial flux machine will increase quadratic. Constructing a stator and rotor out of laminated steel is easier and cheaper for a radial flux topology, since laminations can be stacked, while in the case of an axial flux topology the lamination of the steel has to be made in rotational direction. Another disadvantage of the axial flux topology is the larger length of the end windings, which means an increase in the copper losses.

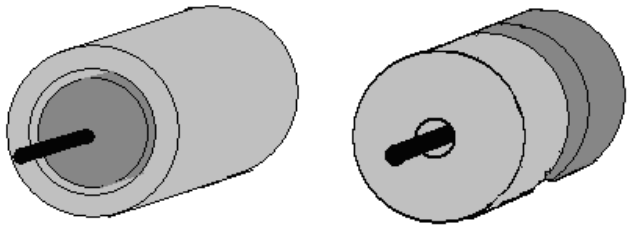

(a) ***(b)***

Figure 2.1: Radial flux machine construction (a), axial flux machine construction (b)

The rotor for the generator of the prototype HPRE will be constructed around the combustion engine. By applying an axial flux topology the advantage of a large air gap area is lost, because most of the area perpendicular to the rotational axis can not be used since it is occupied by the combustion engine. Therefore a radial flux topology is chosen to be designed for the prototype HPRE. It appears easier and cheaper in production and less copper losses can be expected.

The rotor construction:
The most common rotor topology is acquired by placing the PM's on the rotor surface. This is called a surface mounted permanent magnet (SMPM) rotor construction. For this construction type it is required to shape the magnets into arcs, which can be placed on the rotor outer surface. Another method of construction is to embed the magnets into the rotor steel. A rotor constructed in this way is called an inset magnet permanent magnet (IMPM) machine. The advantage of the inset magnet topology is the possibility to use straight magnets. Another advantage is the possibility to place the magnets to acquire flux concentration in the air gap. The disadvantage is that some flux from the PM's will 'leak' trough the rotor steel. This means that this flux doesn't cross the air gap and contribute to the induced voltage.

Since it is not clear from a literature survey which rotor construction type is best suited for this particularly HPRE application, both SMPM and IMPM constructions will be considered in the design process.

2.3. Used magnetic material

Permanent magnets (PM's), also referred to as hard magnetic material are capable of maintaining a magnetic field without any excitation magneto motive force MMF[A-t]. They are characterized by a large B-H loop. The B-H characteristic is temperature dependant. The characteristic tends to shrink to the origin when temperature increases. PM's have a high remanent flux density B_r[T] and a high coercive field strength H_c[T]. Table 2.1 shows a typical overview of different magnet types that are in use today. Ferrite magnets and the rare earth element magnets have a fairly linear demagnetization characteristic. This means that the relative permeability μ_{rec}, for these magnet types, is constant over most of the working area. This can be seen in figure 2.2.

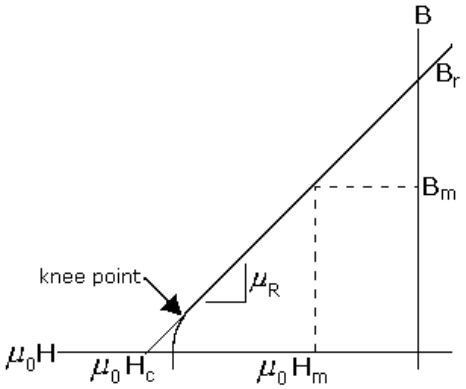

Figure 2.2: Magnet B-H characteristic.

Material	Typical B_r[T]	Typical H_c[kA/m]	Price	extra
NdFeB	1. 2	950	+++	
SmCo	1. 0	900	++++	Low temperature coefficient
Bonded NdFeB	0. 7	500	++	Low Eddy-currents
Ferrite	0. 4	300	+	Low Eddy currents
Alnico	1..2	100	+	High knee point

Table 2.1: Overview of magnetic materials

When choosing a magnetic material for a rotor construction of the generator for the prototype HPRE, the following has to be considered:
The operating temperature of the magnets is not yet a sure thing. It is known that the magnets are implemented in the rotor which is positioned between the stator and the combustion engine of the HPRE. The engines cooling water temperature is around 100°C. Future magnetic field calculations are done with a magnet operating temperature of 120°C in mind. When assuming this, rotor losses must be kept as low as possible.

For automotive applications sintered NdFeB magnets are most suited. They are relatively cheap. They have a high remanent flux density, which mean a higher rotor excitation field. Therefore less copper is needed to induce the same voltage in the windings. Current NdFeB magnets are also useful in high temperature applications as the HPRE. Because of these reasons the NdFeB magnet type is chosen to be used for the development of the generator for the prototype HPRE.

2.4. Coil winding arrangements

The winding arrangement of an electrical machine determines the configuration of the coils in the stator. Coils can be placed in the air gap or in slots around teeth, in the stator. The turns of a coil can then be placed, concentrated in one slot, or they can be distributed over several slots when it concerns a slotted design or around the air gap circumference when it concerns a slotless design. When a slotted construction is considered, the number of slots and number of magnet poles can still vary. All these construction variations will be further considered in this sub-chapter.

Coil placement:
Placing the coils in the air gap leads to a slotless design. By doing this, the air gap length between stator and rotor will increase and the reluctance seen by the PM's will increase, which leads to a decrease in flux density. More PM material or copper windings are needed to compensate for the decrease in flux density. A slotless design has less steel and therefore less hysteresis and Eddy current losses. According to [Com 03] the power density of a slotless design is three times lower than in a slotted design.

Coil winding distribution:
In a slotted stator, the stator windings can be placed as concentrated coils around the teeth, or the windings can be distributed in the slots. According to [Fir 08] concentrated coil constructions have the advantage of a higher winding factor; this increases the amplitude of the induced output voltage. Less copper is needed, due to shorter end windings. They are also easier to manufacture automatically. The disadvantage of concentrated coil windings is the increase of harmonic components in the air gap flux. This causes an increase of losses in the rotor magnets and back iron due to Eddy currents.

For the HPRE a slotted concentrated coil construction appears to be the smallest and cheapest solution. A radial flux PMSM with concentrated coils has already proven to be an excellent choice for hybrid automotive applications [Hsu 04].

Pole slot combinations:
The combinations of the number of stator slots N_s and the number of magnet poles N_m that can be used in an electrical machine design are countless. For a 3 phase machine using concentrated

coils the number of combinations is still large. It is beyond the scope of this thesis to model an electrical machine for all slot pole combinations. Therefore the choice of slot pole combinations has to be made, using a qualitative discussion of different slot pole combinations. Much research on this topic has already been done. According to [Pol 07] a combination of 3 coils around 3 teeth with 2 magnet poles appears to have the lowest Eddy current losses in the magnets and rotor back iron. However this combination has a poor winding factor. An interesting slot pole combination, with a high winding factor and acceptable losses is the combination of 9 coils around 9 teeth with 8 magnet poles. The high winding factor of this slot pole combination is also found in the work of [Ska 06]. Therefore a pole slot combination of 9 coils around 9 teeth with 8 magnets will be considered for modeling.

Due to high electrical frequencies, Eddy current losses can be expected to contribute substantially to the total losses. Therefore a pole slot combination of 3 coils around 3 teeth with 2 magnet poles will also be modeled. Low rotor Eddy currents cause less temperature rise in the magnets, which will enhance efficiency and decrease the risk of demagnetizing the magnets.

2.5. Suitable construction types for the generator of the prototype HPRE

From the presented overview of machine construction types it can be concluded that the generator to be developed for the HPRE has to be a SMPM radial flux generator with concentrated coils. The used magnetic material will be NdFeB magnets. Both SMPM and IMPM rotor constructions must be considered. For this purpose generator models must be developed, suitable to calculate the machine parameters of radial flux PM concentrated coil electrical machines, for both generators with pole slot combinations which are a multiple of 9 coils around 9 teeth with 8 magnet poles and pole slot combinations which are a multiple of 3 coils around 3 teeth with 2 magnet poles. The models to be developed must be suitable for both SMPM and IMPM rotor constructions.

Chapter 3: Modeling a generator using analytical calculations

In this chapter models are derived to analytically represent an electrical machine. Using these models helps to predict the behavior of a newly developed machine designs. A model is a representation of reality. Accurately describing reality results in a precise but complex model. To reduce complexity, a model is often made under a set of predefined assumptions simplifying reality. The derived models in this thesis are useful for generator types that meet the following requirements:

- Radial flux machines.
- PM machines, without large reluctance torque components.
- Concentrated coil machines.
- Machines with sinusoidal output voltages.
- Machines with three phases.

These models could of course be modified to make them suitable for other machine types.

3.1. Permanent magnet flux model

The effective flux Φ[Wb] in a PM machine is the flux linking the stator coils. This linked flux is responsible for inducing a voltage e[V] in the coils and will be called flux linkage λ[Wb-t] from now on. There are different methods for calculating the induced voltage of an electrical machine, but they all start by calculating the flux distribution within that machine. In this thesis the flux linkage and induced voltage is calculated from the flux density B_g[T] in the air gap. For calculating the flux distribution in the machine this PM flux model is set up. It is a model suitable for circuit theory analysis.

The PM flux model represents the flux in a PM machine due to the permanent magnets. First consider the following assumptions:

- The used materials have homogeneous and isotropic properties.
- Consider a generator with a full pitch winding configuration. This is achieved by assuming $N_s=N_m$
- No load is applied.

Figure 3.1 represents a generator configuration with PM's according to this set of assumptions. The figure shows the flux in the air gap that will link the stator coils, for a fixed rotor position.

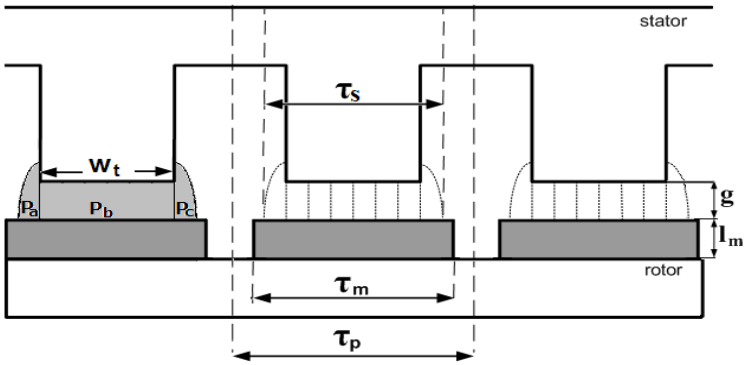

Figure 3.1: Full pitch PM generator construction.

Because of fringing, the flux density distribution, in the air gap, over one slot pitch τ_s[m] is not homogeneous. To calculate the average flux density in the air gap, over one slot pitch, the following is assumed:

- The effective flux linking the stator coils crosses the air gap perpendicular.
- The flux density distribution, in the air gap, over one magnet pitch, is homogeneous.

To apply these assumptions, the model will be further adapted. The stator teeth width w_t[m] will be modeled with the same width as the slot pitch, or when the slot angle θ_s[rad] is larger then the magnet angle θ_m[rad], the stator teeth width will be modeled with the same width as the magnet pitch τ_m[m]. To compensate for the fringing, an effective air gap length g_{eff}[m] is introduced:

$$g_{eff} = g \cdot k_c \tag{3.1}$$

k_c is the air gap length compensating factor. This factor can be found by dividing the air gap permeance P_g[Wb/A] into three parts, as is done in figure 3.1:

$$\begin{aligned} P_g &= P_a + P_b + P_c \\ &= \mu_0 \cdot l_{stk} \cdot \left(\frac{w_t}{g} + \frac{4}{\pi} \cdot \log\left(1 + \frac{\pi \cdot (\tau_s - w_t)}{4 \cdot g} \right) \right) \end{aligned}$$

With some algebraic manipulation [Han 94],[Vio 07], this solution can be written as an air gap correction factor:

$$k_c = \left(1 - \frac{\tau_s - w_t}{\tau_s} + \frac{4 \cdot g}{\pi \cdot \tau_m} \cdot \log\left(1 + \frac{\pi \cdot (\tau_s - w_t)}{4 \cdot g} \right) \right)^{-1} \tag{3.2}$$

The generator is now presented as in figure 3.2. The flux density in the magnets B_m[T] and the effective flux density in the air gap B_g[T], as function of position, are shown.

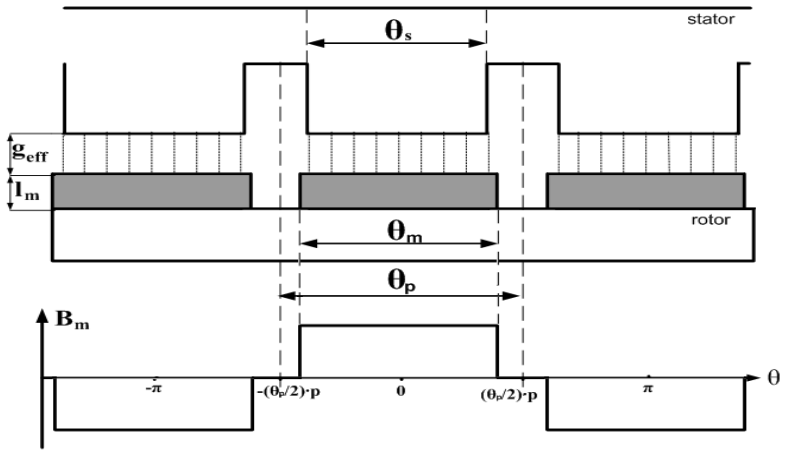

Figure 3.2: PM generator model with effective air gap and the flux density distribution as as function of position.

Not all flux coming from the magnets will link the stator coils through the air gap. Some flux will leak through the air gap. This leakage flux does not contribute to the induced voltage. Figure 3.3 shows two paths the flux can follow. The path of the flux crossing the air gap perpendicular and linking the stator coils, as described earlier in this model, and a path for the leakage flux.

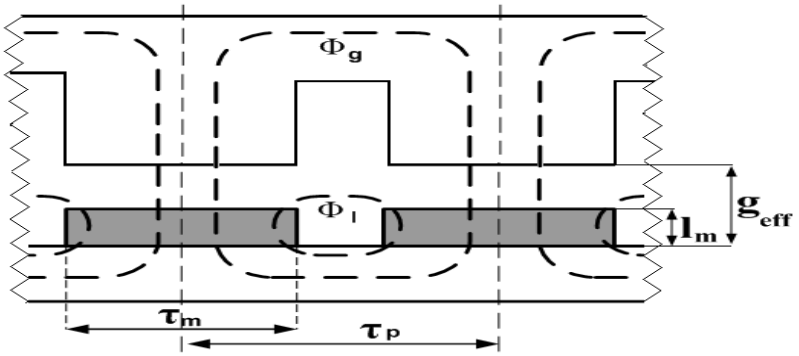

Figure 3.3: effective flux contour and leakage flux contour.

The derived model, under the given set of assumptions, is suitable for using circuit theory, to calculate the magnet flux, effective air gap flux and the leakage flux. The permanent magnets will be presented as flux sources and the model is further presented as reluctance circuit as in figure 3.4(a). This reluctance circuit can then be simplified to the circuit of figure 3.4(b).

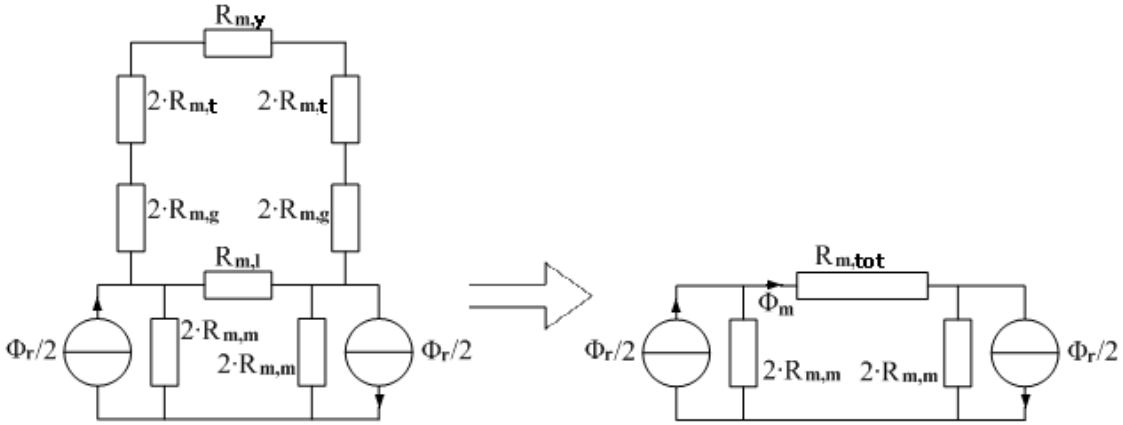

(a) ***(b)***

Figure 3.4: Reluctance circuit representation of the PM flux model (a), simplified form (b)

The calculation of the different reluctance components will now be discussed.

The leakage reluctance $R_{m,l}$[A/Wb] is calculated as is done by [Han 94]. A leakage area is assumed as in figure 3.5. Using this representation a leakage reluctance component is calculated:

$$R_{m,l} = \frac{\pi}{\mu_0 \cdot L_{stk} \cdot \log\left(1 + \pi \cdot \frac{g}{\tau_p - \tau_m}\right)} \tag{3.3}$$

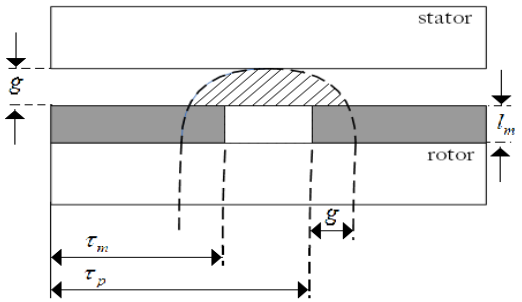

Figure 3.5: Area for modeling leakage reluctance

The air gap reluctance $R_{m,g}$[A/Wb] and magnet reluctance $R_{m,m}$[A/Wb] are calculated using the following equations derived from figure 3.2:

$$R_{m,g} = \frac{g \cdot k_c}{\mu_0 \cdot \tau_s \cdot l_{stk}} \quad (3.4)$$

$$R_{m,m} = \frac{l_m}{\mu_0 \cdot \mu_{rec} \cdot \tau_m \cdot l_{stk}} \quad (3.5)$$

The reluctance components of the stator yoke $R_{m,y}$[A/Wb] and stator teeth $R_{m,t}$[A/Wb] are modeled in the circuit because these are the spots that saturate the most. These reluctance components are calculated using the following equations [Pol 03]:

$$R_{m,y} = \frac{w_{sb}}{\mu_0 \cdot \mu_{r,steel,sy}(B_{sy,tot}) \cdot w_{sy} \cdot l_{stk}} \quad (3.6)$$

$$R_{m,t} = \frac{2}{3} \cdot \frac{d_1 + d_2 + d_3}{\mu_0 \cdot \mu_{r,steel,tooth}(B_{tooth,tot}) \cdot w_{ti} \cdot l_{stk}} \quad (3.7)$$

The factor 2/3 is there in equation 3.8, because the flux will concentrate most in 2/3 of the tooth length. The relative permeability of steel $\mu_{r,steel,sy}$ in the stator yoke is a non linear function of the total flux density $B_{sy,tot}$[T] in the stator yoke and the relative steel permeability $\mu_{r,steel,tooth}$ in the stator teeth is a non linear function of the total flux density $B_{tooth,tot}$[T] in the stator teeth. Appendix 4 presents a function for modeling the non linear relative steel permeability. Calculating the relative steel permeability and the flux densities within the machine must be done by means of an iterative process for every single time step. This is complex and time consuming. During normal operation conditions the reluctance components of the steel parts are of little influence, therefore it is useful to neglect them by making the relative permeability of the steel zero. In chapter 3.3 however, the permeability of the steel as function of flux density is considered and an iterative scheme for taking into account non-linear modeling of the steel reluctance parts is given (figure 3.18). This is done to determine the generators behavior when used as starting motor and the reluctance components of the steel parts can no longer be neglected.

The simplified reluctance circuit of figure 3.4(b) has a total reluctance component $R_{m,tot}$[A/Wb] which is derived according the following equation:

$$R_{m,tot} = \frac{\left(4\cdot\left(R_{m,g}+R_{m,t}\right)+R_{m,y}\right)\cdot R_{m,l}}{\left(4\cdot\left(R_{m,g}+R_{m,t}\right)+R_{m,y}\right)+R_{m,l}} \quad (3.8)$$

The remanent flux Φ_r[Wb] is calculated by using the remanent flux density B_r[T] from the PM datasheet, and adjust it for the right working temperature. This is done using the following equations:

$$B_{r(T)} = B_r\cdot\left(1+\frac{T_{emp}-20°}{100}\cdot T_{k,Br}\right) \quad (3.9)$$

$$\Phi_r = B_{r(T)}\cdot\tau_m\cdot l_{stk} \quad (3.10)$$

Using the superposition principle, the reluctance circuit representing the PM flux model of the generator can now be solved:

$$\Phi_{m1} = \Phi_r\cdot\frac{1}{2}\cdot\frac{2\cdot R_{m,m}}{4\cdot R_{m,m}+R_{m,tot}}$$

$$\Phi_{int1} = \Phi_r\cdot\frac{1}{2}\cdot\frac{2\cdot R_{m,m}+R_{m,tot}}{4\cdot R_{m,m}+R_{m,tot}}$$

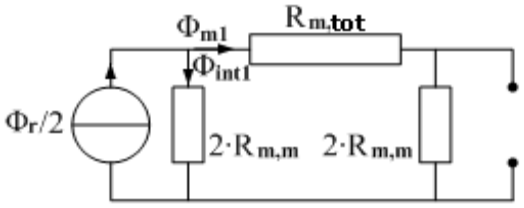

$$\Phi_{m2} = \Phi_{m1}$$

$$\Phi_{int2} = \Phi_{int1}$$

$$\Phi_m = \Phi_{m1}+\Phi_{m2}$$

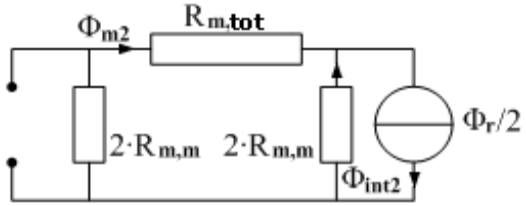

With the magnet flux Φ_m[Wb] known, the air gap flux Φ_g[Wb] and leakage flux Φ_l[Wb] components can be calculated:

$$\Phi_g = \Phi_m\cdot\frac{R_{m,l}}{4\cdot R_{m,g}+4\cdot R_{m,t}+R_{m,y}+R_{m,l}}$$

$$\Phi_l = \Phi_m\cdot\frac{4\cdot R_{m,g}}{4\cdot R_{m,g}+4\cdot R_{m,t}+R_{m,y}+R_{m,l}}$$

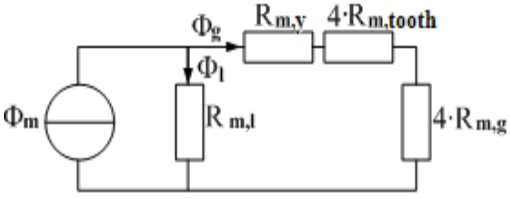

$$k_{ml} = \frac{\Phi_g}{\Phi_m} \quad (3.11)$$

$$B_g = \frac{\Phi_g}{0.5\cdot\tau_m\cdot l_{stk}} \quad (3.12)$$

$$B_m = \frac{\Phi_m}{0.5\cdot\tau_m\cdot l_{stk}} \quad (3.13)$$

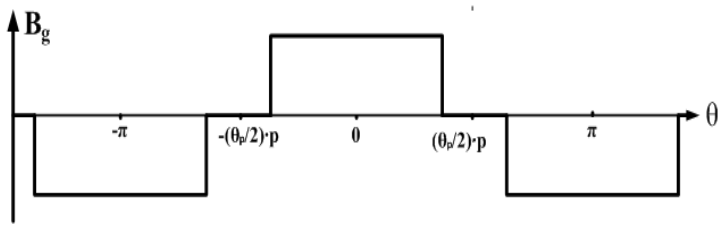

Figure 3.6: Effective air gap flux density as function of position

k_{ml} is the leakage factor and B_g[T] is the effective air gap flux density. Now the effective air gap flux density as function of rotor angle will be given and is also presented in figure 3.6. In this thesis the rotor position angle θ[rad] is expressed in electrical radians.

$$B_g(\theta) = \begin{cases} B_g & for \quad -\frac{\theta_m \cdot p}{2} + \left(2 \cdot \pi \cdot \sum_{-\infty}^{\infty} k\right) \le \theta \le \frac{\theta_m \cdot p}{2} + \left(2 \cdot \pi \cdot \sum_{-\infty}^{\infty} k\right) \\ -B_g & for \quad \pi - \frac{\theta_m \cdot p}{2} + \left(2 \cdot \pi \cdot \sum_{-\infty}^{\infty} k\right) \le \theta \le \pi + \frac{\theta_m \cdot p}{2} + \left(2 \cdot \pi \cdot \sum_{-\infty}^{\infty} k\right) \\ 0 & for \quad \theta = else \end{cases} \qquad (3.14)$$

When the rotor is rotating with speed ω_m[rad/s] the flux densities in the stator tooth B_{tooth}[T] and in the stator yoke B_{sy}[T] can be expressed as functions of time:

$$\theta = \omega_e \cdot t$$

$$\omega_e = \omega_m \cdot p$$

$$B_{tooth}(\theta) = \frac{1}{\theta_s \cdot p} \cdot \int_{-\frac{\theta_s \cdot p}{2} + \theta}^{\frac{\theta_s \cdot p}{2} + \theta} B_g(\theta) d\theta \cdot \frac{\tau_s}{w_{ti} \cdot k_{stk}} \qquad (3.15)$$

$$
= \begin{cases}
B_g \cdot \dfrac{\tau_s}{w_{ti} \cdot k_{stk}} & \text{for} \quad 0 \le \theta \le \dfrac{\theta_m - \theta_s}{2} \cdot p \\
\left(\dfrac{1}{2} + \dfrac{\theta_m}{2 \cdot \theta_s} - \dfrac{\theta}{\theta_s \cdot p} \right) \cdot B_g \cdot \dfrac{\tau_s}{w_{ti} \cdot k_{stk}} & \text{for} \quad \dfrac{\theta_m - \theta_s}{2} \cdot p < \theta \le \theta_p \cdot p - \dfrac{\theta_m + \theta_s}{2} \cdot p \\
\left(\dfrac{\theta_p}{\theta_s} - \dfrac{2 \cdot \theta}{\theta_s \cdot p} \right) \cdot B_g \cdot \dfrac{\tau_s}{w_{ti} \cdot k_{stk}} & \text{for} \quad \theta_p \cdot p - \dfrac{\theta_m + \theta_s}{2} \cdot p < \theta \le \dfrac{\theta_m + \theta_s}{2} \cdot p \\
\left(\dfrac{\theta_p}{\theta_s} - \dfrac{1}{2} - \dfrac{\theta_m}{2 \cdot \theta_s} - \dfrac{\theta}{\theta_s \cdot p} \right) \cdot B_g \cdot \dfrac{\tau_s}{w_{ti} \cdot k_{stk}} & \text{for} \quad \dfrac{\theta_m + \theta_s}{2} \cdot p < \theta \le \theta_p \cdot p - \dfrac{\theta_m - \theta_s}{2} \cdot p \\
-B_g \cdot \dfrac{\tau_s}{w_{ti} \cdot k_{stk}} & \text{for } \theta_p \cdot p - \dfrac{\theta_m - \theta_s}{2} \cdot p < \theta \le \theta_p \cdot p + \dfrac{\theta_m - \theta_s}{2} \cdot p \\
\left(-\dfrac{\theta_p}{\theta_s} - \dfrac{1}{2} - \dfrac{\theta_m}{2 \cdot \theta_s} + \dfrac{\theta}{\theta_s \cdot p} \right) \cdot B_g \cdot \dfrac{\tau_s}{w_{ti} \cdot k_{stk}} & \text{for } \theta_p \cdot p + \dfrac{\theta_m - \theta_s}{2} \cdot p < \theta \le 2 \cdot \theta_p \cdot p - \dfrac{\theta_m + \theta_s}{2} \cdot p \\
\left(-3 \cdot \dfrac{\theta_p}{\theta_s} + \dfrac{2 \cdot \theta}{\theta_s \cdot p} \right) \cdot B_g \cdot \dfrac{\tau_s}{w_{ti} \cdot k_{stk}} & \text{for } 2 \cdot \theta_p \cdot p - \dfrac{\theta_m + \theta_s}{2} \cdot p < \theta \le \theta_p \cdot p + \dfrac{\theta_m + \theta_s}{2} \cdot p \\
\left(-2 \cdot \dfrac{\theta_p}{\theta_s} + \dfrac{1}{2} + \dfrac{\theta_m}{2 \cdot \theta_s} + \dfrac{\theta}{\theta_s \cdot p} \right) \cdot B_g \cdot \dfrac{\tau_s}{w_{ti} \cdot k_{stk}} & \text{for } \theta_p \cdot p + \dfrac{\theta_m + \theta_s}{2} \cdot p < \theta \le 2 \cdot \theta_p \cdot p - \dfrac{\theta_m - \theta_s}{2} \cdot p \\
B_g \cdot \dfrac{\tau_s}{w_{ti} \cdot k_{stk}} & \text{for } 2 \cdot \theta_p \cdot p - \dfrac{\theta_m - \theta_s}{2} \cdot p < \theta \le 2 \cdot \theta_p \cdot p
\end{cases}
$$

$$B_{tooth}(t) = B_{tooth}\left(\frac{\theta}{\omega_e}\right) \tag{3.16}$$

$$B_{sy}(t) = B_{tooth}(t) \cdot \frac{w_{ti}}{2 \cdot w_{sy}} \tag{3.17}$$

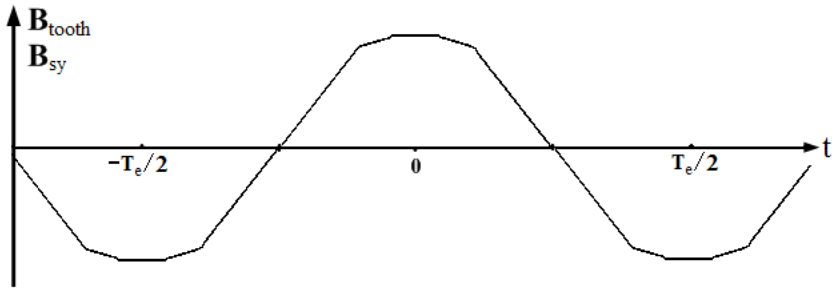

Figure 3.7: Flux density in stator tooth and stator yoke due to PM's as function of time.

Here p is the number of pole pairs. The flux density in the rotor yoke B_{ry}[T] as function of position does rotate with the same speed as the rotor. This means that the rotor yoke flux density does not vary with time. The constant flux density in the rotor yoke due to the PM's is expressed by equation 3.18:

$$B_{ry} = \frac{B_m \cdot \tau_m}{2 \cdot w_{ry} \cdot k_{stk}} \tag{3.18}$$

3.1.2. Induced voltage calculations

In the generator the rotor with magnets will rotate and produces a changing magnetic field in the stator coils. This induces a voltage in the stator coils. The voltage induced in a single coil e[V] can be calculated by deriving Maxwell's second equation, presented in appendix 2 under the following assumptions:

- The induced voltage in the generator is purely sinusoidal.
- A balanced three phase system.
- No load is applied

$$\begin{aligned} e(t) &= -\frac{d\lambda(\theta)}{dt} \\ e(t) &= -\frac{\partial\lambda(\theta)}{\partial\theta} \cdot \frac{\partial\theta}{\partial t} \end{aligned} \tag{3.19}$$

This is also called Faradays law for generator convention. The voltage is a function of the flux linkage λ[Wb-t] and the flux linkage is a function of the rotor position angle θ[rad] in electrical radians.

$$\lambda(\theta) = n_c \cdot \iint_s B_g(\theta) \cdot dA \tag{3.20}$$

Because the generator output voltage is expected to be sinusoidal, the function $B_g(\theta)$, which is derived in the PM flux model, will be written in the form of a Fourier series, in order to calculate the induced voltage. Calculating the induced voltage, using this method, simplifies calculations. First the full Fourier-series representation of the function is given. The point θ = 0 rad. is chosen such that the effective air gap distribution is symmetric with respect to the orthogonal axis. In this way the sin(kθ) terms in the series and the DC offset becomes zero [Sah 01]. See also figure 3.8.

$$\begin{aligned} B_g(\theta) &= \sum_{k=1}^{\infty} \left(a_k \cdot \cos(k\theta) + b_k \cdot \sin(k\theta) \right) \\ a_k &= \frac{1}{\pi} \cdot \int_0^{2\pi} B_g(\theta) \cdot \cos(k\theta)\, d\theta = \hat{B}_{g(k)} \\ b_k &= \frac{1}{\pi} \cdot \int_0^{2\pi} B_g(\theta) \cdot \sin(k\theta)\, d\theta = 0 \end{aligned} \tag{3.21}$$

$$B_g(\theta) = \sum_{k=1}^{\infty} \hat{B}_{g(k)} \cdot \cos(k\theta) \tag{3.22}$$

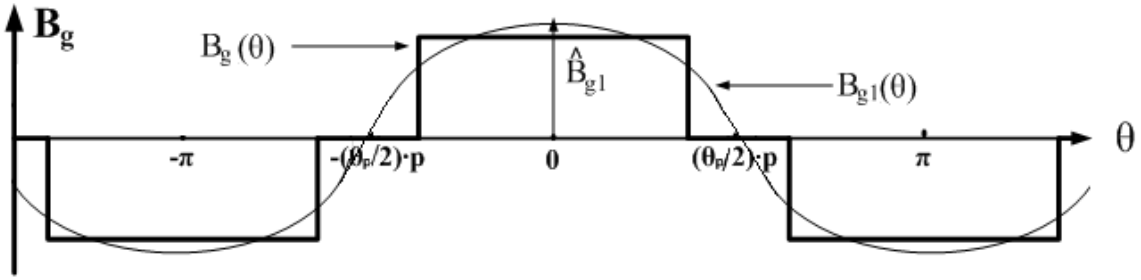

Figure 3.8: Effective air gap flux density function and its first harmonic component.

Since the assumption of purely sinusoidal voltages only the first harmonic component of the effective air gap flux density $B_{g(1)}$[T] is contributing to the induced voltage. Therefore only the first harmonic component of the Fourier series will be calculated.

$$B_{g(1)}(\theta) = \hat{B}_{g(1)} \cdot \cos(\theta) \tag{3.23}$$

$$\begin{aligned}
\hat{B}_{g(1)} &= \frac{1}{\pi} \cdot \int_0^{2\pi} B_g(\theta) \cdot \cos(\theta)\, d\theta \\
&= \frac{1}{\pi} \cdot \left(\int_{\frac{-\theta_m \cdot p}{2}}^{\frac{\theta_m \cdot p}{2}} B_g \cdot \cos(\theta)\, d\theta + \int_{\pi - \frac{\theta_m \cdot p}{2}}^{\pi + \frac{\theta_m \cdot p}{2}} B_g \cdot \cos(\theta)\, d\theta \right) \qquad (3.24) \\
&= \frac{4}{\pi} \cdot B_g \cdot \sin\left(\frac{\theta_m \cdot p}{2} \right) = \frac{4}{\pi} \cdot B_g \cdot \sin\left(\frac{\pi \cdot \alpha_m}{2} \right)
\end{aligned}$$

With the first harmonic component of the effective air gap flux, the first harmonic components of the flux linage $\lambda_{(1)}$[Wb-t] and the induced voltage $e_{(1)}$[V] can be derived as function of time. They are presented in figure 3.9.

$$\begin{aligned}
\lambda_{(1)}(\theta) &= n_c \cdot \iint_s \overline{B_{g(1)}}(\theta) \cdot dA_m \\
&= n_c \cdot l_{stk} \cdot r_{ri} \cdot \frac{1}{p} \cdot \int_{-(\pi/2)+\theta}^{(\pi/2)+\theta} \hat{B}_{g(1)} \cdot \cos(\theta)\, d\theta \qquad (3.25) \\
&= n_c \cdot l_{stk} \cdot r_{ri} \cdot \frac{1}{p} \cdot \hat{B}_{g1} \cdot \left(\sin(\pi/2 + \theta) - \sin(-\pi/2 + \theta) \right) \\
&= n_c \cdot l_{stk} \cdot r_{ri} \cdot \frac{1}{p} \cdot \hat{B}_{g1} \cdot 2 \cdot \cos(\theta)
\end{aligned}$$

$$\lambda_{(1)}(t) = n_c \cdot l_{stk} \cdot r_{ri} \cdot \frac{1}{p} \cdot \hat{B}_{g1} \cdot 2 \cdot \cos(\omega_e \cdot t) \tag{3.26}$$

$$\frac{d\lambda_{(1)}(t)}{dt} = -\omega_e \cdot n_c \cdot l_{stk} \cdot r_{ri} \cdot \frac{1}{p} \cdot \hat{B}_{g1} \cdot 2 \cdot \sin(\omega_e \cdot t)$$

$$e_{(1)}(t) = \omega_m \cdot n_c \cdot l_{stk} \cdot r_{ri} \cdot \hat{B}_{g1} \cdot 2 \cdot \sin(\omega_e \cdot t) \qquad (3.27)$$

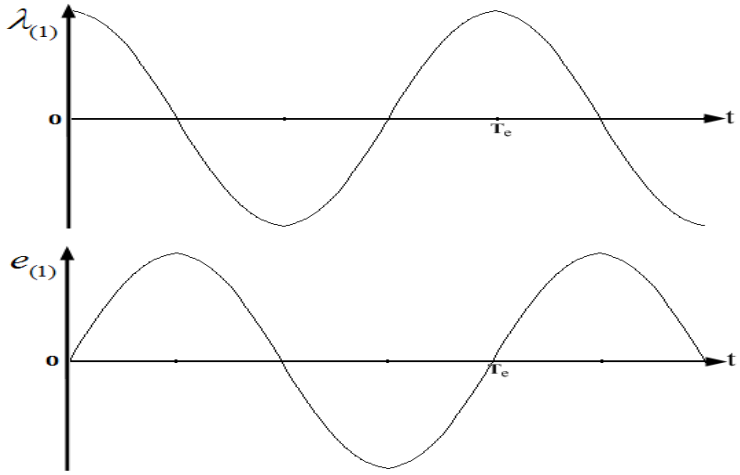

Figure 3.9: first harmonic components of flux linkage and induced voltage of a coil.

This is the voltage induced in one coil. The voltage induced in a phase winding is the sum of the coil voltages that are connected in series. Within the generator the distribution and placement of magnets and stator teeth has influence on the induced voltage. Different factors influencing the induced voltage are:

- *Chorded or fractional pitched windings:*
  When the slot pitch angle and pole pitch angle aren't equal as assumed earlier, less flux will link the stator teeth. When the slot pitch is smaller than the pole pitch the generator has chorded windings. This effect will be taken into account by the pitch factor k_p and is derived in appendix 3.
- *Distribution of the coils in a winding:*
  When the coils in a winding are distributed in a manner that their induced voltages are slightly out of phase, the total winding voltage will be smaller. This effect will be taken into account by the distribution factor k_d and is derived in appendix 3.
- *Skewing of the magnets:*
  Skewing of the magnets is applied to reduce cogging torque and reduce harmonic components in the induced voltage. But the induced winding voltage will decrease. The skew factor k_{skew} will take the reduction of winding voltage into account and will be derived in appendix 3.
- All effects together are taken into account by the winding factor k_w. The winding factor is stated by the following equation:

$$k_w = k_p \cdot k_d \cdot k_{skew}$$

The induced voltage in a phase winding e_{ph}[V] can be calculated using the following equation:

$$e_{ph}(t) = \frac{N_s}{N_{ph}} \cdot k_w \cdot \omega_m \cdot n_c \cdot l_{stk} \cdot r_{ro} \cdot \hat{B}_{g1} \cdot 2 \cdot \sin(\omega_e \cdot t) \quad (3.28)$$

$$\hat{e}_{ph} = \frac{N_s}{N_{ph}} \cdot k_w \cdot \omega_m \cdot n_c \cdot l_{stk} \cdot r_{ro} \cdot \hat{B}_{g1} \cdot 2 \quad (3.29)$$

Because a balanced three phase system is assumed the induced voltages in the three phases e_a[V], e_b[V] and e_c[V] are given by the following functions:

$$\begin{aligned} e_a(t) &= \hat{e}_{ph} \cdot \sin\left(\omega_e \cdot t\right) \\ e_b(t) &= \hat{e}_{ph} \cdot \sin\left(\omega_e \cdot t - \frac{2}{3} \cdot \pi\right) \\ e_b(t) &= \hat{e}_{ph} \cdot \sin\left(\omega_e \cdot t - \frac{4}{3} \cdot \pi\right) \end{aligned} \quad (3.30)$$

Also the RMS (Root Mean Square) value of the voltage E_{ph}[V] can be calculated:

$$\begin{aligned} E_{ph} &= \sqrt{\frac{1}{T_e} \cdot \int_0^{T_e} {e_{ph}}^2(t)dt} \\ &= \hat{e}_{ph} / \sqrt{2} \\ &= \frac{N_s}{N_{ph}} \cdot k_w \cdot \omega_m \cdot n_c \cdot l_{stk} \cdot r_{ro} \cdot \hat{B}_{g1} \cdot \sqrt{2} \end{aligned} \quad (3.31)$$

3.1.3. Resistance calculations

The DC-resistance R_{DC}[Ω] of a conductive wire with length l[m] and area A[m^2], with a resistivity ρ[Ω·m] can be calculated using the following equation:

$$R_{DC} = \rho \cdot \frac{l}{A} \quad (3.32)$$

The resistance of a phase winding R_{ph}[Ω] in a generator is calculated under the following assumption:

- Skin and proximity effects are neglected, since the skin depth δ_{skin}[m] is larger than two times the copper radius r_{cu}[m]. Therefore the phase resistance can be calculated using the DC-resistance equation 3.32.

The resistivity of copper ρ_{cu}[Ω·m] is temperature dependant and an equation is given for the change in resistivity due to temperature T_{emp}[°C]:

$$\rho_{cu(T_{emp})} = \rho_{cu} \cdot \left(1 + k_{cu} \cdot (T_{emp} - 20)\right) \quad (3.33)$$

Here k_{cu}[1/°C] is the copper temperature coefficient. The total length of the copper around one tooth is given by the length of one copper turn l_{turn}[m] multiplied by the number of turns n_c around one coil. The area of a copper winding A_{cu}[m^2] can be calculated from the copper radius r_{cu}[m]. The resistance per phase winding can now be calculated:

$$\begin{aligned} R_{ph} &= \frac{\rho_{cu(120)} \cdot n_c \cdot l_{turn}}{A_{cu}} \cdot \frac{N_s}{N_{ph}} \\ &= \frac{\rho_{cu(120)} \cdot n_c \cdot \left(\pi \cdot \tau_c + 2 \cdot l_{stk}\right)}{r_{cu}{}^2 \cdot \pi} \cdot \frac{N_s}{N_{ph}} \end{aligned} \tag{3.34}$$

It is important to keep in mind that $\delta_{skin} > 2 \cdot r_{cu}$. Therefore the skindepth δ_{skin}[m] can be calculated using the following equation:

$$\delta_{skin} = \sqrt{\frac{2 \cdot \rho_{cu(T_{emp})}}{\omega_e \cdot \mu_0}} \tag{3.35}$$

3.2. Armature reaction model

When applying an electric load to a generator, due to the induced voltage in the coils a current will start to flow. This current produces a magnetic field of its own. The induced magnetic field will oppose the change of flux due to the magnets and therefore the rotational movement of the machine. Higher currents mean more opposing force and therefore the machine has to deliver a higher torque. This phenomenon is called armature reaction and it affects the flux density distribution within the machine. The total magnetic field in the generator is the superposition of the armature reaction field and the permanent magnet field.

Due to armature reaction the flux density in the magnets can be pushed beneath the minimum allowed flux density $B_{m,min}$[T] (see fig 2.2) and there is a risk of demagnetizing the magnets. During normal steady state operation the effect of armature reaction on the magnets is small. But when the generator is also used as a starting machine, or during fault conditions, high currents will flow through the stator coils and there is a real threat of demagnetizing the magnets. When designing a generator armature reaction has to be considered. The thickness of the magnets must be customized, so the magnets are safe for armature reaction magnetic fields due to high currents.

Using circuit theory, the magnetic field due to armature reaction is calculated. Two models are derived, for generator with different concentrated coil winding configurations:

- A model for generator constructions with a fractional pitch winding with a multiple of 9 coils around 9 teeth and 8 magnet poles. This model can also be used for fractional pitch windings with a multiple of 9 coils around 9 teeth and 10 magnet poles.
- A model for generator constructions with a fractional pitch winding with a multiple of 3 coils around 3 teeth and 2 magnet poles. This model can also be used for fractional pitch windings with a multiple of 3 coils around 3 teeth and 4 magnet poles.

The models represent the magnetic field in a generator due to current in one phase of the generator. Modeling only one phase current gives the possibility to calculate the armature reaction component of the flux density in different parts of the machine. The phase self inductance L_s[H] and the mutual inductance M_{ab}[H] components under normal operation conditions can be calculated. And it is possible to calculate the space harmonic components in the rotor due to armature reaction. The model is made under the following set of assumptions:

- The phase currents in the model are purely sinusoidal.
- The air gap reluctance $R_{m,g}$[A/Wb] and magnet reluctance $R_{m,m}$[A/Wb] is not a function of position. This can be assumed since the magnets and the air between them have essentially the same relative permeability μ_r.
- A balanced three phase system.
- The PM flux source does not appear since it does not contribute to the armature reaction flux.

The currents induced in the armature windings are responsible for the armature reaction magnetic field. They lag the no-load voltage by an angle φ[rad]. The phase currents i_a[A], i_b[A] and i_c[A] are given by the following functions:

$$\begin{aligned} i_a(t) &= \hat{i}_{ph} \cdot \sin\left(\omega_e \cdot t - \varphi\right) \\ i_b(t) &= \hat{i}_{ph} \cdot \sin\left(\omega_e \cdot t - \frac{2}{3} \cdot \pi - \varphi\right) \\ i_c(t) &= \hat{i}_{ph} \cdot \sin\left(\omega_e \cdot t - \frac{4}{3} \cdot \pi - \varphi\right) \end{aligned} \tag{3.36}$$

For a defined slot area A_s[m^2] and current density J_{nom}[A/m^2] during normal operation, the slot current I_s[A] flowing through all the turns of a single coil added together is calculated using equation 3.37. With use of the slot current, the RMS phase current I_{ph}[A] for normal operation is calculated (eq. 3.38) and also the phase peak current $\hat{i}_{ph}$ [A] is calculated (eq. 3.39):

$$I_s = \tfrac{1}{2} \cdot A_s \cdot k_{fill} \cdot J_{nom} \tag{3.37}$$

$$I_{ph} = \frac{I_s}{n_c} \tag{3.38}$$

$$\hat{i}_{ph} = I_{ph} \cdot \sqrt{2} \tag{3.39}$$

3.2.1. Fractional pitch windings with a multiple of 9 coils around 9 teeth and 8 magnet poles

A reluctance circuit to model the armature reaction in a generator, due to current in one phase, phase a, is build as in figure 3.11. This circuit represents an electrical machine with a pole slot combination which is a multiple of 9 coils around 9 teeth with 8 magnet poles, as is presented in figure 3.10.

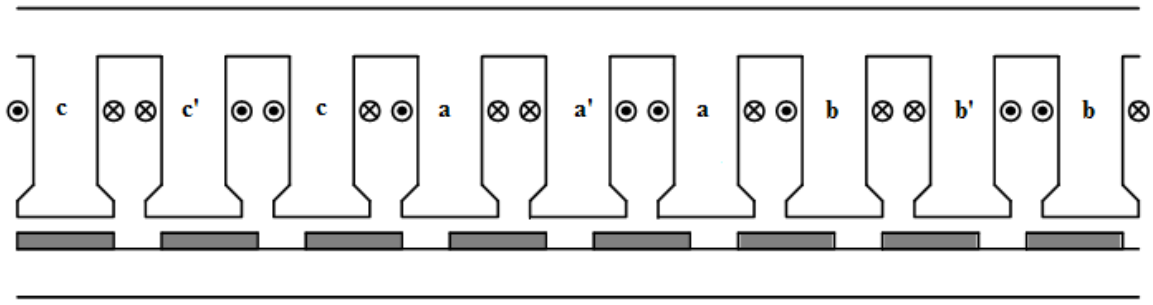

Figure 3.10: Fractional pitch winding with 9 coils around 9 teeth and 8 magnet poles

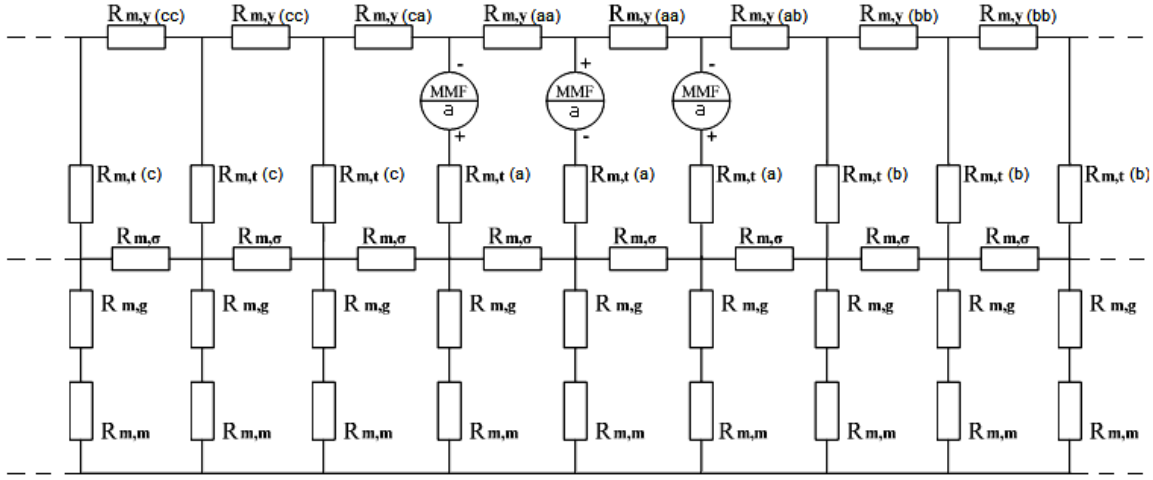

Figure 3.11: Circuit representation for modeling armature reaction due to current in one phase.

The reluctance circuit of figure 3.11 is then simplified to the reluctance circuit of figure 3.12. This can be done by presenting the phases b and c both as a single reluctance path and only take into account the steel reluctance components of the teeth and yoke in phase a. Since these are the spots that will first saturate when the phase current increases. For the circuit of figure 3.12, a reluctance matrix will be set up to calculate the loop fluxes 1 till 8.

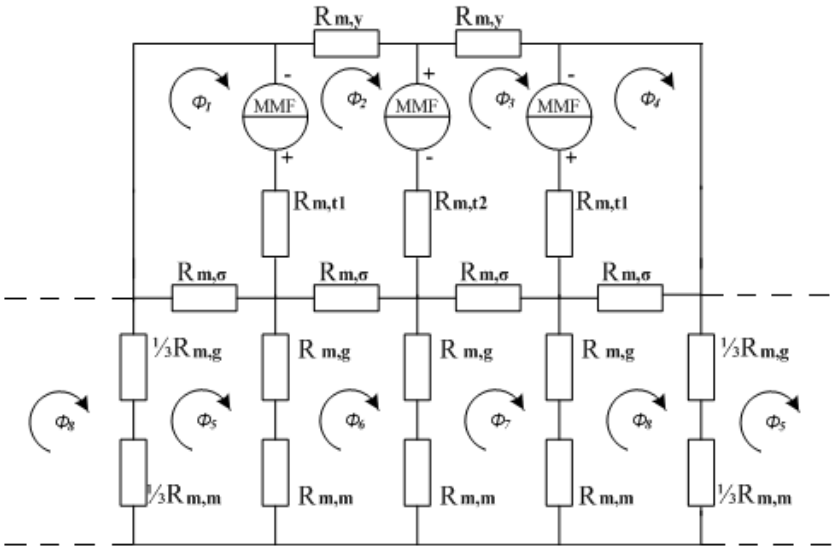

Figure 3.12: Simplified armature reaction reluctance circuit.

First equations for the different components in the circuit are derived. The air gap reluctance $R_{m,g}$[A/Wb] is calculated in the same way as is done in the PM flux model. The armature reluctance flux crosses the air gap over the whole slot pitch. Therefore an effective air gap length g_{eff}[m] is applied. In this way the air gap can be modeled as a lumped reluctance component.

$$R_{m,g} = \frac{g_{eff}}{\mu_0 \cdot \tau_s \cdot l_{stk}} \tag{3.4}$$

The magnet reluctance $R_{m,m}$[A/Wb] is calculated different from the PM flux model magnet reluctance, because the armature reaction flux crosses the air gap and magnets over one slot pitch τ_s[m]:

$$R_{m,m} = \frac{l_m}{\mu_0 \cdot \mu_{rec} \cdot \tau_s \cdot l_{stk}} \tag{3.40}$$

The leakage reluctance consists of different parts. Some flux will leak through the slots, and some flux will leak through the air gap. These leakage flux components do not interact with the PM flux in the magnets and the air gap. However they do contribute to the inductance of the machine. An equation for the air gap leakage reluctance $R_{m,\sigma(gap)}$[A/Wb] is given by [Gie 02]:

$$R_{m,\sigma(gap)} = \frac{1}{l_{stk} \cdot \mu_0 \cdot \frac{5 \cdot (g / w_s)}{5 + 4 \cdot (g / w_s)}} \tag{3.41}$$

An equation for the slot leakage reluctance $R_{m,\sigma(slot)}$[A/Wb] is given by [Han 94]:

$$R_{m,\sigma(slot)} = \frac{1}{\mu_0 \cdot L_{stk} \cdot \left(\frac{d_3}{3 \cdot \frac{w_{sb} + w_{si}}{2}} + \frac{d_2}{\frac{w_{si} + w_s}{2}} + \frac{d_1}{w_s} \right)} \tag{3.42}$$

The total leakage reluctance $R_{m,\sigma}$[A/Wb] used in this model is calculated by taking the separate leakage components together, following equation 3.43:

$$R_{m,\sigma} = \frac{R_{m,\sigma(slot)} \cdot R_{m,\sigma(gap)}}{R_{m,\sigma(slot)} + R_{m,\sigma(gap)}} \tag{3.43}$$

The reluctance components of the steel are modeled to represent the spaces that saturate the most when currents are applied in phase a. These spaces are the stator yoke $R_{m,y}$[A/Wb] and the stator teeth $R_{m,t}$[A/Wb] of phase a. To reduce complexity it can be useful to also neglect these reluctance components during normal operation conditions. This can be done by making the relative permeability in the steel parts infinite. Equations for the reluctance components representing the steel parts are presented:

$$R_{m,y} = \frac{w_{sb}}{\mu_0 \cdot \mu_{r,steel,sy}(B_{sy,tot}) \cdot w_{sy} \cdot l_{stk}} \quad (3.6)$$

$$R_{m,t} = \frac{2}{3} \cdot \frac{d_1 + d_2 + d_3}{\mu_0 \cdot \mu_{r,steel,tooth}(B_{tooth,tot}) \cdot w_{ti} \cdot l_{stk}} \quad (3.7)$$

The relative permeability of steel $\mu_{r,steel}$ is a non linear function of the flux density in the steel. This function is derived in appendix 4. Calculations must be done by means of an iterative process, as presented in figure 3.18. For normal operation conditions however, the relative steel permeability can be assumed infinite.

The magneto motive force MMF[A-t] of a coil is given by:

$$MMF_a(t) = n_c \cdot i_a(t) \quad (3.44)$$

With the use of a reluctance matrix the loop fluxes in the circuit are calculated. For a generator with a winding configuration of 9 coils around 9 teeth and 8 magnet poles this is done according equation 3.45:

$$\overline{\Phi_a}(t) = \mathbf{R^{-1}} \bullet \overline{MMF_a}(t) \quad (3.45)$$

$$\begin{bmatrix} \phi_1(t) \\ \phi_2(t) \\ \phi_3(t) \\ \phi_4(t) \\ \phi_5(t) \\ \phi_6(t) \\ \phi_7(t) \\ \phi_8(t) \end{bmatrix} = \begin{bmatrix} \left(R_{m,\sigma}+R_{m,t1}\right) & -R_{m,t1} & 0 & 0 & -R_{m,\sigma} & 0 & 0 & 0 \\ -R_{m,t1} & \left(R_{m,\sigma}+R_{m,t1}+R_{m,t2}+R_{m,y}\right) & -R_{m,t2} & 0 & 0 & -R_{m,\sigma} & 0 & 0 \\ 0 & -R_{m,t2} & \left(R_{m,\sigma}+R_{m,t1}+R_{m,t2}+R_{m,y}\right) & -R_{m,t1} & 0 & 0 & -R_{m,\sigma} & 0 \\ 0 & 0 & -R_{m,t1} & \left(R_{m,\sigma}+R_{m,t1}\right) & 0 & 0 & 0 & -R_{m,\sigma} \\ -R_{m,\sigma} & 0 & 0 & 0 & \left(\frac{4}{3}\cdot\left(R_{m,m}+R_{m,g}\right)+R_{m,\sigma}\right) & -\left(R_{m,m}+R_{m,g}\right) & 0 & 0 \\ 0 & -R_{m,\sigma} & 0 & 0 & -\left(R_{m,m}+R_{m,g}\right) & \left(2\cdot\left(R_{m,m}+R_{m,g}\right)+R_{m,\sigma}\right) & -\left(R_{m,m}+R_{m,g}\right) & 0 \\ 0 & 0 & -R_{m,\sigma} & 0 & 0 & -\left(R_{m,m}+R_{m,g}\right) & \left(2\cdot\left(R_{m,m}+R_{m,g}\right)+R_{m,\sigma}\right) & -\left(R_{m,m}+R_{m,g}\right) \\ 0 & 0 & 0 & -R_{m,\sigma} & 0 & 0 & -\left(R_{m,m}+R_{m,g}\right) & \left(\frac{4}{3}\cdot\left(R_{m,m}+R_{m,g}\right)+R_{m,\sigma}\right) \end{bmatrix}^{-1} \bullet \begin{bmatrix} -n_c \cdot i_a(t) \\ 2 \cdot n_c \cdot i_a(t) \\ -2 \cdot n_c \cdot i_a(t) \\ n_c \cdot i_a(t) \\ 0 \\ 0 \\ 0 \\ 0 \end{bmatrix}$$

3.2.1.1. Armature reaction flux densities

Using the loop fluxes the armature reaction component of the flux density is calculated at different places in the machine. The flux generated in and under the middle tooth of phase a is chosen for flux density calculations, because this tooth has little influence from flux generated by the other phase currents. This makes calculations accurate even though other phases are neglected.

The armature reaction component of the flux density in a stator tooth as function of time:

$$B_{ar,tooth}(t) = \frac{\phi_2(t)-\phi_3(t)}{w_{ti}\cdot l_{stk}\cdot k_{stk}} = \hat{B}_{ar,tooth}\cdot\sin\left(\omega_e\cdot t\right) \quad (3.46)$$

$$\hat{B}_{ar,tooth} = B_{ar,tooth}\left(\frac{T_e}{4}\right) \quad (3.47)$$

The armature reaction component of the flux density in the stator yoke as function of time:

$$B_{ar,sy}(t) = \frac{\phi_2(t)}{w_{sy}\cdot l_{stk}\cdot k_{stk}} = \hat{B}_{ar,sy}\cdot\sin\left(\omega_e\cdot t\right) \quad (3.48)$$

$$\hat{B}_{ar,sy} = B_{ar,sy}\left(\frac{T_e}{4}\right) \quad (3.49)$$

The armature reaction component of the flux density in the rotor yoke, seen from the stator, as function of time:

$$B_{ar,ry}(t) = \frac{\phi_7(t)}{w_{ry}\cdot l_{stk}\cdot k_{stk}} = \hat{B}_{ar,ry}\cdot\sin\left(\omega_e\cdot t\right) \quad (3.50)$$

$$\hat{B}_{ar,ry} = B_{ar,ry}\left(\frac{T_e}{4}\right) \quad (3.51)$$

The armature reaction component of the flux density in the air gap and magnets, seen from the stator, as function of time:

$$B_{ar,magnet}(t) = \frac{\phi_6(t)-\phi_7(t)}{\tau_s\cdot l_{stk}} = \hat{B}_{ar,magnet}\cdot\sin\left(\omega_e\cdot t\right) \quad (3.52)$$

$$\hat{B}_{ar,magnet} = B_{ar,magnet}\left(\frac{T_e}{4}\right) \quad (3.53)$$

The armature reaction flux in the magnets $B_{ar,magnet}$[T] interacts with the flux of the PM's in the PM's. These two flux components can be superimposed. This superimposed flux must be greater than the minimum allowed flux density in the magnets $B_{m,min}$[T]. Otherwise there is a threat of partly demagnetizing the magnets. This is shown in figure 3.13.

$$B_m - \hat{B}_{ar,magnet} > B_{m,\min} \quad (3.54)$$

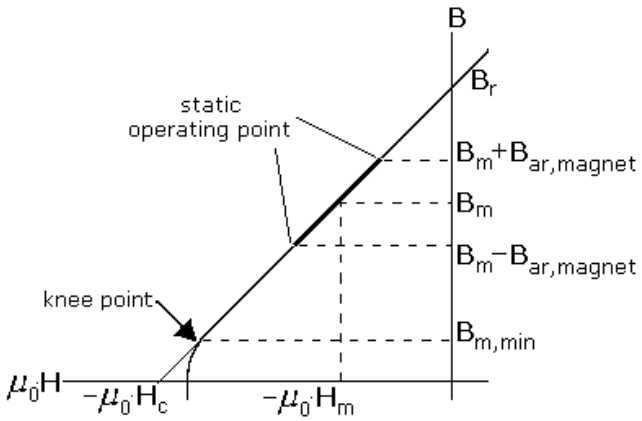

Figure 3.13: Effect of armature reaction flux on a permanent magnet.

3.2.1.2 Inductance calculations

The self inductance L_s[H] of a phase winding is a measure for the capacity to store magnetic energy. This energy is stored in a magnetic field around the coils of the phase winding. When the permeabilities of the materials in the generator are constant, which can be assumed during normal operation condition, the self inductance of phase a is a constant, relating the current in phase a to flux of phase a linking the coils of phase a. And the mutual inductance M_{ab}[H] relates the current in phase a to flux of phase a linking coils in phase b.

$$\begin{aligned} L_{sa} &= \frac{\lambda_{aa}(t)}{i_a(t)} \\ &= \frac{n_c \cdot \Phi_{aa}(t)}{i_a(t)} \end{aligned} \tag{3.55}$$

$$M_{ab} = \frac{\lambda_{ab}(t)}{i_a(t)} \tag{3.56}$$

Keep in mind that the flux from phase a linking phase b has an opposite direction as the flux from phase a linking phase a and therefore has a negative value. Because a balanced three phase system is assumed, it can be shown that inductance and mutual inductance components are the same for every phase:

$$\begin{aligned} L_s &= L_{sa} = L_{sb} = L_{sc} \\ M_{ab} &= M_{ac} = M_{ba} = M_{bc} = M_{ca} = M_{cb} \end{aligned}$$

The total flux linking every phase can then be calculated using the following set of equations:

$$\begin{bmatrix}\lambda_a(t)\\ \lambda_b(t)\\ \lambda_c(t)\end{bmatrix} = \begin{bmatrix} L_s & M_{ab} & M_{ab}\\ M_{ab} & L_s & M_{ab}\\ M_{ab} & M_{ab} & L_s\end{bmatrix}\cdot\begin{bmatrix} i_a(t)\\ i_b(t)\\ i_c(t)\end{bmatrix}$$
$$\begin{bmatrix}\lambda_a(t)\\ \lambda_b(t)\\ \lambda_c(t)\end{bmatrix} = \left(L_s - M_{ab}\right)\cdot\begin{bmatrix} i_a(t)\\ i_b(t)\\ i_c(t)\end{bmatrix} \tag{3.59}$$

The self inductance can further be divided in a main inductance L_{sm}[H] part and a leakage inductance part $L_{s\sigma}$[H]. The main inductance is related to the flux interacting with the PM flux in the air gap. The leakage inductance is related to the flux not interacting with the PM flux.

$$L_s = L_{sm} + L_{s\sigma} \tag{3.60}$$

In this model the leakage inductance is divided in two parts, the slot leakage inductance $L_{s\sigma(slot)}$[H] and the gap leakage inductance $L_{s\sigma(gap)}$[H]:

$$L_{s\sigma} = L_{s\sigma(slot)} + L_{s\sigma(gap)} \tag{3.61}$$

Another component often taken into account is the end leakage inductance $L_{s\sigma(end)}$[H], this is the inductance component due to the end windings. This is the smallest leakage component and will be neglected to make a better comparison between the analytical model and the FEM model, which is discussed in chapter 5.

Using the armature reaction model and with use of equations 3.45, 3.55, 3.56 and 3.60 all inductance components can be calculated:

$$L_s = \frac{N_s}{3\cdot N_{ph}}\cdot\frac{n_c\cdot\left(\left|\hat{\phi}_1-\hat{\phi}_2\right|+\left|\hat{\phi}_2-\hat{\phi}_3\right|+\left|\hat{\phi}_3-\hat{\phi}_4\right|\right)}{\hat{i}_{ph}} \tag{3.62}$$

$$L_{sm} = \frac{N_s}{3\cdot N_{ph}}\cdot\frac{n_c\cdot\left(\left|\hat{\phi}_5-\hat{\phi}_6\right|+\left|\hat{\phi}_6-\hat{\phi}_7\right|+\left|\hat{\phi}_7-\hat{\phi}_8\right|+\left|\hat{\phi}_8-\hat{\phi}_5\right|\right)}{\hat{i}_{ph}} \tag{3.63}$$

$$L_{s\sigma} = L_s - L_{sm} \tag{3.64}$$

$$M_{ab} = -\frac{N_s}{3\cdot N_{ph}}\cdot\frac{n_c\cdot\left|\hat{\phi}_4\right|}{\hat{i}_{ph}} \tag{3.65}$$

3.2.2. Fractional pitch windings with a multiple of 9 coils around 9 teeth and 8 magnet poles

A reluctance circuit to model the armature reaction in a generator, due to current in one phase, phase a, is build as in figure 3.15. This circuit represents an electrical machine with a pole slot combination which is a multiple of 3 coils around 3 teeth with 2 magnet poles, as is presented in figure 3.14. Only the steel reluctance component of the tooth of phase a is considered, since this is the first spot to saturate.

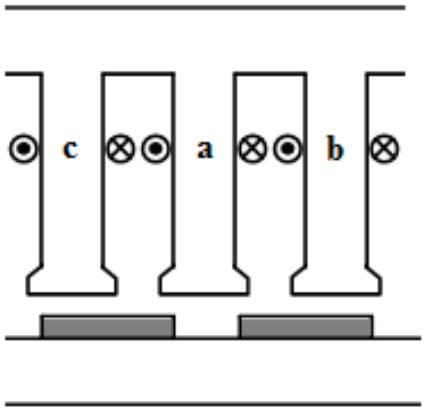

Figure 3.14: Fractional pitch winding with 3 coils around 3 teeth and 2 magnet poles

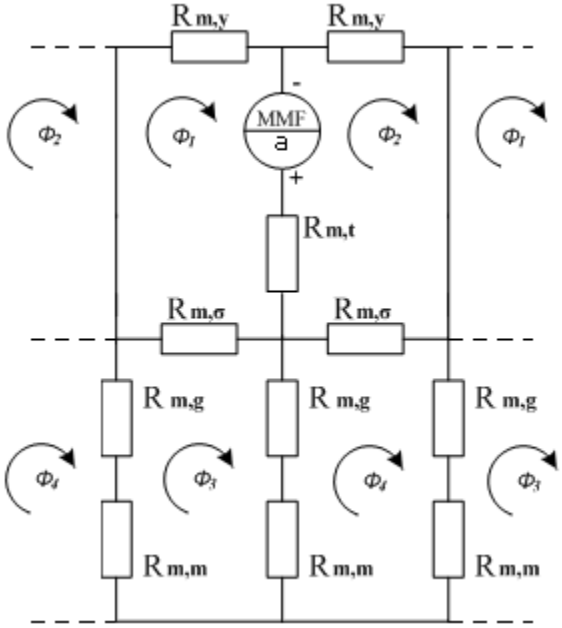

Figure 3.15: Circuit representation for modeling armature reaction due to current in one phase.

The reluctance circuit components in the circuit can be derived using the equations 3.4, 3.6, 3.7 and 3.40 to 3.44. from chapter 3.2.1. The loop fluxes will be calculated according equation 3.66:

$$\overline{\Phi_a}(t) = \mathbf{R}^{-1} \bullet \overline{MMF_a}(t) \tag{3.66}$$

$$\begin{bmatrix} \phi_1(t) \\ \phi_2(t) \\ \phi_3(t) \\ \phi_4(t) \end{bmatrix} = \begin{bmatrix} \left(R_{m,\sigma} + R_{m,t} + R_{m,y}\right) & -R_{m,t} & -R_{m,\sigma} & 0 \\ -R_{m,t} & \left(R_{m,\sigma} + R_{m,t} + R_{m,y}\right) & 0 & -R_{m,\sigma} \\ -R_{m,\sigma} & 0 & \left(2 \cdot R_{m,g} + R_{m,\sigma}\right) & -R_{m,g} \\ 0 & -R_{m,\sigma} & -R_{m,g} & \left(2 \cdot R_{m,g} + R_{m,\sigma}\right) \end{bmatrix}^{-1} \bullet \begin{bmatrix} -n_c \cdot i_a(t) \\ n_c \cdot i_a(t) \\ 0 \\ 0 \end{bmatrix}$$

3.2.2.1. Armature reaction flux densities

Using the loop fluxes calculated with equation 3.66 the armature reaction component of the flux density is calculated at different places in the machine. Because of a balanced three phase system and phase symmetry armature reaction flux densities due to current in one phase are a factor 2/3 lower than armature reaction flux densities due to a balanced three phase current.

Therefore all flux densities will be multiplied with a factor 3/2 to compensate for the fact that only one phase is considered:

The armature reaction component of the flux density in a stator tooth as function of time:

$$B_{ar,tooth}(t) = \frac{3}{2}\cdot\frac{\phi_1(t)-\phi_2(t)}{w_{ti}\cdot l_{stk}\cdot k_{stk}} = \hat{B}_{ar,tooth}\cdot\sin\left(\omega_e\cdot t\right) \quad (3.67)$$

$$\hat{B}_{ar,tooth} = B_{ar,tooth}\left(\frac{T_e}{4}\right) \quad (3.68)$$

The armature reaction component of the flux density in a stator yoke as function of time:

$$B_{ar,sy}(t) = \frac{3}{2}\cdot\frac{\phi_1(t)}{w_{sy}\cdot l_{stk}\cdot k_{stk}} = \hat{B}_{ar,sy}\cdot\sin\left(\omega_e\cdot t\right) \quad (3.69)$$

$$\hat{B}_{ar,sy} = B_{ar,sy}\left(\frac{T_e}{4}\right) \quad (3.70)$$

The armature reaction component of the flux density in the rotor yoke, seen from the stator, as function of time:

$$B_{ar,ry}(t) = \frac{3}{2}\cdot\frac{\phi_3(t)}{w_{ry}\cdot l_{stk}\cdot k_{stk}} = \hat{B}_{ar,ry}\cdot\sin\left(\omega_e\cdot t\right) \quad (3.71)$$

$$\hat{B}_{ar,ry} = B_{ar,ry}\left(\frac{T_e}{4}\right) \quad (3.72)$$

The armature reaction component of the flux density in the air gap and magnets, seen from the stator, as function of time:

$$B_{ar,magnet}(t) = \frac{3}{2}\cdot\frac{\phi_3(t)-\phi_4(t)}{\tau_s\cdot l_{stk}} = \hat{B}_{ar,magnet}\cdot\sin\left(\omega_e\cdot t\right) \quad (3.73)$$

$$\hat{B}_{ar,magnet} = B_{ar,magnet}\left(\frac{T_e}{4}\right) \quad (3.74)$$

3.2.2.2. Inductance calculations

Using the armature reaction model and with help of equations 3.55, 3.56, 3.60 and 3.66, all inductance components can be calculated:

$$L_s = \frac{N_s}{N_{ph}}\cdot\frac{n_c\cdot\left(\hat{\phi}_1-\hat{\phi}_2\right)}{\hat{i}_{ph}} \quad (3.75)$$

$$L_{sm} = \frac{N_s}{N_{ph}} \cdot \frac{n_c \cdot \left(\hat{\phi}_3 - \hat{\phi}_4\right)}{\hat{i}_{ph}} \quad (3.76)$$

$$L_{s\sigma} = L_s - L_{sm} \quad (3.77)$$

$$M_{ab} = -\frac{N_s}{N_{ph}} \cdot \frac{n_c \cdot \left|\hat{\phi}_1\right|}{\hat{i}_{ph}} \quad (3.78)$$

3.2.3. Space harmonic components in the rotor due to armature reaction

When having an electrical machine with sinusoidal distributed windings, the armature reaction flux density in the air gap and magnets will have a sinusoidal space distribution. This armature reaction flux density distribution, will rotate trough the machine with an electrical rotational speed ω_e[rad]. Since the PM flux distribution also rotates at this speed, the flux distribution, seen from the rotor, as function of space and time does not change. This means; no Eddy current losses in the rotor.

When developing an electrical machine with concentrated coil fractional pitch windings the armature reaction flux density distribution does not have a sinusoidal space distribution. When a Fourier transformation of this space distribution is made, it becomes clear that the armature reaction flux density distribution in the air gap and magnets has different space harmonic components that move at different speeds, seen from the rotor. These space harmonics can add substantially to the losses in the magnets and rotor back iron. Therefore a space-time composition of the harmonic components in the air gap and rotor magnets will be made in this sub-chapter.

The method to present the armature reaction component of the flux density in the air gap and magnets, as function of position and time, is derived according the work of [pol 07]. The method is derived under the following set of assumptions:

- Flux crosses the air gap and magnets perpendicular.
- Armature reaction magneto motive force is due to perfectly sinusoidal currents.

The flux density in the air gap and magnets $B_{ar,a}$[T], due to the magneto motive force of one phase, phase a, will be presented as function of stator position θ_{st}[rad]. $B_{ar,a}$[T] will then be written in the form of a Fourier series with a fundamental wave length of λ_1[rad]. The position $\theta_{st} = 0$ rad. is chosen such that the flux density distribution is symmetric with respect to the orthogonal axis. In this way the sin(kθ) terms in the series and the DC offset becomes zero. As is done with the induced voltage calculations in chapter 3.1.2:

$$B_{ar,a}\left(\theta_{st}\right) = \sum_{k=1}^{\infty} \hat{B}_{ar(k)} \cdot \cos\left(k \cdot \frac{2 \cdot \pi \cdot \theta_{st}}{\lambda_1}\right) \quad (3.79)$$

$$\hat{B}_{ar(k)} = \frac{2}{\lambda_1} \cdot \int_0^{\lambda_1} B_{ar,a}\left(\theta_{st}\right) \cdot \cos\left(k \cdot \frac{2 \cdot \pi \cdot \theta_{st}}{\lambda_1}\right) d\theta_{st} \quad (3.80)$$

The flux density distributions of the other phases are equal to the distribution of phase a, except for a phase shift in the position. When the amplitudes of the space harmonics are also a function of time, induced by the armature currents, the armature reaction components of the magnet flux density $B_{ar,a}$[T], $B_{ar,b}$[T], $B_{ar,c}$[T] can be expressed as functions of stator position θ_{st}[rad] and time t[s]:

$$\begin{aligned} B_{ar,a}(\theta_{st},t) &= \sum_{k=1}^{\infty} \hat{B}_{ar(k)} \cdot \cos\left(k \cdot \frac{2\cdot\pi\cdot\theta_{st}}{\lambda_1}\right) \cdot \cos(\omega_e \cdot t) \\ B_{ar,b}(\theta_{st},t) &= \sum_{k=1}^{\infty} \hat{B}_{ar(k)} \cdot \cos\left(k \cdot \left(\frac{2\cdot\pi\cdot\theta_{st}}{\lambda_1} - \frac{2\cdot\pi}{3}\right)\right) \cdot \cos\left(\omega_e \cdot t - \frac{2\cdot\pi}{3}\right) \\ B_{ar,c}(\theta_{st},t) &= \sum_{k=1}^{\infty} \hat{B}_{ar(k)} \cdot \cos\left(k \cdot \left(\frac{2\cdot\pi\cdot\theta_{st}}{\lambda_1} - \frac{4\cdot\pi}{3}\right)\right) \cdot \cos\left(\omega_e \cdot t - \frac{4\cdot\pi}{3}\right) \end{aligned} \quad (3.81)$$

The total armature reaction component of the flux density in the air gap and magnets, as function of stator position and time, can be obtained by adding the three separate functions. This results in equation 3.82:

$$B_{ar}(\theta_{st},t) = \sum_{k=1}^{\infty} B_{ar,a(k)}(\theta_{st},t) + B_{ar,b(k)}(\theta_{st},t) + B_{ar,c(k)}(\theta_{st},t) \quad (3.82)$$

Where:

$$\begin{aligned} B_{ar(k)}(\theta_{st},t) &= \frac{3}{2} \cdot \hat{B}_{ar(k)} \cdot \cos\left(k \cdot \frac{2\cdot\pi\cdot\theta_{st}}{\lambda_1} - \omega_e \cdot t\right) \quad for \quad k = 1,4,7,... \\ B_{ar(k)}(\theta_{st},t) &= \frac{3}{2} \cdot \hat{B}_{ar(k)} \cdot \cos\left(k \cdot \frac{2\cdot\pi\cdot\theta_{st}}{\lambda_1} + \omega_e \cdot t\right) \quad for \quad k = 2,5,8,... \\ B_{ar(k)}(\theta_{st},t) &= 0 \quad for \quad k = 3,6,9,... \end{aligned} \quad (3.83)$$

Here p_λ is the number of pole pairs that fit within the wavelength λ_1.
The calculated space harmonics are presented as function of stator position. Seen by the stator all harmonic components change with speed ω_e[rad]. The magnets are positioned on the rotor. The rotor position angle θ[rad] moves with a fixed speed relative to the stator position angle. The speed ω_r[rad/s] at which the space harmonic components as function of time change, seen by the rotor, can be calculated according equations 3.84:

$$\omega_{r(k)} = \begin{cases} \left(\frac{p_\lambda}{k} - 1\right) \cdot \omega_e & for \quad k = 1,4,7,... \\ -\left(\frac{p_\lambda}{k} + 1\right) \cdot \omega_e & for \quad k = 2,5,8,... \end{cases} \quad (3.84)$$

For machines with a fractional pitch winding with a multiple of 9 coils around 9 teeth and 8 magnet poles:

First the change of flux in the air gap and magnets B_{ar}[T] due to armature reaction, will be considered for a generator with fractional pitch windings with 9 coils around 9 teeth and 8 magnet poles.

The peak flux density in the magnets $\hat{B}_{ar,magnet}$ [T], due to the armature reaction mmF of one phase has already been calculated in chapter 3.2.1.1 equation 3.53. The flux density was calculated only for the static position $\theta_{st} = 0$ rad. it follows:

$$B_{ar,a}(0) = \hat{B}_{ar,magnet}$$

Figure 3.16 presents the armature reaction component of the air gap and magnet flux density $B_{ar,a}$[T], as function of stator position.

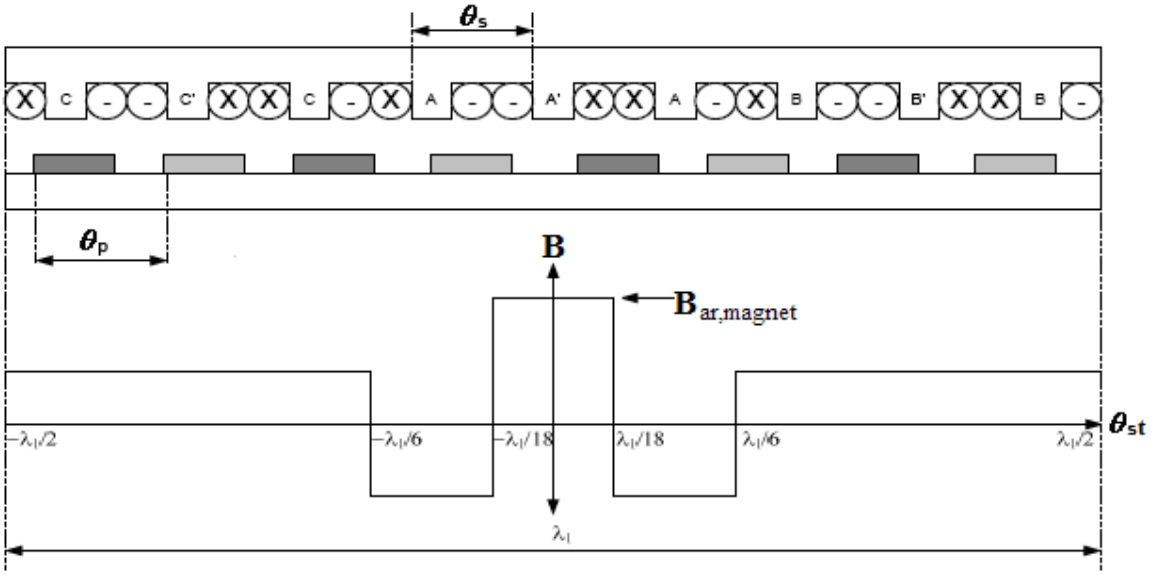

Figure 3.16: Armature reaction component of the flux density in the air gap and rotor magnets as function of stator position

For Fourier transformation the fundamental wave length λ_1[rad] becomes:

$$\lambda_1 = 9 \cdot \theta_s \cdot p$$
$$= 8 \cdot \pi$$

The number of pole pairs that fit within the fundamental waveform is:

$$p_\lambda = 4$$

The armature reaction component of the magnet flux density $B_{ar,a}$[T], as function of stator position, can be expressed according equation 3.85:

$$B_{ar,a} = \begin{cases} \hat{B}_{ar,magnet} & for \quad -\frac{\lambda_1}{18} < \theta_{st} < \frac{\lambda_1}{18} \\ -\frac{8}{10} \cdot \hat{B}_{ar,magnet} & for \quad -\frac{\lambda_1}{6} < \theta_{st} < -\frac{\lambda_1}{18} \\ & \quad \frac{\lambda_1}{18} < \theta_{st} < \frac{\lambda_1}{6} \\ \frac{1}{10} \cdot \hat{B}_{ar,magnet} & for \quad -\frac{\lambda_1}{2} < \theta_{st} < -\frac{\lambda_1}{6} \\ & \quad \frac{\lambda_1}{6} < \theta_{st} < \frac{\lambda_1}{2} \end{cases} \tag{3.85}$$

With use of equation 3.80 the magnitudes of the space harmonics become:

$$\hat{B}_{ar(k)} = \frac{9}{5 \cdot k \cdot \pi} \cdot \hat{B}_{ar,magnet} \cdot \left(2 \cdot \sin\left(\frac{k \cdot \pi}{9} \right) - \sin\left(\frac{k \cdot \pi}{3} \right) \right) \tag{3.86}$$

For machines with fractional pitch windings with a multiple of 3 coils around 3 teeth and 2 magnet poles:

The peak flux density in the magnets $\hat{B}_{ar,magnet}$, due to the armature reaction mmF in three phases has already been calculated in chapter 3.2.2.1. equation 3.74. The flux density was calculated only for the static position $\theta_{st} = 0$ rad. Because of a symmetric balanced three phase system, the flux density in the magnets due to armature reaction in one phase for the position $\theta_{st} = 0$ rad follows:

$$B_{ar,a}(0) = \frac{2}{3} \cdot \hat{B}_{ar,magnet}$$

Figure 3.17 will present the armature reaction component of the air gap and magnet flux density $B_{ar,a}$[T], as function of stator position:

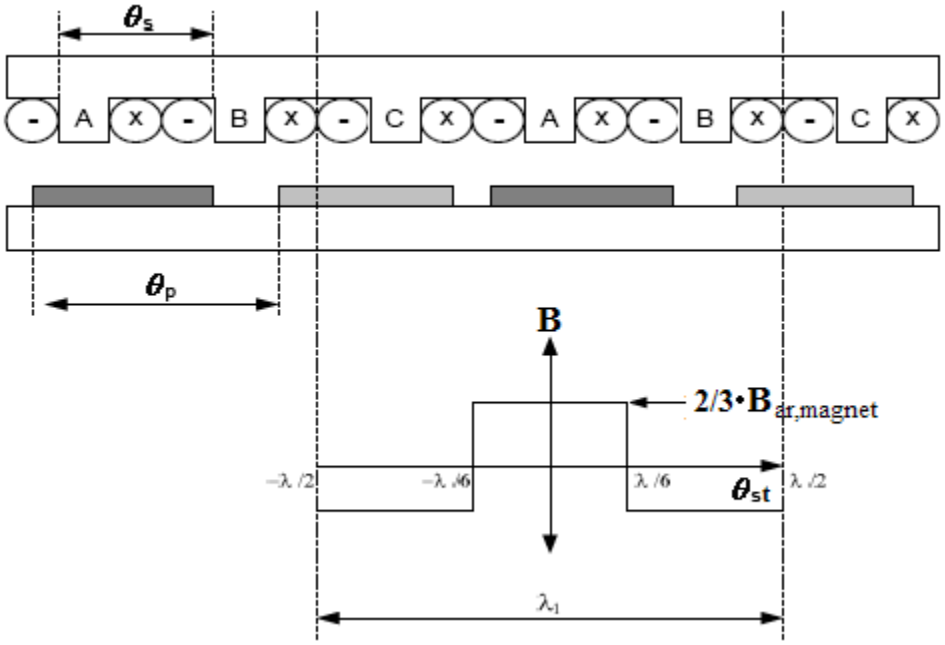

Figure 3.17: Armature reaction component of the flux density in the air gap and rotor magnets as function of stator position

For Fourier transformation the fundamental wave length λ_1[rad] becomes:

$$\begin{aligned} \lambda_1 &= 3 \cdot \theta_s \cdot p \\ &= 2 \cdot \pi \end{aligned}$$

The number of pole pitch angles that fit within the fundamental waveform is:

$$p_\lambda = 1$$

The armature reaction component of the magnet flux density $B_{ar,a}$[T], as function of stator position, can be expressed according equation 3.87:

$$B_{ar,a} = \begin{cases} \frac{2}{3} \cdot \hat{B}_{ar,magnet} & for \quad -\frac{\lambda_1}{6} < \theta_{st} < \frac{\lambda_1}{6} \\ -\frac{1}{3} \cdot \hat{B}_{ar,magnet} & for \quad -\frac{\lambda_1}{2} < \theta_{st} < -\frac{\lambda_1}{6} \\ & \quad \frac{\lambda_1}{6} < \theta_{st} < \frac{\lambda_1}{2} \end{cases} \qquad (3.87)$$

With use of equation 3.80 the magnitudes of the space harmonics become:

$$\hat{B}_{ar(k)} = \frac{2}{k \cdot \pi} \cdot \hat{B}_{ar,magnet} \cdot \sin\left(\frac{k \cdot \pi}{3}\right) \qquad (3.88)$$

3.2.4. Short circuit current effects

Fault conditions can cause high currents, which can demagnetize the permanent magnets. The generator should be designed in such way that no harm is inflicted to the permanent magnets during fault conditions. For this purpose the short circuit current has to be calculated. The following equation is an estimation of the peak short circuit current $\hat{i}_{scc}$ [A] [Nie 08]:

$$\hat{i}_{scc} = 2 \cdot \frac{\sqrt{2} \cdot E_{ph}}{\sqrt{R_{ph}{}^2 + (\omega_e \cdot L_s)^2}} \tag{3.89}$$

The factor 2 in this equation accounts for the peak value that can be reached by the current in the transient period just after short-circuit, assuming that the electric time constant $\tau_e = L_s/R_{ph}$ is sufficiently large to allow the current to double. Using the armature reaction model the effect of the armature reaction magnetic field on the permanent magnets $B_{ar,max}$[T], due to a short circuit current, can be estimated. This is done in equation 3.90 for a generator with a winding configuration with a multiple of 9 coils around 9 teeth and 8 magnet poles. Equation 3.91 calculates the effect for a generator configuration which is a multiple of 3 coils around 3 teeth and 2 magnet poles:

$$\begin{aligned} \overline{MMF_{scc}} &= \begin{bmatrix} -n_c \cdot I_{scc} & 2 \cdot n_c \cdot I_{scc} & -2 \cdot n_c \cdot I_{scc} & n_c \cdot I_{scc} & 0 & 0 & 0 & 0 \end{bmatrix}^T \\ \overline{\Phi_a} &= \mathbf{R^{-1}} \bullet \overline{MMF_{scc}} \\ B_{ar,\max} &= \frac{\phi_6 - \phi_7}{\tau_s \cdot l_{stk}} \end{aligned} \tag{3.90}$$

$$\begin{aligned} \overline{MMF_{scc}} &= \begin{bmatrix} -n_c \cdot I_{scc} & n_c \cdot I_{scc} & 0 & 0 \end{bmatrix}^T \\ \overline{\Phi_a} &= \mathbf{R^{-1}} \bullet \overline{MMF_{scc}} \\ B_{ar,\max} &= \frac{\phi_3 - \phi_4}{\tau_s \cdot l_{stk}} \end{aligned} \tag{3.91}$$

The Permanent magnets in a generator design are safe, if equation 3.92 holds:

$$B_m - B_{ar,\max} > B_{m,\min} \tag{3.92}$$

3.3. The generator as starter motor

The generator integrated in the HPRE with the combustion engine must also have the ability to start the combustion engine. The generator has to work as a starter motor. The required peak starting torque T_{start}[Nm] to get the generator into motion is much higher as the nominal generator torque T_{nom}[Nm]. High starting currents will flow, which produce a large magnetic field in the stator. The stator iron will saturate and the reluctance of the stator teeth and stator yoke will increase non-linear. This influences the produced torque and even higher currents are needed to produce the same torque compared to a machine without saturation.

The model described in this chapter approximates the generated torque T_{gen}[Nm] as function of start current I_{start}[A]. If the generated torque is calculated in a machine where saturation doesn't play a role, the torque increases linear with the increase of current:

$$I_{start,nosat} = \frac{T_{gen}}{T_{nom}} \cdot I_{ph} \tag{3.93}$$

If saturation does play a role and a current I_{start}[A] is applied at the machine, then the generated torque T_{gen}[Nm] can be calculated using a derivation of the magnetic term of the Lorentz force equation, into the law of force. This derivation is found in appendix 2. Here the force F[N] is calculated on a current I[A] carrying wire of length l[m], where perpendicular a magnetic field with flux density B[T] is applied. The law of force is independent of the magnetic field produced by the current.

$$F = B \cdot I \cdot l \tag{A.2.15}$$

In a slotted machine design, as is applied in this thesis, the conductors however are laid in the slots, and the magnet flux goes through the teeth, not through the conductors themselves. This makes it uncertain if the force law is valid. Still the force law is a widespread and accepted law used for machine designing. It is used in this thesis because it gives the same results as deriving the Torque from faraday's law and the law of conservation of energy. This will be done in chapter 3.5. Therefore the force law will be used to calculate the generated starting force F_{gen}[N] and starting torque T_{gen}[Nm] under the following assumption:

- The conductors are presented in the machines air gap.

$$\begin{aligned} F_{gen} &= N_s \cdot 2 \cdot n_c \cdot k_w \cdot \frac{\hat{B}_{g(1)}}{\sqrt{2}} \cdot l_{stk} \cdot I_{start} \\ T_{gen} &= N_s \cdot \sqrt{2} \cdot n_c \cdot k_w \cdot \hat{B}_{g(1)} \cdot l_{stk} \cdot r_{ro} \cdot I_{start} \end{aligned} \tag{3.94}$$

Because there is no phase angle assumed between voltage and current when starting the machine, the PM magnetic field and the armature reaction magnetic field are assumed π/2 radians out of phase when the generator starts to move. The flux density due to the total magnetic field in the stator teeth $B_{tooth,tot}$[T] and stator yoke $B_{sy,tot}$[T] can be calculated using the following equations:

$$B_{sy,tot}(t) = B_{sy}(t) + B_{ar,sy}(t) \quad (3.95)$$

$$B_{tooth,tot}(t) = B_{tooth}(t) + B_{ar,tooth}(t) \quad (3.96)$$

Due to high starting currents, and therefore high armature reaction flux densities, infinite high relative steel permeability can not be assumed, as can be done for normal operation. Therefore the relative steel permeability will be modeled as a function of the flux density $\mu_{r,steel}(B_{steel})$. This function is derived in appendix 4. Using an iterative process as in figure 3.18, the generated starting torque as function of starting current can be calculated.

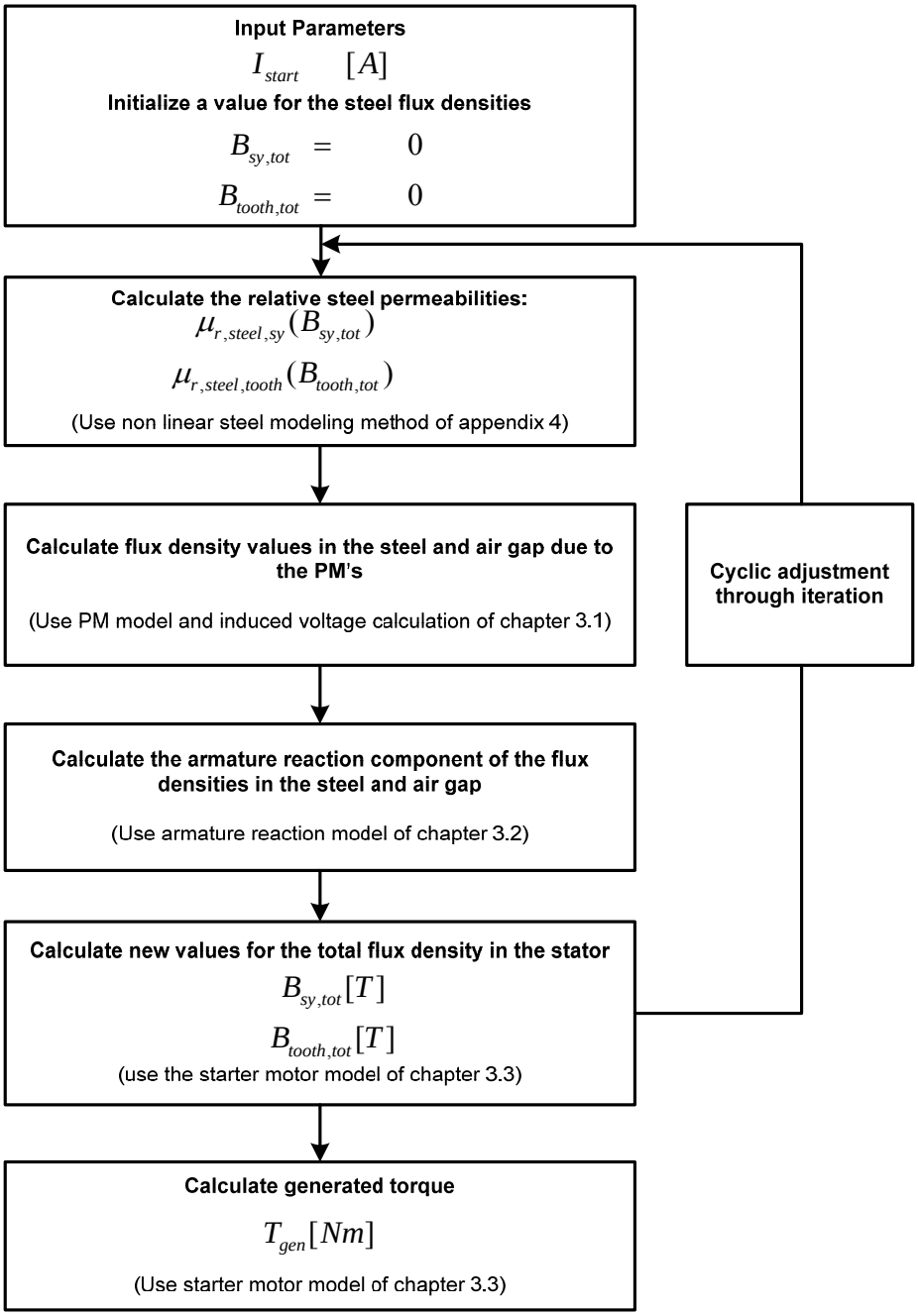

Figure 3.18: Iterative scheme for calculating the generated starting torque. Including saturation effects.

3.4. Generator loss modeling

In this thesis only the electric loss components are discussed. Mechanical losses are not considered since this thesis is concerned with the development of the generator for the prototype HPRE. Mechanical losses are dealt with by the engineers of the combustion engine and coupling interface, for the HPRE. When converting mechanical power into electrical power, there are two major loss components, the copper losses and the Eddy current and hysteresis losses. All losses are converted into heat. Figure 3.19 presents a flowchart with different loss components during the conversion.

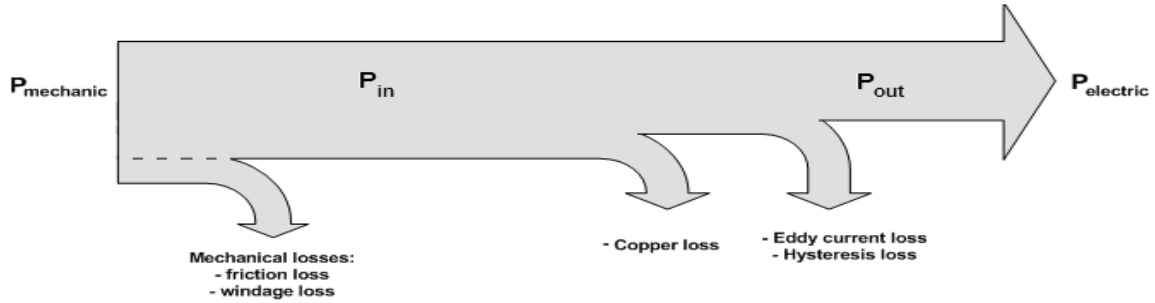

Figure 3.19: Power flowchart for a generator.

3.4.1 Copper losses

Copper losses are resistive losses due to the current in the copper windings of the machine. The total copper losses $P_{loss,cu}$[W] can be calculated using the following equation:

$$P_{loss,cu} = N_{ph} \cdot I_{ph}^{2} \cdot R_{ph} \tag{3.97}$$

3.4.2. Iron losses

The iron losses consist of two parts. Hysteresis losses and Eddy current losses. Hysteresis losses originate when magnetizing and demagnetizing the steel within the magnetic flux path. During the change of polarity the Weiss-domains in the steel have to turn over, during this process some energy is dissipated [Hoe 97]. Hysteresis losses are a function of frequency f_e[Hz] and flux density squared B[T]^2. The other loss component is the Eddy current loss. When a changing magnetic field is present in a conductive material, following ampere's law, a current is induced in that material. This current will flow in the direction such that it will create a magnetic field opposing it's origin of existence. In the generator the stator steel, rotor steel, magnets and copper conductors are conductive and Eddy currents could arise. Within the copper conductors no changing magnetic field is present, since all flux follows a contour path through the stator steel around the conductors. Hence the conductors are free of Eddy current losses. All other materials will induce Eddy currents. For the generator prototype designs laminated steel is used for the stator and rotor and also laminated magnets are used. With use of a laminated material, the Eddy current flow in that part can be disrupted, reducing the Eddy current losses. The Eddy current losses are a function of frequency, flux density and lamination thickness squared $(fB\Delta x)^2$.

The following equation [pol 98] is used to approximate the total iron losses $P_{loss,Fe}$[W] in the generator:

$$P_{loss,Fe} = 2 \cdot p_{Fe,spec} \cdot \left(\frac{\omega_e}{2\pi 500} \right)^{\frac{3}{2}} \cdot \left(m_{s,teeth} \cdot \left(\frac{B_{tooth,tot}}{1.3T} \right)^2 + m_{s,sy} \cdot \left(\frac{B_{sy,tot}}{1.3T} \right)^2 + m_{s,ry} \cdot \left(\frac{B_{ar,ry}}{1.3T} \right)^2 \right) \tag{3.98}$$

An empirical correction factor of 2 compensates for the higher specific losses $p_{Fe,spec.}$[W/kg] at the boundaries of the sheet steel and for the higher specific losses because of non-homogeneous fields within the steel. The rotor steel losses are due to flux variations of the armature reaction space harmonics, calculated in chapter 3.2.3. Because laminated steel is used for the rotor, rotor steel losses are not expected to be excessive. Therefore the rotor steel losses are approximated by incorporating them in equation 3.98, to calculate the total steel losses. Iron losses can be reduced by:

- Making the machine steel volume bigger, so the flux density in the steel will drop.
- Lower the number of magnet poles to lower the machine frequency.
- Use thinner laminations.

3.4.3. Magnet losses

Calculating the iron losses in the rotor magnets is a very difficult task. The change in magnetic field in the rotor back iron and in the magnets due to the armature reaction currents has already been described in chapter 3.2.3. In this chapter the losses in the magnets will be calculated. The Eddy current losses will be calculated for the different space harmonic components of the changing flux density in the magnets due to armature reaction.

First the Eddy current losses due to a changing magnetic flux density are approximated by considering Maxwell's second law [Pol 98], [Hoe 97], under the following set of assumptions:

- The effect of the Eddy currents on the magnetic field is negligible.
- The magnetic flux density in the magnets has only a radial flux component, which is not a function of the radius. In figure 3.20 this means the flux density has only a y-component which is not a function of y.
- The magnetic flux is considered constant over the magnet width τ_m[m] and in the direction of the machine axis. This means in figure 3.20, that the flux density is not a function of x and z.
- The changing magnetic field in the magnets changes purely sinusoidal.
- End effects are negligible. Therefore the electric field strength $\overline{E}$ [V/m] and current density $\overline{J}$ [A/m^2] only have a z-component. Considering end effects would increase the resistance and therefore decrease the losses. By neglecting end effects an overestimated approximation of the magnet losses is made.

Consider, as assumed, a purely sinusoidal flux density as function of time

$$B = \hat{B} \cdot \sin(\omega \cdot t)$$

Consider Maxwell's second law, derived from equation A.2.2. of appendix 2:

$$\oint_C \overline{E} \cdot dl \quad = \quad -\frac{d}{dt}\iint_S \overline{B} \cdot dA$$

Because the end effects are neglected, the contour is chosen such that the length of the contour in z-direction l_c[m] is larger than the width of the contour in x-direction. The width of the magnet τ_m[m] represents the contour in x-direction in figure 3.20 (a). To reduce Eddy currents, laminated magnets could be used. To apply a contour on a piece of a laminated magnet the length of the magnet lamination l_{ml}[m] now represents the contour in x-direction. As can be seen in figure 3.20 (b).

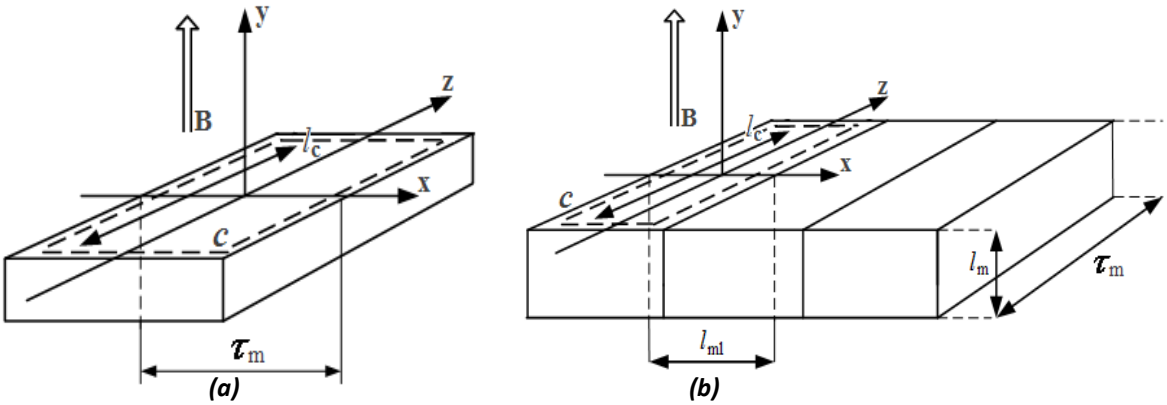

Figure 20: Magnet representation (a), laminated magnet (b)

There is only a z-component of the electric field strength. These can be calculated by deriving Maxwell's second law (equation A.2.2) to the following equation:

$$\begin{aligned} -l_c \cdot E_z(x) + l_c \cdot E_z(-x) = \quad & -l_c \cdot \frac{d}{dt}\int_{-x}^{x} B(t)dx \\ = \quad & -2 \cdot l_c \cdot x \cdot \frac{dB(t)}{dt} \\ = \quad & -2 \cdot l_c \cdot x \cdot \omega_e \cdot \hat{B} \cdot \cos(\omega \cdot t) \end{aligned} \tag{3.99}$$

Because the contour is applied in the middle of the magnet, due to symmetry the next equation is true:

$$-E_z(x) = \quad E_z(-x)$$

With use of the magnet resistivity ρ_m[Ω·m] the current density (in z-direction) in the magnet can be found using the following equations:

$$E_z(x) \quad = \quad \rho_m \cdot J_z(x) \tag{3.100}$$

$$J_z(x) = \frac{1}{\rho_m} \cdot x \cdot \omega \cdot \hat{B} \cdot \cos(\omega \cdot t) \tag{3.101}$$

Using the current density, a function can be made to express the magnet losses per unit of volume $p_{m,spec}$[W/kg] as a function of width x and time.

$$\begin{aligned} p_{m,spec}(x,t) &= \rho_m \cdot J_z{}^2(x) \\ &= \rho_m \cdot \left(\frac{1}{\rho_m} \cdot x \cdot \omega \cdot \hat{B} \cdot \cos(\omega \cdot t) \right)^2 \end{aligned} \tag{3.102}$$

By taking the average losses per unit of volume over one period of time T[s] the function can be expressed as only a function of the width x.

$$p_{m,spec}(x) = \frac{1}{2 \cdot \rho_m} \cdot \left(x \cdot \omega \cdot \hat{B} \right)^2 \tag{3.103}$$

The average magnet loss per unit of volume, in a magnet with width x, is now calculated using the following equations:

$$\begin{aligned} p_{m,spec} &= \frac{1}{x} \cdot \int_{-\frac{x}{2}}^{\frac{x}{2}} \frac{1}{2 \cdot \rho_m} \cdot \left(x \cdot \omega \cdot \hat{B} \right)^2 dx \\ &= \frac{1}{24 \cdot \rho_m} \cdot \left(x \cdot \omega \cdot \hat{B} \right)^2 \end{aligned} \tag{3.104}$$

Looking again at figure 3.20 (a) and figure 3.20 (b), the specific losses for magnets $p_{m,spec}$[W/ m^3] can be calculated by substitute the magnet width τ_m in x. And the specific losses for laminated magnets $p_{ml,spec}$[W/ m^3] can be calculated by substituting the magnet lamination length l_{ml}[m] into x.

$$\begin{aligned} p_{m,spec} &= \frac{1}{24 \cdot \rho_m} \cdot \left(\tau_m \cdot \omega \cdot \hat{B} \right)^2 \\ p_{ml,spec} &= \frac{1}{24 \cdot \rho_m} \cdot \left(l_{ml} \cdot \omega \cdot \hat{B} \right)^2 \end{aligned} \tag{3.105}$$

The specific losses in the magnets are due to many different armature reaction flux density space harmonic components, with their own frequency's. This is clear from chapter 3.2.3. The total specific losses due to all harmonic components of the armature flux density in the magnets $B_{s(k)}$ follow:

$$\begin{aligned} p_{m,spec} &= \sum_{k=1}^{\infty}\left(\frac{1}{24\cdot\rho_m}\cdot\left(\tau_m\cdot\omega_{r(k)}\cdot\hat{B}_{ar(k)}\right)^2\right) \\ p_{ml,spec} &= \sum_{k=1}^{\infty}\left(\frac{1}{24\cdot\rho_m}\cdot\left(l_{ml}\cdot\omega_{r(k)}\cdot\hat{B}_{ar(k)}\right)^2\right) \end{aligned} \qquad (3.106)$$

By calculating the total magnet volume V_m[m^3] with the use of appendix 1 and apply it in equation 3.107 the magnet losses can be calculated for normal surface magnets $P_{loss,m}$[W] and laminated surface magnets $P_{loss,ml}$[W].

$$\begin{aligned} P_{loss,m} &= V_m\cdot p_{m,spec} \\ P_{loss,ml} &= V_m\cdot p_{ml,spec} \end{aligned} \qquad (3.107)$$

3.5. Performance calculations

Phase angle calculation:
Now that phase inductances, current and voltages are calculated, the machine performance characteristics can be calculated using the following set of assumptions:

- A balanced three phase system.
- The current phasor I_{ph}[A] is kept in between the middle of the terminal phase voltage U_t[V] and the induced voltage E_{ph}[V], by means of active rectifiers. This means: $\psi = \phi = \frac{1}{2}\cdot\delta$ As is shown in figure 3.21
- Rectifier losses are neglected.

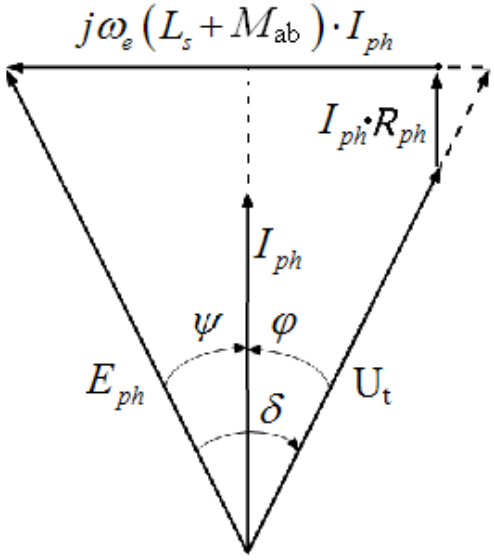

Figure 3.21: Electrical phasor representation of the generator.

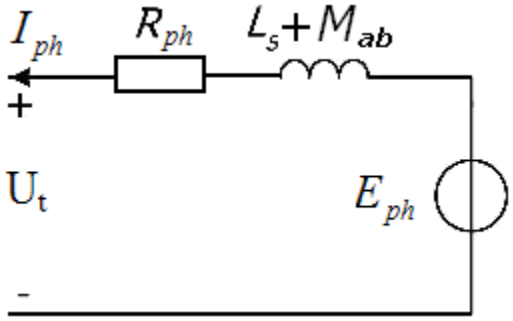

Figure 3.22: Electric circuit diagram of a Generator phase.

Figure 3.21 is a phasor diagram of the generator and figure 3.22 is an electric circuit representation of one phase of the generator. The phase angle φ[rad] between phase terminal voltage and phase current and the phase angle ψ[rad] between induced phase voltage E_{ph}[V] and current can be derived from figure 3.21, with use of the trigoniometric sine rule, while the voltage drop due to copper losses is neglected:

$$\frac{\omega_e \cdot (L_s + M_{ab}) \cdot I_{ph}}{\sin(\varphi - \psi)} = \frac{E_{ph}}{\sin\left(\frac{\pi + 2 \cdot \psi}{2}\right)}$$

$$\frac{\omega_e \cdot (L_s + M_{ab}) \cdot I_{ph}}{\sin(2 \cdot \varphi)} = \frac{E_{ph}}{\cos(\psi)}$$

$$\varphi = \frac{1}{2} \cdot \sin^{-1}\left(\frac{\omega_e \cdot (L_s + M_{ab}) \cdot I_{ph} \cdot \cos(\psi)}{E_{ph}}\right) \quad (3.108)$$

$$\psi = \varphi$$

Use the law of conservation of energy, which states: 'Energy can neither be created nor destroyed'. Applying this for the three phase generator, the following equation must hold during generator convention:

$$P_{out} + P_{loss,cu} = P_{in} - P_{loss,Fe} - P_{loss,ml} = 3 \cdot E_{ph} \cdot I_{ph} \cdot \cos\psi \quad (3.109)$$

Using equation 3.108 and equation 3.109 the equation for calculating the phase angle φ[rad] becomes:

$$\varphi = \frac{1}{2} \cdot \sin^{-1}\left(\frac{\omega_e \cdot (L_s + M_{ab}) \cdot (P_{in} - P_{loss,Fe} - P_{loss,ml})}{3 \cdot E^2_{ph}}\right) \quad (3.110)$$

Output voltage:
The RMS terminal voltage U_t[V] and the RMS terminal line-line voltage U_{ll}[V] can also be derived from figure 3.21:

$$U_t = E_{ph} - \frac{I_{ph} \cdot R_{ph}}{\cos\varphi} \quad (3.111)$$

$$U_{ll} = U_t \cdot \sqrt{3} \quad (3.112)$$

The terminal phase voltage u_a[V], u_b[V] and u_c[V] can be expressed as functions of time:

$$\begin{aligned} u_a(t) &= e_a - i_a \cdot R_{ph} - L_s \cdot \frac{di_a}{dt} \\ u_b(t) &= e_b - i_b \cdot R_{ph} - L_s \cdot \frac{di_b}{dt} \\ u_c(t) &= e_c - i_c \cdot R_{ph} - L_s \cdot \frac{di_c}{dt} \end{aligned} \quad (3.113)$$

When a lossless DC rectifier is applied the rectified DC voltage U_{dc}[V] can be calculated:

$$U_{dc} = U_{ll} \cdot \frac{3 \cdot \sqrt{2}}{\pi} \quad (3.114)$$

The electric output power P_{out}[W] produced by the machine is calculated using the following equations:

$$p_{out}(t) = u_a(t) \cdot i_a(t) + u_b(t) \cdot i_b(t) + u_c(t) \cdot i_c(t) \quad (3.115)$$

$$\begin{aligned} P_{out} &= \sqrt{\frac{1}{T_e} \cdot \int_0^{T_e} {p_{out}}^2(t) dt} \\ &= 3 \cdot U_t \cdot I_{ph} \cdot \cos\varphi \end{aligned} \quad (3.116)$$

Applied torque:
The torque present in the air gap $T_{air,gap}$[Nm] is the torque component responsible for the induced voltage and current in the generator. Using the law of conservation of energy, the air gap Torque can be calculated.

$$\begin{aligned} T_{air,gap} &= \frac{P_{in} - P_{loss,Fe} - P_{loss,m}}{\omega_m} \\ &= \frac{3 \cdot E_{ph} \cdot I_{ph}}{\omega_m} \\ &= 3 \cdot \sqrt{2} \cdot n_c \cdot k_w \cdot \hat{B}_{g(1)} \cdot l_{stk} \cdot r_{ro} \cdot \frac{N_s}{N_{ph}} \cdot I_{ph} \cdot \cos\varphi \end{aligned} \quad (3.117)$$

With some modification this equation can also be used to calculate the generated output torque T_{gen}[Nm] when using the generator as starting machine. To do so keep the following considerations into mind:

- When the generator is used as starting machine it is used as a motor, therefore the power flow is opposite to the power flow in generator convention.
- When starting the rotational speed ω_m[rad/s] is zero and therefore the iron and magnet losses are assumed zero.
- The electrical speed ω_e is very low and therefore it is assumed that $\cos\varphi=1$.

Applying the law of conservation of energy for motor convention:

$$P_{in} = P_{out} + P_{loss,cu} + P_{loss,Fe} + P_{loss,m} = 3 \cdot U_t \cdot I_{ph} \cdot \cos\varphi \tag{3.118}$$

Then the generated output Torque T_{gen}[Nm] when starting the machine is calculated:

$$\begin{aligned} T_{gen} &= \frac{P_{out}}{\omega_m} \\ &= \frac{P_{in} - P_{cu}}{\omega_m} \\ &= \frac{3 \cdot U_t \cdot I_{start} - I^2{}_{start} \cdot R_{ph}}{\omega_m} \\ &= \frac{3 \cdot (E_{ph} + I_{start} \cdot R_{ph}) \cdot I_{start} - I^2{}_{start} \cdot R_{ph}}{\omega_m} \\ &= \frac{3 \cdot E_{ph} \cdot I_{start}}{\omega_m} \\ &= 3 \cdot \sqrt{2} \cdot n_c \cdot k_w \cdot \hat{B}_{g(1)} \cdot l_{stk} \cdot r_{ro} \cdot \frac{N_s}{3} \cdot I_{start} \end{aligned} \tag{3.119}$$

This is the same equation as derived using the Lorentz force law in chapter 3.3. It proofs that the Lorentz force law is useful for force calculations in slotted electrical machines.

Efficiency:
Using the output power and the loss components the machine efficiency η[%] is calculated, while generator conventions are applied.:

$$\eta = \frac{P_{out}}{P_{out} + P_{loss,cu} + P_{loss,Fe} + P_{loss,ml}} \times 100\% \tag{3.120}$$

Chapter 4: Generator geometrics optimizing routine

This chapter first describes the optimizing routine, used for finding an optimal generator design. Then the generator designs for the prototype HPRE, developed using the optimizing routine and analytical models, are presented.

4.1. Optimizing routine description

With the use of the analytical models of chapter 3 an optimal design has to be found. For that purpose a generator geometric optimizing routine program is made, using the Matlab 7.5 computer software. Designing starts by fixing some of the parameters and use them as input for the optimizing routine. The fixed parameters for the HPRE generator concern the geometric constraints, parameters describing the electrical output requirements and the given mechanical input parameters.

Generator geometric constraints:

Rotor inner radius:	r_{ri}	=	0.1125	[m]
Stator outer radius:	r_{so}	=	0.19	[m]

Generator given mechanical input parameters:

Rotational speed:	n_m	=	3000	[RPM]
Starting torque:	T_{start}	=	220	[Nm]
Operating temperature:	T_{emp}	=	120	[°C]

Generator required electrical output parameters:

Output power:	P_{out}	=	$35 \cdot 10^3$	[W]
Rectified DC output voltage:	U_{dc}	=	600	[V]
Number of phases:	N_{ph}	=	3	
Nominal current density:	J_{nom}	=	$7 \cdot 10^6$	[A/m^2]

When designing a generator the current density J_{nom}[A/m^2] in the copper windings of the machine is an important design consideration. Higher current densities ensure the use of less copper and therefore a smaller machine design. The drawback is the quadratic increase in copper losses when the current density is increased. Losses have to be minimized; otherwise excessive heating of the generator will occur. The choice of the nominal current density is a thermal problem. It is beyond the scope of this thesis to generate a thermal model. Instead a current density is chosen according the work of Miller [Mil 94], where a current density table is set up for different applications. For the prototype HPRE generator a current density of J_{nom} = 7 A/mm^2 is chosen. This is a safe choice for generators with forced liquid cooling. The thermal behavior within the generator can be adjusted by adjusting the flow of the liquid cooling.

The used materials for designing the generator are presented in appendix 7. The material properties are also used as input for the optimizing routine. The magnet fraction α_m is chosen 5/6, which means 5/6 of a pole pitch is covered with magnet. Further increase of the magnet fraction leads to excessive flux leakage.

Magnet material properties:

Magnet type:			N38UH		
Magnet fraction:	α_m	=	5/6		
Remanent flux density:	$B_{r(20°)}$	=	1.24	[T]	
Coercive field strength:	H_c	=	940000	[A/m]	
Temperature coefficient:	$T_{k,Br}$	=	-0.11	[%/°C]	
Magnet resistivity:	ρ_m	=	$1.3 \cdot 10^{-6}$	[Ω.m]	
Magnet mass density:	ρ_{magnet}	=	7350	[kg/m^3]	
Min. allowed flux density:	$B_{m,min}$	=	0.0	[T]	
Cost price per kg. weight:	C_{magnet}	=	60	[€/kg]	

Copper conductor properties:

Copper resistivity:	$\rho_{cu(20°)}$	=	$1.72 \cdot 10^{-8}$	[Ω.m]	
Copper mass density:	ρ_{copper}	=	8900	[kg/m^3]	
Temperature coefficient:	k_{cu}	=	0.0043	[/°C]	
Slot fill factor:	k_{fill}	=	0.4		
Cost price per kg. weight:	C_{copper}	=	15	[€/kg]	

Magnetic sheet steel properties:

Steel mass density:	ρ_{steel}	=	7650	[kg/m^3]	
Specific iron loss:	$p_{Fe,spec}$	=	43.35	[W/kg]	@500Hz,1.3T
Stacking factor:	k_{stk}	=	0.95		
Cost price per kg weight:	C_{steel}	=	3	[€/kg]	

Generator geometric optimizing routine:

Part of the remaining parameters is found by cyclic adjustment through an iterative process, another part of the optimal machine parameters is found by varying them over a range and searching the optimal values according to the given design criteria.
Choosing the right search range for the variables is essential for finding the optimal design. The optimizing program ranges the following parameters:

Number of magnets:	N_m	range:		
Magnet length:	l_m	range:		[m]
Stator outer radius:	r_{so}	range:		[m]
Air gap length:	g	range:		[m]
Max. PM no load flux density:	B_{max}	range:		[T]
Consider tooth shoes:		range:	yes – no	

The minimum allowed magnet length l_m range is set at 0.005 m. For a prototype it is not recommended by the machine manufacturer to design thinner magnets.

The minimum allowed air gap range g is set at 0.001 m. A smaller air gap can lead to problems when building a prototype, since the actual air gap length will decrease due to glue between magnets and rotor surface, and due to bandaging of the rotor, to keep the magnets attached to the rotor.

The maximum flux density in the steel during no load conditions B_{max} is given a range beneath the saturation limit of the steel. The total magnetic field in the machine depends on electric loading and can reach a higher value.

When the input parameters, material properties and variable parameter ranges are known, the program can start to calculate every possible design to find the optimal design geometrics according the given design criteria. The flowchart in figure 4.1 schematically presents the optimizing routine for calculating an optimal design.

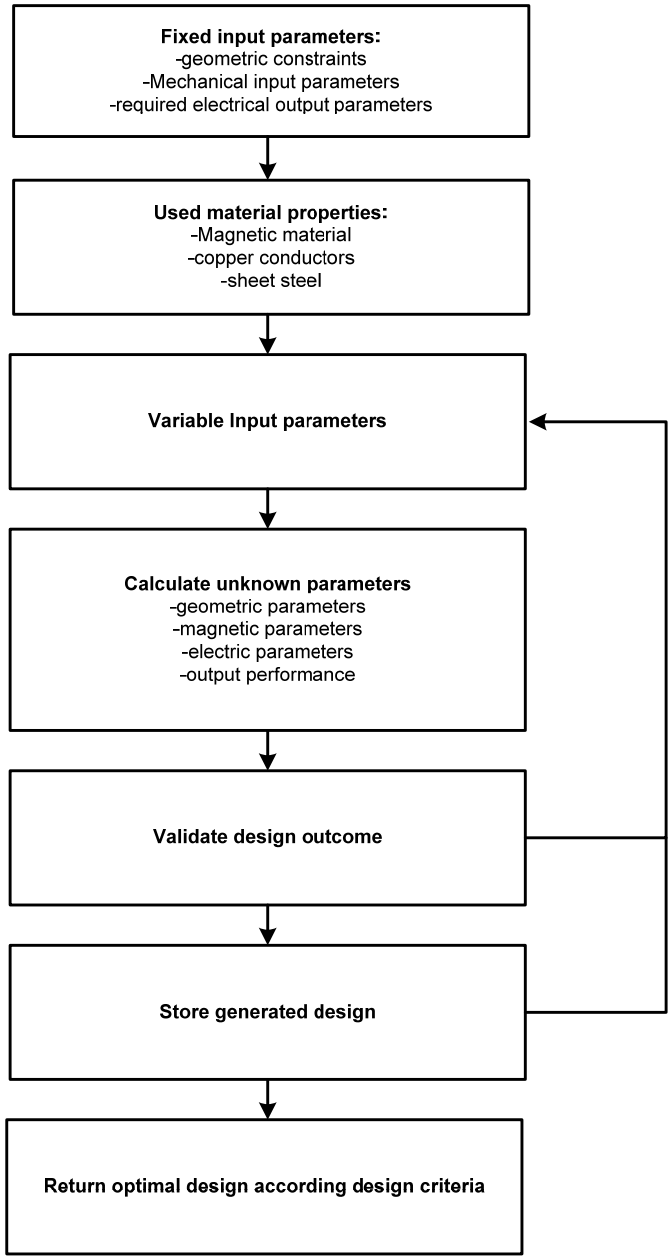

Figure 4.1: Flowchart of optimizing routine.

Calculation of the unknown parameters during the optimizing process presented in figure 4.1 is done by using the analytical models of chapter 3 and the geometric equations of appendix 1. They are used in an iterative process. This iterative process for calculation of the unknown parameters is schematically presented in figure 4.2.

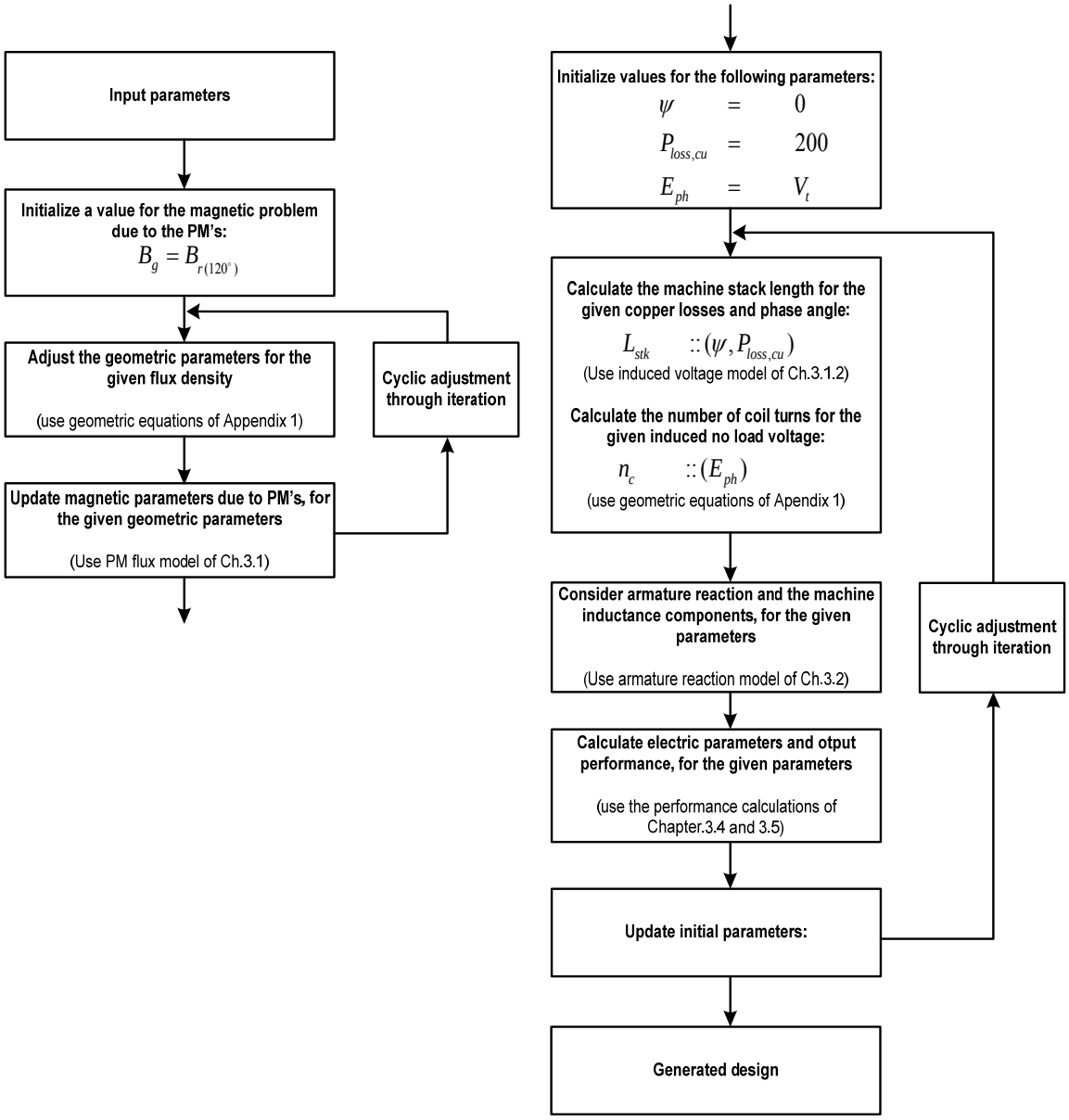

Figure 4.2: Flowchart of the iterative process for calculating unknown machine parameters.

All generated designs will be validated according a set of validation rules. Only designs that meet the requirements are stored in a database. From this database the optimal generator design, according the design criteria, is found. The validation rules are listed and explained below:

- $B_m - \hat{B}_{ar,\max} > B_{m,\min}$ (3.54)
  According equation 3.54 this expression must be true, in order to avoid the risk of demagnetization.

- The angle δ[rad] between the terminal voltage U_t[V] and induced voltage E_{ph}[V] must not exceed π/2 rad. in order to have an efficient design. Therefore the self inductance L_s[H] must not exceed:

$$L_{\max} = \sqrt{2} \cdot \frac{E_{ph}}{\omega_e \cdot I_{ph}} \quad (4.1)$$

An increase of inductance causes a decrease of the cosφ, this is not beneficial for the machine efficiency. Because deviations can occur between the calculated inductance and the real inductance and because the negative effect on efficiency the limit for the self inductance is set according:

$$L_s < L_{\max}$$
$$L_{\max} = 0.8 \cdot \frac{E_{ph}}{\omega_e \cdot I_{ph}} \quad (4.2)$$

- $\hat{B}_{sy,tot} < 1.8T$
  $\hat{B}_{tooth,tot} < 1.8T$

  Higher flux density values, during normal operations, provide heavily saturated stator steel. This affects the machines starting behavior.

- A limit for the machine length in axial direction l_{stk}[m] is included:

  $l_{stk} > 0.0045\,m$

  A longer machine axial stack length, means less coil turns for inducing the same voltage, and a larger air gap area is created. Therefore the armature reaction flux densities can be expected smaller. Since designs with a smaller stack length are theoretically possible, this is a safety measure. It is included because of neglected end effects and possible deviations of the calculated armature reaction magnetic fields, from the real armature reaction magnetic fields.

- To meet the third design criterion, a limit to minimum allowed efficiency is also given:

  $\eta > 90\%$

4.2 Generator designs for the prototype high power range extender

Using the optimizing routine the optimal geometric dimensions for a generator design, with a fractional pitch winding configuration with a multiple of 9 coils around 9 teeth and 8 magnet poles and surface mounted magnets on the rotor, are found. The geometric dimensions of the generator are the dimensions of lowest cost price. Since cost usually decreases with a decrease in mass, the generator of lowest cost turned out to be also the one of lowest mass.

The optimal geometric dimensions were altered a bit to make a generator design suitable for manufacturing. The rotor yoke outer radius r_{ro}[m] had been increased by 2 mm. In this way the rotor is a bit larger, but this made it possible to also design an IMPM rotor with V-shape magnets, of the same size. The SMPM and IMPM rotors can be exchanged and used, for testing purposes, with the same generator. More about the IMPM rotor design can be found in appendix 5. Also a second generator was designed, which has a fractional pitch winding with a multiple of 3 coils around 3 teeth and 2 magnet poles. This generator was designed in a way, that it has the same stator outer radius r_{so}[m], stator inner radius r_{si}[m] axial stack length l_{stk}[m] and number of rotor magnet poles as the first optimized generator. This makes it possible to exchange the different rotors to test them in both generators. The different exchangeable stators and rotors provide a number of different design variations. The best design variation can be determined during the test phase of the prototype HPRE.

The generator with a slot pole combination which is a multiple of 9 coils around 9 teeth with 8 poles is optimal for a stator with 36 teeth and a rotor with 32 poles. Therefore the generator with a slot pole combination which is a multiple of 3 coils around 3 teeth with 2 poles had to be designed for a 32 pole rotor. Therefore the stator of this generator must have 48 teeth. The generator design dimensions for a generator with a 36 teeth stator and for a generator with a 48 teeth stator are presented in table 4.1. Figure 4.3 and 4.4 presents a linearized sketch of a quarter of the generator, for the two different generator designs with the SMPM rotor design. The definite design drawings, including the stator outer house with forced liquid cooling, the rotor inner bus and the winding drawings can be found in appendix 6.

The two generator designs and the different rotors are in production and are expected in Oktober 2010.

Parameter	unit	Description	36 teeth stator	48 teeth stator
Stator steel dimensions				
θs	rad	Slot angle		
τ_s	m	Slot pitch		
A_s	m^2	Slot area		
d_1	m	Stator tooth shoe top length		
d_2	m	Stator tooth shoe bottom length		
d_3	m	Stator teeth length without shoe tooth		
l_{stk}	m	stator length in axial direction		
Ns		Number of slots	36	48
r_{sb}	m	Stator yoke inner radius		
r_{si}	m	Stator inner radius		
r_{so}	m	Stator outer radius		
w_s	m	Slot opening width		
w_{sb}	m	Slot width at slot bottom		
w_{si}	m	Slot width beneath the tooth shoe		
w_{sy}	m	Stator yoke width		
w_t	m	Tooth width at tooth shoe		
w_{tb}	m	Tooth width at tooth bottom		
w_{ti}	m	Tooth width beneath tooth shoe		
$V_{s,sy}$	m^3	Volume of steel used in the stator yoke	$3.47 \cdot 10^{-4}$	$3.47 \cdot 10^{-4}$
$V_{s,teeth}$	m^3	Volume of steel used in the stator teeth	$6.46 \cdot 10^{-4}$	$6.11 \cdot 10^{-4}$
$m_{s,teeth}$	kg	Mass of steel used in the stator teeth	4.94	4.68
$m_{s,sy}$	kg	Mass of steel used in the stator yoke	2.66	2.66
p_s	€	Price of steel used in the stator	22.78	22.00
Copper winding dimensions				
A_{cu}	m^2	Area of copper conductor		
J_{nom}	A/m^2	Nominal current density in the copper		
k_{fill}		Slot fill factor		
n_c		Number of coil turns around a tooth		
r_{cu}	m	Radius of copper conductor		
V_{cu}	m^3	Volume of used copper in the windings	$3.49 \cdot 10^{-4}$	$3.48 \cdot 10^{-4}$
m_{cu}	kg	Mass of used copper in windings	3.10	3.10
p_{cu}	€	Price of used copper in the windings	46.52	46.50
Coil winding configuration				
k_d		Coil distribution factor	0.960	1
k_p		Slot pitch factor	0.985	0.866
k_w		Winding factor	0.945	0.866

Table 4.1: Generator geometric dimensions and parameters, for the two developed generator designs.

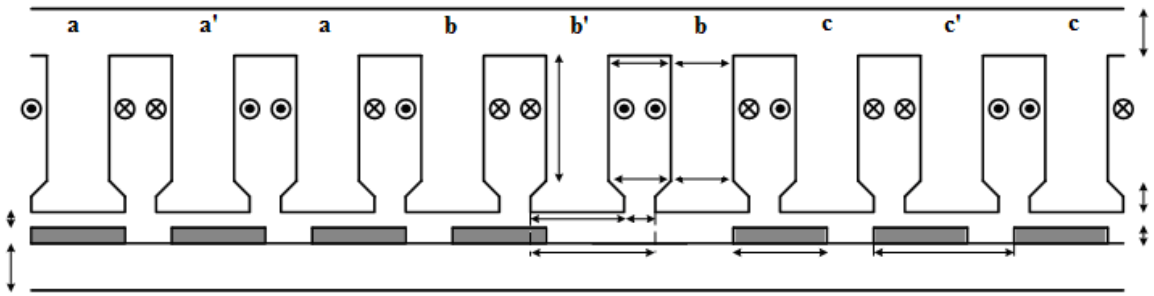

Figure 4.3: Generator design with a concentrated coil fractional pitch winding configuration with 36 slots and 32 magnet poles.

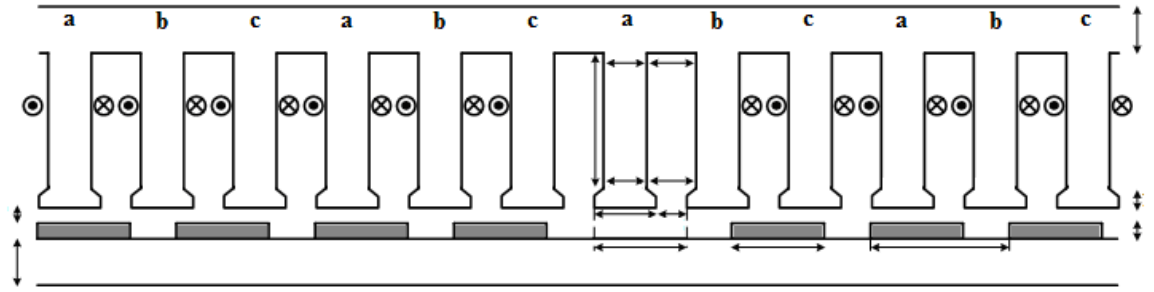

Figure 4.4: Generator design with a concentrated coil fractional pitch winding configuration with 48 slots and 32 magnet poles.

The rotor design dimensions for the rotor with surface mounted magnets and for the rotor with V-shape inset magnets are given in Table 4.2. Figure 4.5 presents a pole of an IMPM rotor with V-shape magnets

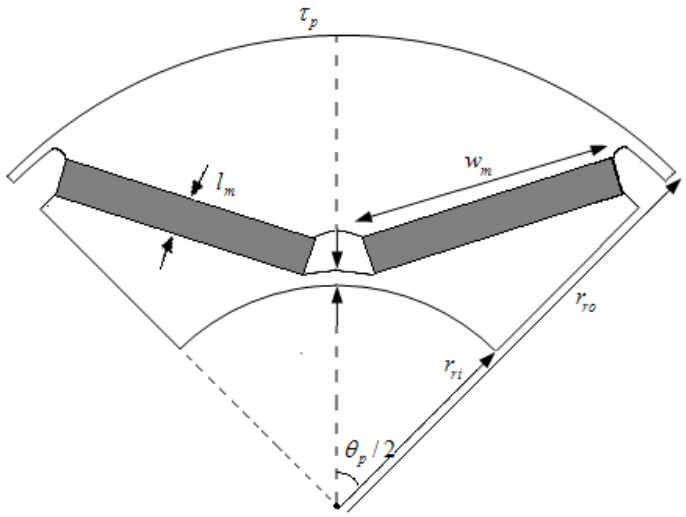

Figure 4.5: IMPM rotor design with V-shape inset magnets.

Parameter	unit	Description	SMPM rotor	IMPM rotor
Rotor steel dimensions				
θ_p	rad	Pole angle		
τ_p	m	Pole pitch		
l_{stk}	m	Rotor length in axial direction		
N_m		Number of poles	32	32
r_{rb}	m	Rotor steel outer radius		
r_{ri}	m	Rotor inner radius		
r_{ro}	m	Rotor outer radius		
w_{ry}	m	Rotor yoke width		
$V_{s,ry}$	m^3	Volume of steel used in the rotor yoke	$2.73 \cdot 10^{-4}$	$2.73 \cdot 10^{-4}$
$m_{s,ry}$	kg	Mass of steel used in rotor yoke	2.09	2.09
$p_{s,ry}$	€	Price of steel used in rotor yoke	6.26	6.26
Magnet dimensions				
α_c		Flux concentrating factor		
α_m		Magnet fraction	5/6	-
θ_m	rad	Magnet angle		
τ_m	m	Magnet pitch		
l_m	m	Magnet length in the flux flow direction		
l_{stk}	m	Magnet length in axial direction		
w_m	m	Magnet width		
V_m	m^3	Volume of used magnets	$1.53 \cdot 10^{-4}$	$1.12 \cdot 10^{-4}$
m_m	kg	Mass of used magnets	1.12	0.82
p_m	€	Price of used magnets	67.41	49.39

Table 4.2: Rotor geometric dimensions and parameters for the two developed rotor designs.

Chapter 5: Modeling a generator using FEM

The purpose of modeling with a finite element method (FEM), in this thesis, is to verify the analytical model. A FEM model is easily made more accurate than an analytical model, but the drawback is the execution time of the calculations, which is much longer. Therefore FEM modeling is less suitable for machine geometric optimizing routines. However it is suitable to verify an analytical model with the purpose of improving the model. Furthermore FEM analysis of electrical machines provides a better insight and understanding of the electric and magnetic fields in that electric machine.

The FEM models in this thesis are made with the Comsol 3.5a computer software. This is a finite element analysis program suitable for modeling electric machines. The modeling of electric machines with the program is done by executing the following steps [CM 08a]

Geometry modeling:
First a model is drawn in 2D or 3D. When a model is symmetric in one direction, or axial symmetric, a 2D model is easier to generate and calculations on 2D models save a lot of computing time.

Subdomain settings:
After drawing the models geometry the properties, material coefficients and excitation sources must be applied to the different sub domains within the model. Non-linear properties are modeled using functions or linearized look up tables.

Boundary conditions:
The boundary conditions for electromagnetics between two domains are specified according to Maxwell's boundary conditions (Appendix 2). Specific boundary conditions for the model can be introduced. This is useful when only a segment of an electric machine is modeled but also when a moving boundary is introduced, such as the air gap within an electric machine.

Mesh generation:
The program must mesh the geometry before it can solve the finite element problem. The accuracy of the results is mainly based on the correct discretization (mesh) of the considered regions.

Computing the solution:
Solving the electromagnetic problem is done by means of iterative processes. Settings to limit the rate of convergence and the number of iterations can be applied to make a trade off between computing time and accuracy.

5.1. Permanent magnet flux model in FEM

The PM flux model is modeled in FEM to validate the calculated parameters from the analytical PM flux model, for the developed generator designs. Also the analytical calculated no load phase voltage $e_a(t)$, $e_b(t)$ and $e_c(t)$ can be verified. With use of the calculated machine geometrics (chapter 4.2) a model is drawn in 2D in an x,y-reference plane. Symmetry in the third dimension (in the z or axial direction) is assumed and end effects are neglected. The copper windings are modeled as a single rectangular conductor in the slot and no external current is applied. The windings are assumed to have the same magnetic properties as the surrounding air and the conductivity σ[S/m] is set to zero, to simulate a no load situation. The magnetic field is modeled according to Maxwell's constitutive relations,

$$\begin{aligned} \overline{B} &= \mu \cdot \overline{H} \\ \sigma_{air} &= o \\ \sigma_{copper} &= \sigma_{air} \end{aligned}$$

The magnetic field strength H[A/m] in the steel is modeled as a function of flux density B[T]. The function is made according a linearized lookup table made from the B-H steel characteristic (appendix 4). Modeling the Eddy currents with the use of FEM, in the steel regions of the generator, is beyond the scoop of this thesis and is therefore neglected. Therefore the conductivity of the steel σ_{steel}[S/m] can be made zero.

$$\begin{aligned} \overline{H} &= f\left(\overline{B}\right) \\ \sigma_{steel} &= 0 \end{aligned}$$

The magnets are modeled as excitation sources according to Maxwell's constitutive relations. The Eddy currents in the magnets are also neglected:

$$\begin{aligned} \overline{B} &= \mu_0 \cdot \mu_{rec} \cdot \overline{H} + \overline{B_r} \\ \sigma_{magnet} &= 0 \end{aligned}$$

The remanent flux density vector $\overline{B_r}$ gives direction to the magnetic field of the excitation sources. For PM's with a radial outward magnetization this vector in an x,y-reference plane becomes [CM 08b]:

$$\begin{bmatrix} B_{r,x} \\ B_{r,y} \end{bmatrix} = \begin{bmatrix} B_{r(120)} \cdot \dfrac{x}{\sqrt{x^2 + y^2}} \\ B_{r(120)} \cdot \dfrac{y}{\sqrt{x^2 + y^2}} \end{bmatrix} \qquad (5.1)$$

For radial inward magnetized PM's the remanent flux density vector $\overline{B_r}$ in an x,y- reference plain becomes [CM 08b]:

$$\begin{bmatrix} B_{r,x} \\ B_{r,y} \end{bmatrix} = \begin{bmatrix} -B_{r(120)} \cdot \dfrac{x}{\sqrt{x^2+y^2}} \\ -B_{r(120)} \cdot \dfrac{y}{\sqrt{x^2+y^2}} \end{bmatrix} \tag{5.2}$$

The boundary conditions are left unaffected and are according to Maxwell's boundary conditions (appendix 2), because the whole generator circumference is modeled. The rotor displacement as function of time is modeled by giving the rotor sub domain regions a prescribed displacement in the x and y directions as a function of time t[s]. The displacement is dependant of the given rotational speed n_m[rpm] [CM 08b]:

$$\begin{aligned} \frac{dx}{dt} &= \cos(2\cdot\pi\cdot\frac{n_m}{60}\cdot t)\cdot x - \sin(2\cdot\pi\cdot\frac{n_m}{60}\cdot t)\cdot y - x \\ \frac{dy}{dt} &= \sin(2\cdot\pi\cdot\frac{n_m}{60}\cdot t)\cdot x + \cos(2\cdot\pi\cdot\frac{n_m}{60}\cdot t)\cdot y - y \end{aligned} \tag{5.3}$$

Figure 5.1(a) shows a piece of the drawn and meshed model for the smpm generator with 36 teeth. The discretization in the air gap is much finer because this is the area of most interest, therefore an increased accuracy is necessary.

The electromagnetic problem is solved for one electric time period T_e[s] on 25 intervals. The accuracy of solving the magnetic vector potential A_z using an iterative process is set to $1\cdot10^{-3}$. Figure 5.1(b) shows the solution of the magnetic field problem. The flux density B[T], which is related to the magnetic vector potential, is shown for different regions of the machine. Also a contour plot is plotted in figure 5.1(b) to show the direction of the magnetic field. From this figure the flux density in the stator teeth as function of rotor position can also be determined.

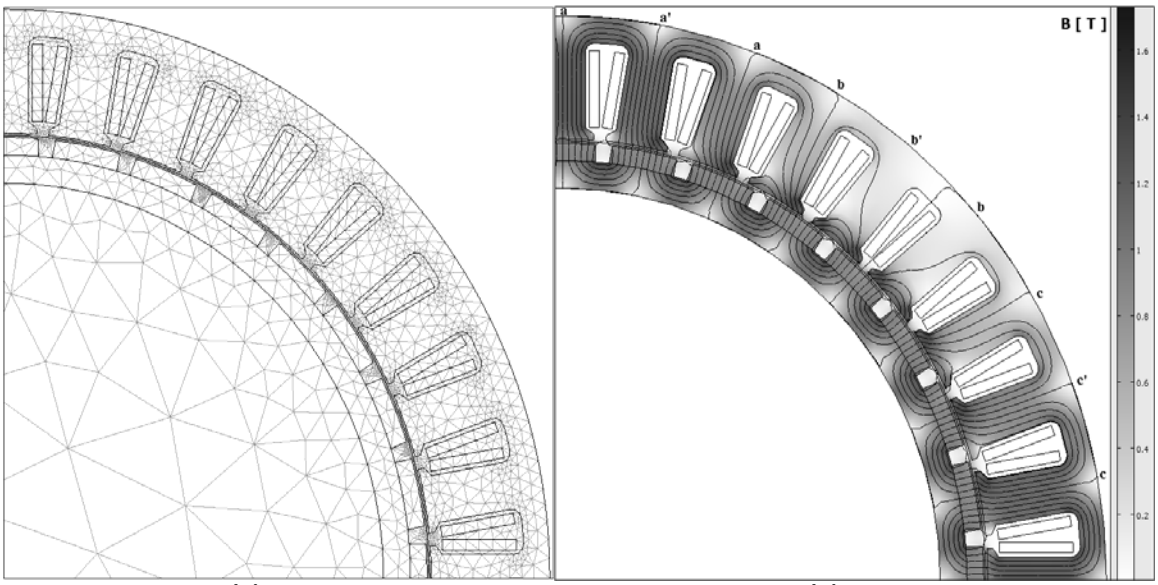

(a) *(b)*

Figure 5.1: Model of the 36 teeth generator design (a). Computational results of the flux density (b)

The voltage induced in the coils can be calculated from the electric field $\overline{E}$ [V/m] solution and deriving Faraday's law. Since the electric field is zero in the x and y directions no voltage is induced in the end windings. The voltage induced in a conductor V_c[V] of length l_{stk}[m] in the z direction is given by equation:

$$\begin{aligned} V_c &= \oint_c \overline{E} \cdot \bar{\tau} ds \\ &= E_z \cdot l_{stk} \end{aligned} \tag{5.4}$$

However the electric field in the conductors near the bottom of the slot could deviate from the electric field in the conductors near the tooth shoe. In order to not have to model every conductor separately one single conductor is modeled, spanning a great area A_{rect}[m^2] of the slot, where normally the conductors are placed. The electric field induced in a random conductor placed in the slot is therefore the average of the electric field induced in the rectangular area. The induced voltage in all conductors $V_{c,tot}$[V] of one coil, placed in a slot, is then calculated using the following equation:

$$V_{c,tot} = n_c \cdot \frac{l_{stk}}{A_{rect}} \cdot \int E_z \cdot dA_{rect} \tag{5.5}$$

The phase voltages $e_a(t)$, $e_b(t)$ and $e_c(t)$ can be calculated by taking the sum of all the calculated conductor voltages $V_{c,tot}$[V] belonging to one phase. The calculated no load phase voltages from the FEM model of the 36 teeth generator are presented in figure 5.2.

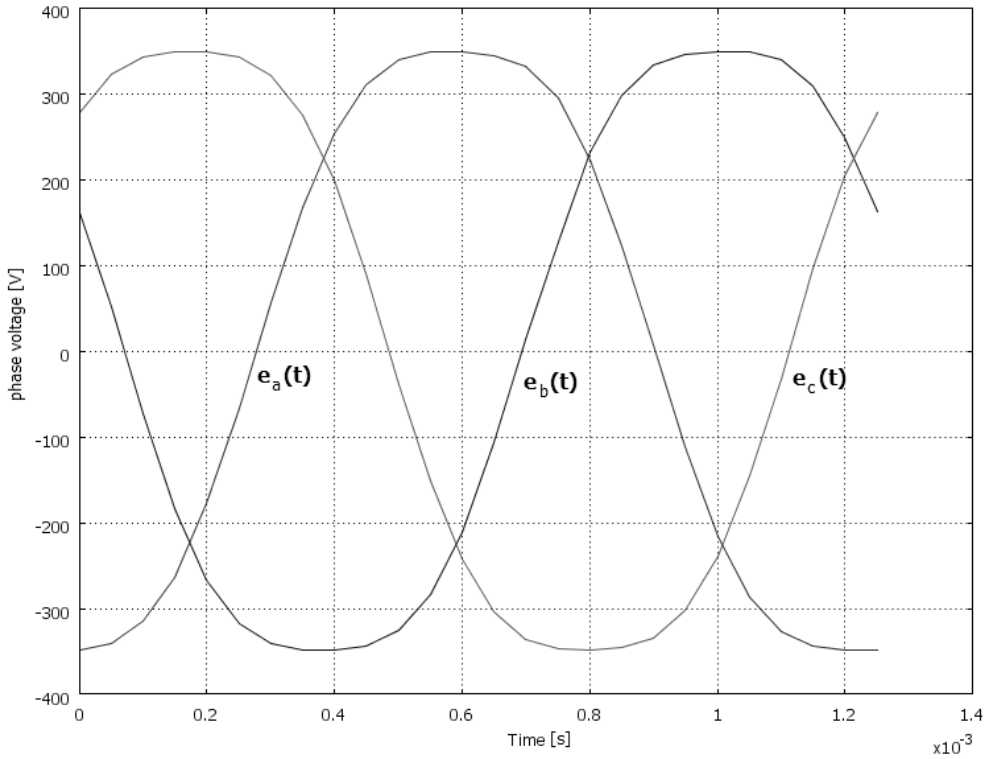

Figure 5.2: No load phase voltages of the 36 teeth generator design according to FEM calculations.

5.2. Armature reaction model using FEM

The armature reaction model made in FEM is suitable to determine an instantaneous armature reaction magnetic field, due to a fixed current. The armature reaction field as function of time is not determined in order to speed up calculations. The model can be used to determine the electric machines self inductance L_s[H] and mutual inductance M_{ab}[H]. Also the peak armature reaction flux density in the teeth $\hat{B}_{ar,tooth}[T]$, during normal operation, can be determined in order to check if a machine design gets saturated. The maximum effect of the armature reaction magnetic field on the magnets $B_{ar,max}$[T] can be determined.

The armature reaction model is made in the same way as the PM flux model, however the PM will not be excited. This is done in order to determine the magnetic energy in the geometry due to the phase currents. Figure 5.3 shows the solution of the magnetic field problem, for one section of the generator, if the rectangular coil sections of phase a are excited with the peak phase current $\hat{i}_a$ [A], multiplied by the number of conductors n_c around one coil. This is the peak current, present during normal operations. The flux density B[T] due to armature reaction is visible for different regions in the machine.

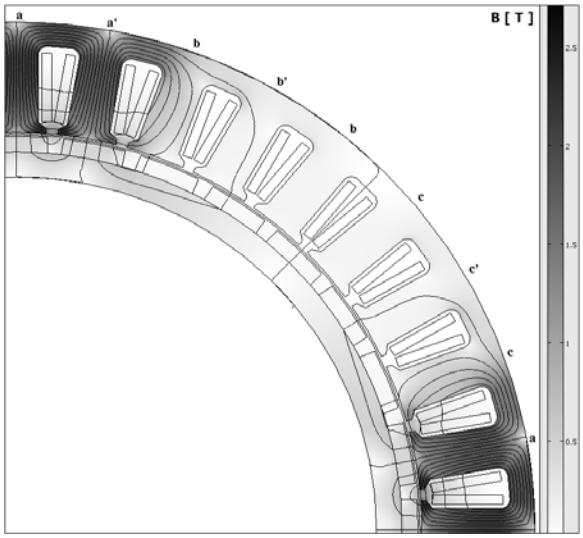

Figure 5.3: Computational results of the magnetic field due to armature reaction in the 36 teeth generator design.

Determining the electrical machines phase self inductance L_s[H] is done by using the magnetic energy W_m[J] equation for a constant current I[A] and inductance L[H]:

$$W_m = \frac{1}{2} \cdot L \cdot I^2 \tag{5.6}$$

Using the FEM armature reaction model, the total magnetic energy within the machine can be determined by integrating the magnetic energy density υ_m[J/m^3] over the total model area $A_{section}$[m^2] and multiplying by the machines length in axial direction l_{stk}[m] :

$$W_m = l_{stk} \cdot \iint \upsilon_m dA_{section} \tag{5.7}$$

From equation 5.6 and equation 5.7 the self inductance per phase follows:

$$L_s = \frac{2 \cdot W_m}{\hat{i}_a^{\,2}} \tag{5.8}$$

The mutual inductance M_{ab}[H] can be determined by applying a current $\hat{i}_a$ [A] in phase a and applying a current $-\hat{i}_b$ in phase b. This represents the current flowing through the machine during normal operation of a balanced three phase system, since $i_a(t) + i_b(t) + i_c(t) = 0$ still holds. Combining equation 3.59 and equation 5.8 the following equation must hold and the mutual inductance can be calculated:

$$\begin{aligned} 2 \cdot \left(L_s - M_{ab} \right) &= \frac{2 \cdot W_m}{\hat{i}_a^{\,2}} \\ M_{ab} &= L_s - \frac{W_m}{\hat{i}_a^{\,2}} \end{aligned} \tag{5.9}$$

Chapter 6: Calculation results and validations for the developed generator designs

In this chapter the calculation results, for the two different generator designs, with a SMPM rotor are discussed. The two different generators differ in their number of teeth and winding configuration. The two different generator designs are:

- A PM generator with concentrated coil fractional pitch windings, with 36 teeth.
- A PM generator with concentrated coil fractional pitch windings, with 48 teeth.

Design drawings and winding drawings, for the different designs can be found in appendix 6. The optimized geometrics were discussed in chapter 4.2. The calculation results of the two different generator designs will be presented as follow:

- Magnetic parameter results.
- Electric parameter results.
- Output performance.

6.1. Magnetic parameter results

The calculated magnetic parameters are presented as flux densities at different locations in the generator. The magnetic parameters are calculated with use of the analytical models from chapter 3, and then verified with the FEM models from chapter 5. For every calculation result there will be a reference to the used analytical equations. The further use or importance of a specific parameter is also made clear.

Effective air gap flux density:
First the effective air gap flux density $B_g(\theta)$, as function of rotor position, during no load is calculated. This parameter is important for calculating the induced voltage, as is clear from equation 3.31. Figure 6.1 shows the calculated effective air gap flux density, calculated according equation 3.14 of the analytical model. The functions are given for both the 36 teeth and 48 teeth generator design.

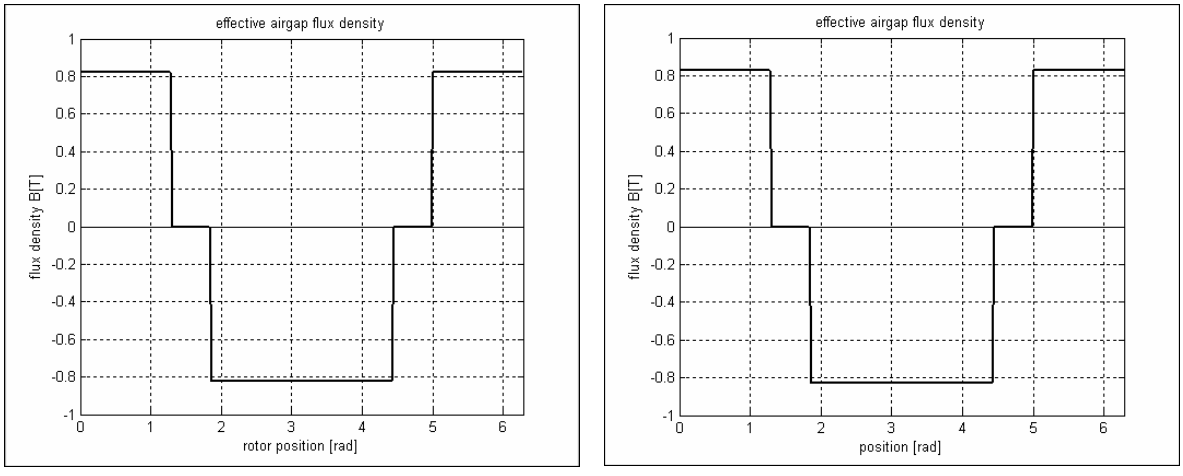

(a) ***(b)***

Figure 6.1: Air gap flux density as function of rotor position, for the 36 teeth generator design (a), for the 48 teeth generator design (b).

Using the FEM models a more accurate estimation of the effective air gap flux density function is made. The results of the FEM calculations are given in figure 6.2 for the 36 teeth generator design and in figure 6.3 for the 48 teeth generator design. These results were obtained when a stator tooth is directly positioned above a PM and no load is applied.

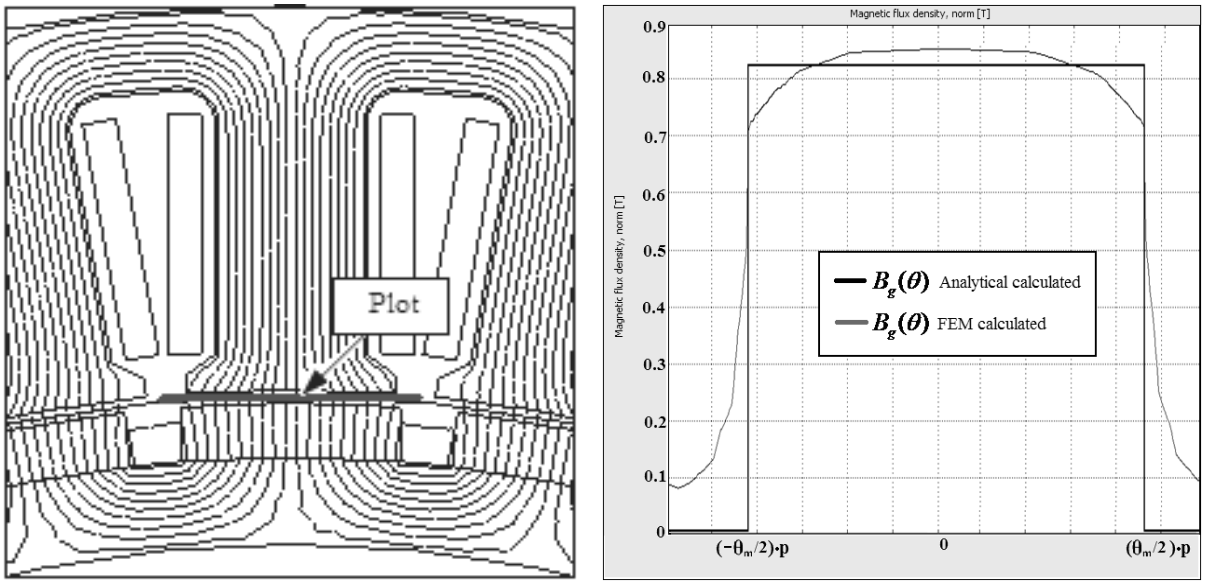

Figure 6.2: FEM result of the calculated air gap flux density as function of position. (36 teeth design)

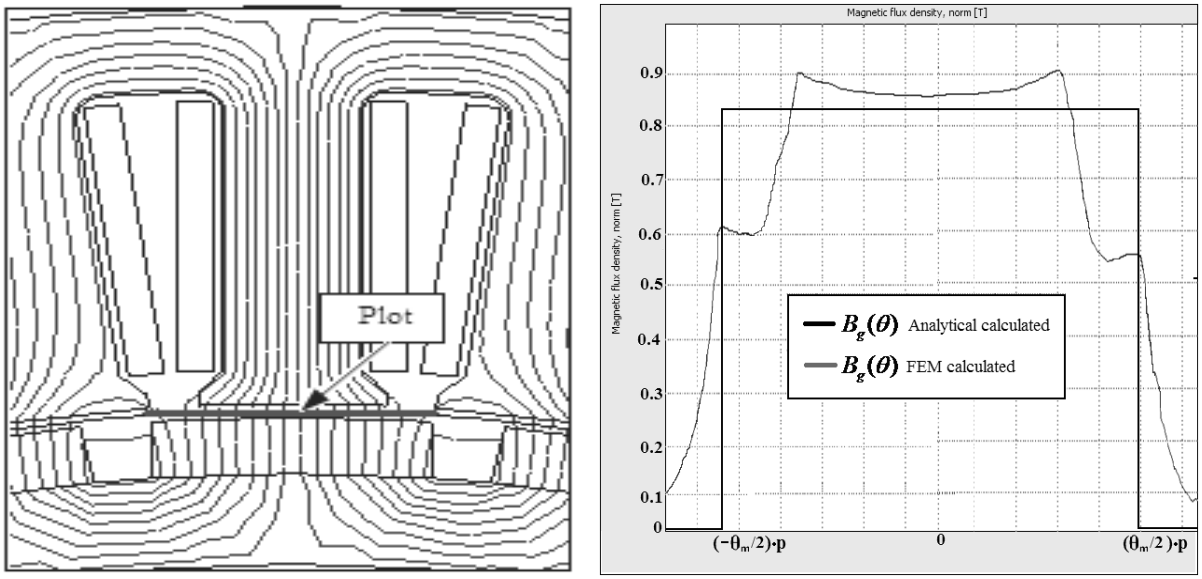

Figure 6.3: FEM result of the calculated air gap flux density as function of position. (48 teeth design)

From the FEM model it becomes clear that the effective air gap flux density, but also the magnet flux density $B_m(\theta)$, are dependant of the position of the stator teeth. When the rotor moves, the flux density in both the magnets and the air gap, as a function of rotor position angle, will change due to the stator slotting. This causes Eddy currents to be induced in the magnets. The analytical model neglects the change of flux density due to the stator slotting. This effect however is of very little influence.

Stator steel flux densities:

The flux densities in the stator steel vary with time and place. In the analytical model the stator steel is divided in two parts: a tooth part and a stator yoke part. The total stator yoke flux density $B_{sy,tot}$[T] and total tooth flux density $B_{tooth,tot}$[T] are important for taking into account saturating effects and iron loss $P_{loss,Fe}$[W] calculations. The steel flux densities are composed of a PM part B_{sy}[T] resp. B_{tooth}[T] and an armature reaction part $B_{ar,sy}$[T] resp. $B_{ar,tooth}$[T]. This is according to equation 3.95 and 3.96. Figure 6.4 presents the analytical calculation results, of the stator flux densities as a function of one electrical time period, during normal operation conditions, for the generator design with 36 teeth. Figure 6.5 presents the same analytical calculation results for a generator design with 48 teeth.

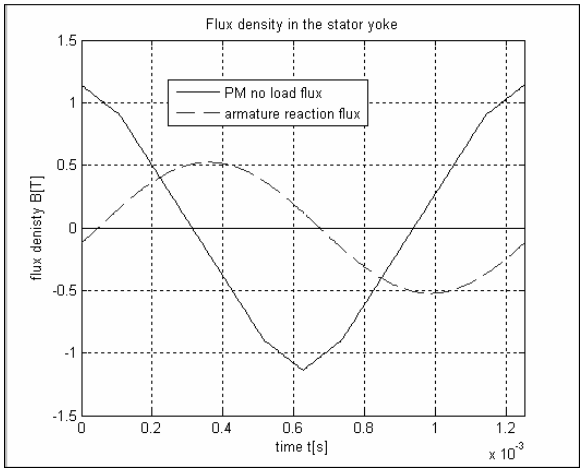

(a) Stator yoke

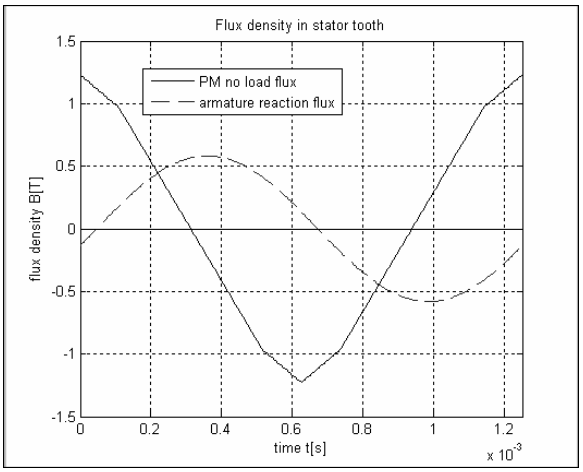

(b) stator tooth

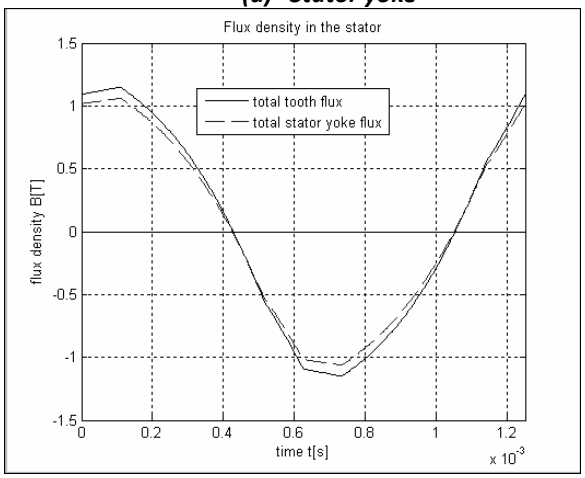

(c) Total flux density in stator

Figure 6.4: Analytical calculation results of the flux density in the stator as function of time, for the 36 teeth generator design

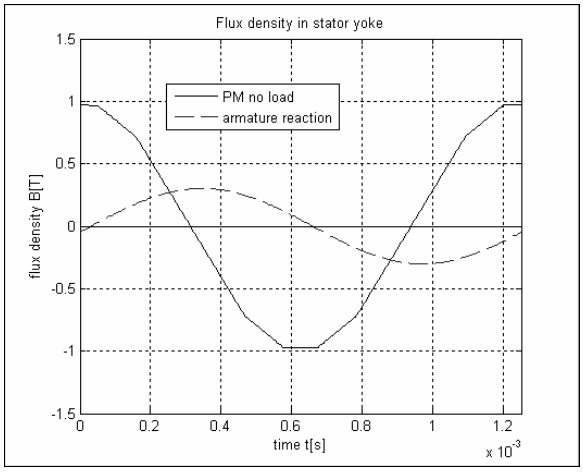

(a) Stator yoke

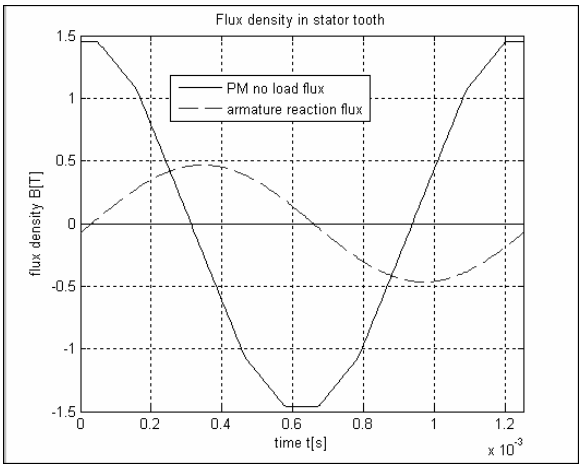

(b) stator tooth

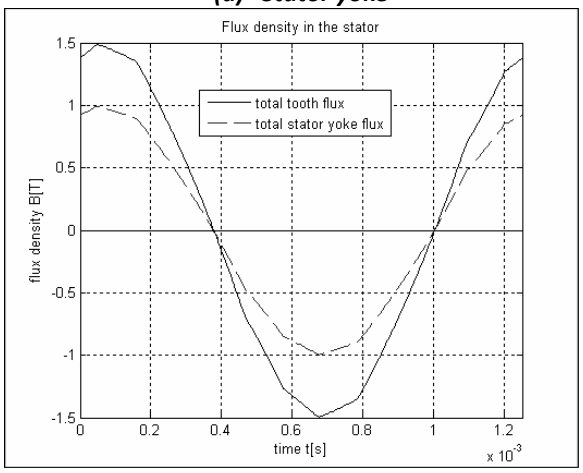

(c) Total flux density in stator

Figure 6.5: Analytical calculation results of the flux density in the stator as function of time, for the 48 teeth generator design

Table 6.1 presents a list of peak values for the different calculated flux density components. The analytical calculated results are presented, but also the results from the FEM calculations are presented. The FEM values are given, to verify the accuracy of the analytical model.

Parameter	Unit	36 teeth stator 32 poles rotor		48 teeth stator, 32 poles rotor	
		Analytical	FEM	Analytical	FEM
B_g	T	0.83	0.87	0.83	0.87
$\hat{B}_{g(1)}$	T	1.03	-	1.03	-
B_m	T	0.87	0.87	0.88	0.88
$\hat{B}_{ar,magnet}$	T	0.12	0.13	0.08	0.08
$\hat{B}_{ry}$	T	1.12	1.1	1.12	1.1
$\hat{B}_{ar,ry}$	T	0.17	0.16	0.09	0.08
$\hat{B}_{sy}$	T	1.11	1.1	0.97	1
$\hat{B}_{ar,sy}$	T	0.52	0.63	0.3	0.40
$\hat{B}_{sy,tot}$	T	1.06	-	0.99	-
$\hat{B}_{tooth}$	T	1.22	1.18	1.45	1.38
$\hat{B}_{ar,tooth}$	T	0.58	0.63	0.47	0.55
$\hat{B}_{tooth,tot}$	T	1.15	-	1.49	-

Table 6.1: Flux density peak values for different generator domains.

Short circuit current armature reaction:

Armature reaction, due to the peak of a short circuit current $\hat{i}_{scc}$ [A], is considered in the analytical model, without taking into account the PM magnetic field and steel saturation.
It is further assumed, in the analytical model, that the armature reaction magnetic field under a tooth is homogeneous. The calculation results of the armature reaction flux density in the magnets $B_{m,max}$[T] are presented in Table 6.2. The analytical results are calculated according equations 3.89 to 3.91, while the FEM result is a peak value.

Parameter	Unit	36 teeth stator 32 poles rotor		48 teeth stator, 32 poles rotor	
		Analytical	FEM	Analytical	FEM
$\hat{i}_{scc}$	A	295	295	597	597
$B_{ar,max}$	T	0.68	0.66	0.67	0.59

Table 6.2: Peak flux densities in the magnets due to short circuit current.

From the FEM model it becomes clear that the flux density under the stator tooth, where a short circuit current is applied, is not homogeneous but a function of position θ_{st} [rad]. This is clear from figure 6.6, where the armature reaction flux density in the magnet $B_{ar,max}$[T] due to a short circuit current, is presented as a function of the stator circumference angle θ_{st} [rad]

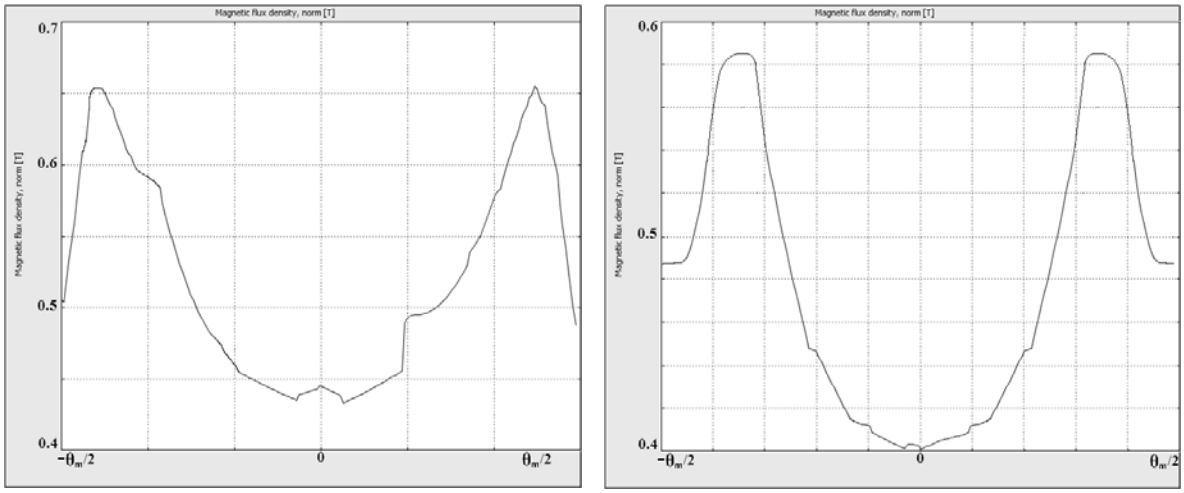

(a) ***(b)***

Figure 6.6: armature reaction flux density in the magnets due to short circuit current, for the 36 teeth generator design (a), for the 48 teeth generator design (b)

The effect of the short circuit current on the PM's, is approximated in the analytical model, by superimposing the PM flux on the maximum armature reaction flux. Following equation 3.92 the total flux density in the PM's must be higher than the minimum allowed flux density $B_{m,min}$[T]:

$$B_m - B_{ar,\max} \quad > \quad B_{m,\min} \tag{3.92}$$

According to the B-H characteristic of the magnet material, the minimum allowed flux density, at a temperature of 120°C is:

$$B_{m,\min} \quad = \quad 0.0T$$

The effect of the armature reaction flux density in the magnets, due to the peak of a short circuit current is also considered, using the FEM model, while taking into account the PM magnet flux. Figure 6.7 and figure 6.8 present plots of the flux density at the PM surface (in the magnet) due to the peak short circuit armature flux. From these figures it becomes clear that, due to a peak short circuit current, the flux at the magnets surface reaches the value of 0.2 T. Since the peak short circuit current is of very short duration, and only at the magnets surface the minimum allowed flux density limit is reached, the magnets can be considered safe from demagnetization, even during fault conditions.

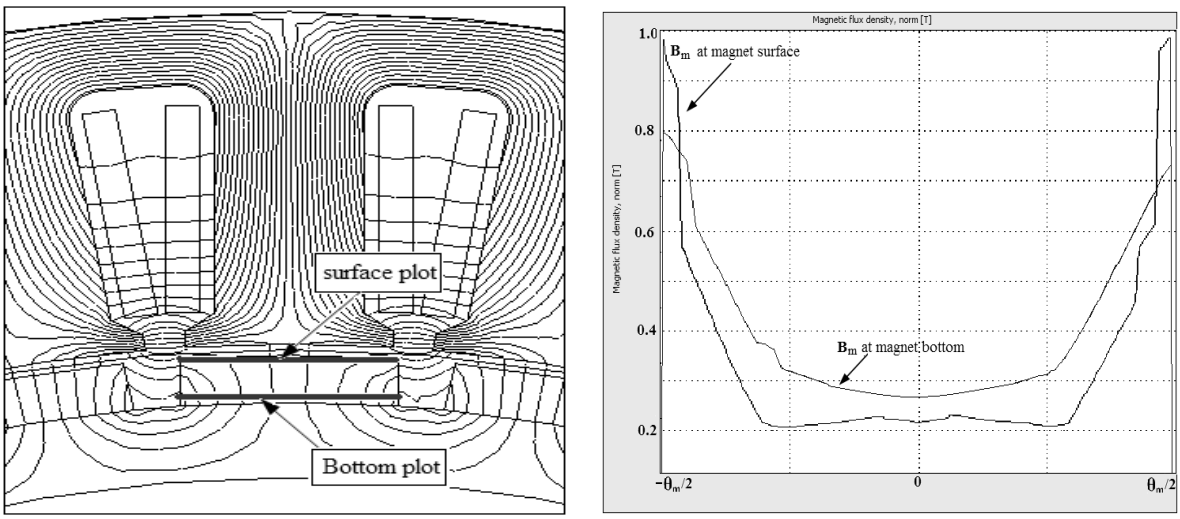

Figure 6.7: armature reaction flux density plot in a magnet due to the peak short circuit current, while taking into account the PM flux. For the 36 teeth generator design.

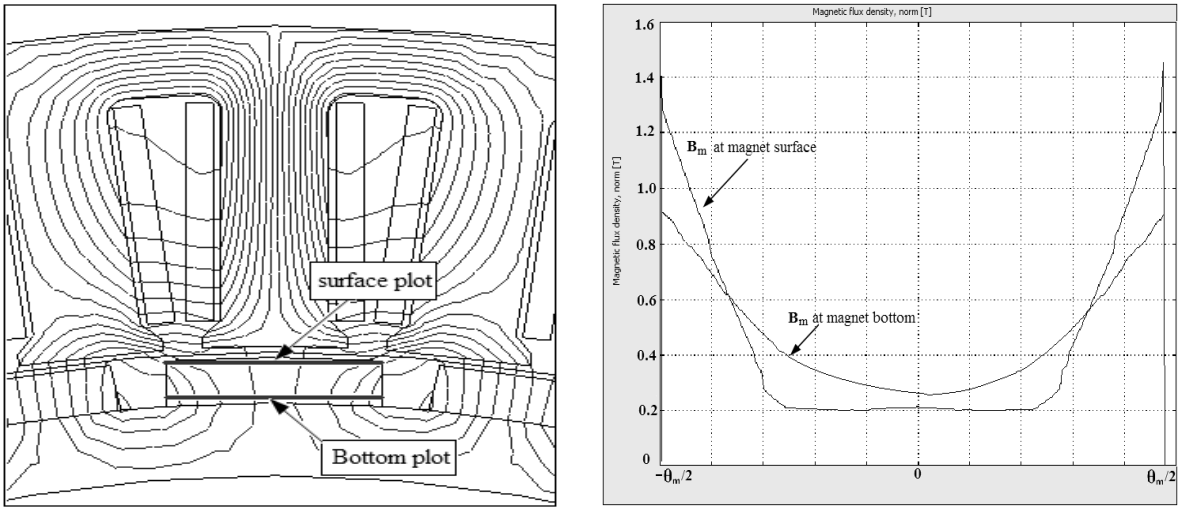

Figure 6.8: armature reaction flux density plot in a magnet due to the peak short circuit current, while taking into account the PM flux. For the 48 teeth generator design.

Starting torque:

Due to the non linear permeability of the steel parts of the generator, torque will not increase linear with current. Figure 6.9 shows the analytical calculation results of the generated starting torque T_{gen}[Nm], when a starting current I_{start}[A] is applied. Results are given for both the 36 teeth generator design and the 48 teeth generator design. Calculations are done according the iterative process of figure 3.18.

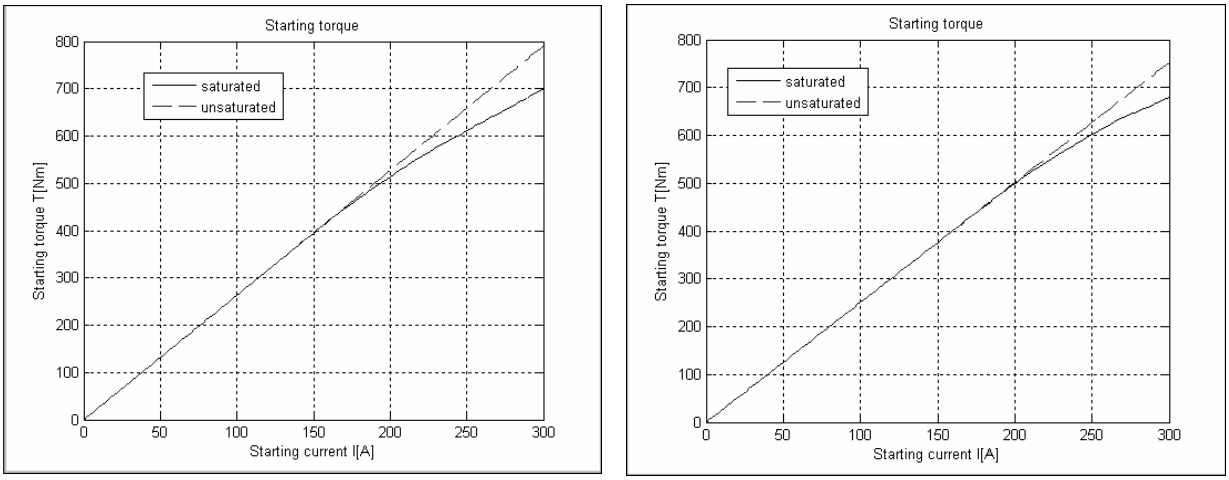

(a) 36 teeth generator design ***(b) 48 teeth generator design***

Figure 6.9: Generated torque as function of the starting current.

From the results it is clear that beneath a starting torque of 400Nm saturation effects are negligible, therefore no problems are expected when using these generator designs as starter motor.

Space harmonic components in the rotor due to armature reaction:
The method presented in chapter 3.2.3 is used for calculating the space harmonic components of the flux density in the magnets due to armature reaction. Table 6.3 presents the calculated amplitudes of the different space harmonic components $\hat{B}_{ar(k)}$ [T] and their relative speed, relative to the rotational speed ω_e[rad] of the electrical phasor.

Harmonic component	36 teeth stator 32 poles rotor		48 teeth stator, 32 poles rotor	
	$\hat{B}_{ar(k)}$ [mT]	$\omega_{r(k)}$	$\hat{B}_{ar(k)}$ [mT]	$\omega_{r(k)}$
k=1	-20.3	$3\cdot\omega_e$	66.2	0
k=2	23.4	$-3\cdot\omega_e$	33.1	$-1.5\cdot\omega_e$
k=3	0	0	0	0
k=4	79.2	0	-16.5	$-0.75\cdot\omega_e$
k=5	63.4	$-1.8\cdot\omega_e$	-13.0	$-1.2\cdot\omega_e$
k=6	0	0	0	0
k=7	6.7	$-0.43\cdot\omega_e$	9.5	$-0.86\cdot\omega_e$
k=8	-2.5	$-1.5\cdot\omega_e$	8.3	$-1.13\cdot\omega_e$
k=9	0	0	0	0

Table 6.3: Amplitudes and frequencies of armature reaction space harmonics, seen from the rotor.

6.2. Electric parameter results

Now the results of the calculated electrical machine parameters will be presented. First the induced voltage is considered, and then results for the calculated inductances and resistances are presented.

Induced voltage:
Using the analytical model for calculating the induced voltages will result in getting the first harmonic component of the induced voltage, because the induced voltage is assumed to be sinusoidal. By doing this harmonic components in the induced voltage are neglected. Therefore also the FEM calculation results are presented. The FEM model doesn't neglect the harmonic components in the induced voltage. Figure 6.10 shows the induced voltages e_a[V], e_b[V] and e_c[V] in the phases a, b and c, calculated using the analytical model according equation 3.30.

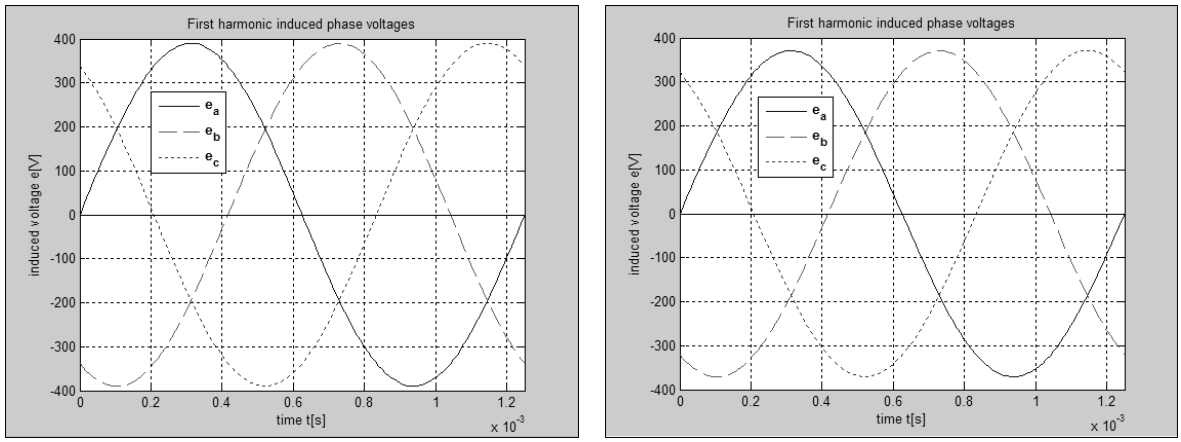

(a) ***(b)***

Figure 6.10: Analytical results of the induced no load phase voltages.
For the 36 teeth generator design (a) and the 48 teeth generator design (b).

Figure 6.11 presents the FEM calculation results for the induced voltages in phase a, b and c, while no load is applied.

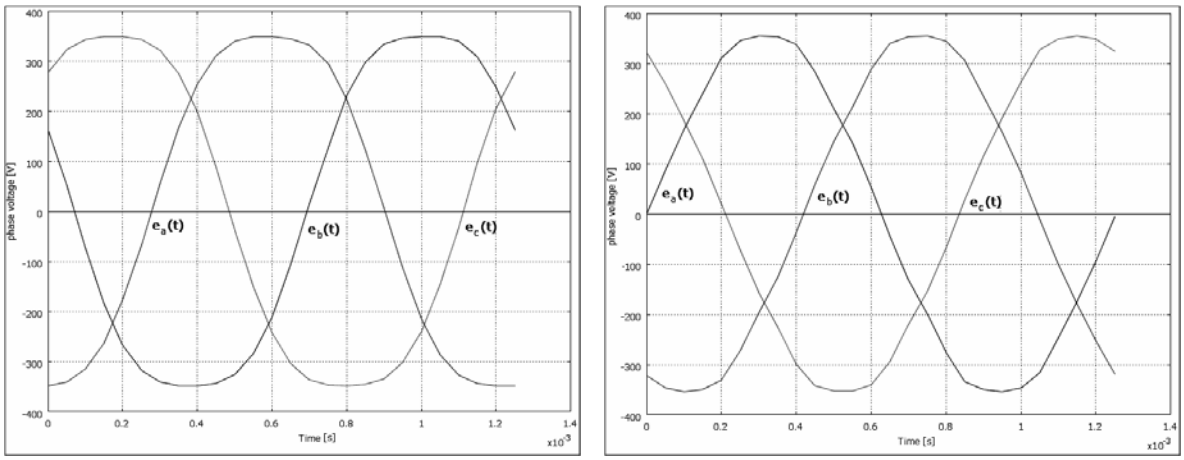

(a) ***(b)***

Figure 6.11: FEM calculation results of the induced no load phase voltages.
For the 36 teeth generator design (a) and the 48 teeth generator design (b).

From the analytical induced voltage results, it becomes clear that the peak of the first harmonic component of the induced voltage, of the generator design with 36 teeth is higher than the peak of the generator design with 48 teeth. The FEM results both give the same peak values as a result. Therefore it is clear, as can be seen, that a stator design with 36 teeth has higher amplitudes of its harmonic voltage components. By connecting a generator in star, all harmonic components with a multiple of 3 can be eliminated. By doing this the resulting line-line voltages $e_{ll,a}$[V] $e_{ll,b}$[V] and $e_{ll,c}$[V] during no load operation, calculated using FEM, are presented in figure 6.12(a) for the 36 teeth generator design and in figure 6.12 (b) for the 48 teeth generator design.

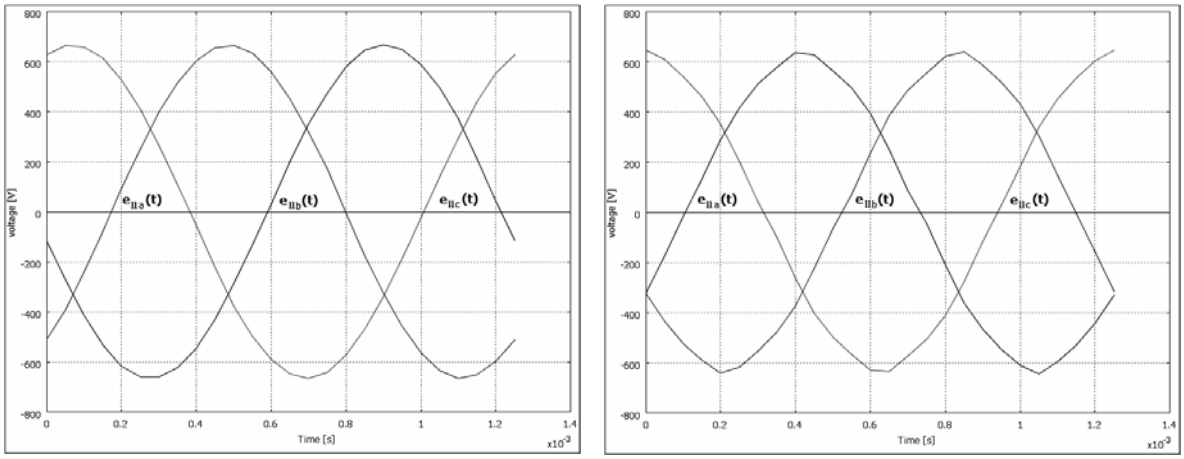

Figure 6.12: FEM calculation results of the induced line-line voltages. (Y-connected phases) For the 36 teeth generator design (a) and the 48 teeth generator design (b).

Table 6.4 presents an overview of the peak values of the induced voltage during no load, calculated both analytical and using FEM, for the two different generator designs.

Parameter	Unit	36 teeth stator 32 poles rotor		48 teeth stator, 32 poles rotor	
		Analytical	FEM	Analytical	FEM
$\hat{E}_{ph}$	V	390	355	372	355
$\hat{E}_{LL}$	V	675	665	644	636

Table 6.4: Calculate amplitudes of the induced generator voltage.

Phase resistance:
The phase resistance is calculated using the analytical model. According to equation 3.34 the phase resistance R_{ph}[Ω], of a generator with a 36 teeth stator design, becomes:

$$R_{ph} = 73.7 \quad m\Omega$$

The phase resistance of a generator with a 48 teeth stator design becomes:

$$R_{ph} = 63.5 \quad m\Omega$$

Inductances:
The different inductance components in a generator are calculated analytical and are verified using FEM calculations. Analytical calculations are done according the analytical model of chapter 3.2.1.2 and chapter 3.2.2.2. Table 6.5 presents the calculation results from both the analytical and FEM calculations, for both the generator designs with 36 teeth and 48 teeth:

Parameter	Unit	36 teeth stator 32 poles rotor		48 teeth stator, 32 poles rotor	
		Analytical	FEM	Analytical	FEM
L_s	H	$526 \cdot 10^{-6}$	$561 \cdot 10^{-6}$	$247 \cdot 10^{-6}$	$277 \cdot 10^{-6}$
L_{sm}	H	$237 \cdot 10^{-6}$	-	$78.9 \cdot 10^{-6}$	-
$L_{s\sigma}$	H	$289 \cdot 10^{-6}$	-	$169 \cdot 10^{-6}$	-
M_{ab}	H	$-56 \cdot 10^{-6}$	$-50 \cdot 10^{-6}$	$-124 \cdot 10^{-6}$	$-137 \cdot 10^{-6}$

Table 6.5: Calculation results of the inductance components.

6.3. Output performance results

In this chapter the following calculation results will be discussed:

- Magnet losses due to space harmonics
- Generator loss calculations
- Output characteristics.

Magnet losses:
The losses in the magnets due to the space harmonic components of the armature reaction flux density are calculated according the analytical model of chapter 3.4.3. The results of the calculated space harmonic components in table 6.3 are used to find the total loss due to Eddy currents in the magnets. Both laminated and unlaminated magnets are considered in table 6.4

	Harmonic component	k=1	k=2	k=4	k=5	k=7	k=8	total
		36 teeth stator, 32 poles rotor						
P_m	W	175.1	232.7	0	612.3	0.4	0.7	1021.3
P_{ml}	W	1.8	2.5	0	6.4	0.0	0.0	10.7
		48 teeth stator, 32 poles rotor						
P_m	W	0	133	8	14	4	5	163
P_{ml}	W	0	1.4	0	0.2	0	0	1.7

Table 6.4: Magnet losses for laminated and unlaminated magnets in both generator designs.

From these results it is obvious that magnet losses in the generator design with a fractional pitch winding configuration with 36 slots and 32 poles can become substantial. Since both generators are developed with laminated magnets the losses in the magnets become negligible.

Generator losses:
Table 6.5 is an overview with results of the analytical calculated generator losses. The losses are calculated according the equations of chapter 3.4.

Parameter	Unit	Description	36 teeth stator 32 poles rotor	48 teeth stator, 32 poles rotor
$P_{loss,cu}$	W	Copper losses	430	397
$P_{loss,Fe}$	W	Iron losses	$0.99 \cdot 10^3$	$1.37 \cdot 10^3$
$P_{loss,m}$	W	Magnet losses (non laminated)	$1.02 \cdot 10^3$	163
$P_{loss,ml}$	W	Magnet losses (laminated magnets)	10.7	1.7
$P_{loss,tot}$	W	Total losses (laminated magnets)	$1.43 \cdot 10^3$	$1.77 \cdot 10^3$

Table 6.5: Generator losses.

Output characteristics:
The output characteristics for both generator designs are calculated only for nominal operation conditions, since the generator will be used at a fixed speed and power input. The output parameters are calculated analytically, according to the equations of chapter 3.5 and are presented in table 6.6.

Parameter	Unit	Description	36 teeth stator 32 poles rotor	48 teeth stator, 32 poles rotor
U_t	V	Terminal phase voltage	273	260
U_{ll}	V	Terminal line-line voltage	473	451
U_{dc}	V	Rectified DC voltage	639	609
I_{ph}	A	Phase current	44.0	45.6
J_{nom}	A/m^2	Current density	$6.78 \cdot 10^6$	$6.52 \cdot 10^6$
cos ϕ		Cosϕ	0.97	0.98
P_{out}	W	Generated output power	$35.1 \cdot 10^3$	$35.1 \cdot 10^3$
η	%	Efficiency	96.1	95.2

Table 6.6: Output performance.

Chapter 7: Conclusions and future work

7.1. Contributions and conclusions

This thesis project deals with the development of a generator for a prototype HPRE. This generator must be optimized for minimum cost and weight, while having a reasonable efficiency. The generator must also be developed to function as starter motor for the combustion engine of the HPRE.

First the best suitable machine construction for the generator is determined. For this purpose a literature survey is held. It appears that a permanent magnet radial flux machine with concentrated coils is preferable, because the most low cost, light weight and efficient generator design can be expected. The generator of the prototype HPRE will therefore be developed according to this machine construction type. Two different fractional pitch winding configurations, for concentrated coil constructions, are considered for development:

- A winding configuration which is a multiple of 9 coils around 9 teeth with 8 magnet poles. Acceptable rotor losses are expected from this configuration and it has a high winding factor k_w.
- A winding configuration which is a multiple of 3 coils around 3 teeth with 2 magnet poles. This is a concentrated coil configuration with the lowest expected rotor losses. But it has a low winding factor k_w.

Also two different rotor configurations, for permanent magnet (PM) excitated machines, are considered for development:

- A rotor with surface mounted permanent magnets (SMPM). This is the smallest and lightest solution. However extra production costs can be expected since the magnets will be arc shaped and have to be attached, using bandaging, to the rotor outer surface.
- A rotor with inset mounted permanent magnets (IMPM). This solution is expected to be cheaper in production, since straight magnet pieces can be used, and no bandaging is needed. Also lower magnet losses are expected, since the magnets are placed further from the stator in comparison to the magnets of a SMPM rotor. A disadvantage is the extra flux leakage in the rotor, which contributes to a less efficient use of magnet material.

Models have been derived for calculations on the considered generator construction types. An optimizing routine is developed in order to generate the designs according the design criteria. The developed models include:

- A PM flux model, modeled both analytical and with use of FEM modeling. This model determines the flux density distribution, due to the PM's, within an electrical machine. From the effective air gap flux density B_g the induced no load voltage E_{ph} is then calculated using the analytical derived induced voltage calculations.
- Two armature reaction models, modeled both analytical and with use of FEM modeling. One for determining the flux density distribution and inductivity components in electrical machines with a winding configuration which is a multiple of 9 coils around 9 teeth and 8 magnet poles. And one for determining the flux density distribution and inductivity components in electrical machines with a winding configuration which is a multiple of 3 coils around 3 teeth and 2 magnet poles.

- A method for analytically calculating the generated starting torque T_{gen} as function of applied start current I_{start}.
- The analytical modeling of losses, including: copper losses, iron losses in both rotor and stator and magnet losses due to the space harmonic components of the armature reaction flux density.

Using the optimizing routine an optimal design for a generator with a winding configuration which is a multiple of 9 coils around 9 teeth and 8 magnet poles is found. This design has 36 teeth and 32 magnet poles. Another generator with the same outer dimensions, but another fractional pitch winding configuration, is designed. This generator design has a slot pole combination of 48 slots and 32 magnet poles. In this way both generator designs can be tested with the same rotors and a good comparison between the two different winding configurations can be made. From the analytical and FEM calculations the following important differences between the two different generator designs can be expected:

- The generator design with a slot pole configuration of 36 teeth and 32 magnet poles has a lower flux density in the stator teeth. Therefore less stator iron losses are expected, which leads to a higher machine efficiency.
- The generator with a slot pole configuration of 48 teeth and 32 magnet poles has lower rotor losses. Therefore less temperature rise in the rotor can be expected, which leads to a more efficient use of magnet material.

Two different rotors are developed which can be used in both machine designs. A SMPM rotor is developed, with a larger rotor yoke as required. In this way it was possible to also develop an IMPM rotor of the same dimensions.

The results of the development have lead to the production of two generator designs with two different rotor designs. The rotors will be made out of laminated steel and the magnets will also be laminated, in order to keep rotor losses as low as possible. Rotors are exchangeable between the two different generators, in order to compare the different design variations during the test phase of the prototype HPRE.

7.2. Future work

Future work consists of two parts:

- Determining the best construction variation for the generator of the HPRE.
- Extending the generator analytical models and FEM models

The produced prototype generators have to be tested in a testing lab. The lab results can then be used for further validation and refinement of the developed calculation models. During the testing phase the different design variations have to be compared. Comparisons for the different generator slot pole configurations in combination with the different rotor constructions include:

- Comparison of production costs.
- Comparison of efficiency.
- Comparison of rotor losses.
- Heat development throughout the machine.

The optimal design variations for the generator of the HPRE have to be determined. The best design variation, for a PM radial flux concentrated coil machine construction, will be further optimized for the development of a final generator design for the production type of the HPRE.

The modeling work for generator constructions has to be further developed. A model must be developed to determine the heat distribution, due to losses, within a generator. This model can be used to determine the optimal current density J_{nom} for an electrical machine design. Future designs can than be optimized with an optimal current density. The generator models can easily be extended with models for different concentrated coil and distributed coil winding configurations. This can be accomplished by approaching the development in the same way as the development of the armature reaction models in this thesis.

REFERENCES

[Com 03] J.C. Compter,*"Mechatronics: Introduction to electro-mechanics",* DUT Lecture notes, 2003.

[CM 08a] Comsol Multiphysics AC/DC module user's guide, 2008.

[CM 08b] Comsol Multiphysics AC/DC module model library, 2008.

[Dub 04] M.R.J. Dubois*,"Optimized Permanent Magnet Generator Topologies for Direct-Drive Wind Turbines",* Ph.D. diss: Delft, 2004.

[Fer 07] J.A. Ferreira, *"Power electromagnetics"*, DUT Lecture notes, 2007.

[Fir 08] M.Firmansyah, *"Eddy current losses calculation in the rotor back iron and magnets for concentrated winding PM generator"*, MSc. thesis: Delft, 2008.

[Gie 02] J.F. Gieras, M.Wing*,"Permanent magnet motor technology"*, Marcel Dekker: New York, 2002.

[Had 99] J.R. Hadji-Minaglou, and G. Henneberger, *"Comparison of different motor types for electric vehicle application",* EPE Journal, vol. 8, pp. 46-55, 1999.

[Hah 08] S. Hahlbeck,*"Design considerations for rotors with embedded V-shape permanent magnets"*, In proceedings of the international conference on electrical machines: paper ID 908, 2008.

[Han 94] D.C. Hanselman*,"Brushless permanent-magnet motor design",* McGraw-Hill: Maine, 1994.

[Har 89] M.R. Harris and T.J.E. Miller, *"Comparison of Design and Performance Parameters in Switched Reluctance and Induction Motors",* IEEE Conference of Electrical Machines and Drives, pp. 303-307, 1989

[Hoe 97] M.J. Hoeijemaker, *"Elektrische omzettingen",* VSSD: Delft, 1997.

[Hol 03] R. Holm,*"Modelling and optimization of a PM machine in a flywheel",* Ph.D. diss: Delft, 2003.

[Hsu 04] J.S. Hsu, C.W. Ayers, C.L. Coomer, *"Report on Toyota/Prius motor design and manufacturing assessment",* Oak Ridge National Laboratory, 2004.

[Kir 05] J.L.Kirtley,*"Inductances and windingfactor calculations in generators"*, MIT. Lecture notes, 2005

[Mil 94] T. Miller, J.R.Hendershot jr. ,*'Design of brushless permanent magnet motors",*Clarendon press, 1994.

[Moh 03] N. Mohan, T.M. Undeland, W.P. Robbins: *"Power electronics",* J.Wiley, 2003.

[Nas 93] S.A. Nasar, I. Boldea, L.E. Unnewehr,*"Permanent magnet, reluctance, and self-synchronous motors",* CRC Press, 1993.

[Nie 08] Lu Nie, *"Design of Fault Tolerant Energy conversion System for Increasing Wind Turbine Reliability"*, MSc. Thesis: Delft, 2008

[Pol 98] H. Polinder,*"On the losses in a high speed PM generator with rectifier"*, Ph.D. diss: Delft, 1998.

[Pol 03] H. Polinder, J.G. Slootweg, M.J. Hoeijmakers, J.C. Compter, *"Modeling of a Linear PM Machine Including Magnetic Saturation and End Effects: Maximum Force-to-Current Ratio."*, IEEE transaction on industry applications, vol. 39, no. 6, 2003.

[Pol 07] H. Polinder, M.J. Hoeijmaker, M. Scuotto, *"Eddy current losses in the solid back iron of PM machines for different concentrated fractional pitch windings",* IEEE machine and drives conference, 2007.

[PP 10] http://www.peec-power.com, s'Gravendeel, 2010

[Sah 01] F.Sahin, *"Design and development of a high speed axial-flux PM machine",* Ph.D. diss: Delft, 2001.

[Sen 97] P.C. Sen,*"Principles of electric machines and power electronics",* J.Wiley, 1997.

[Ska 06] S. E. Skaar, O. Krovel, R. Nilssen, *"Distribution, coil span and winding factors for PM machineswith concentrated windings",* NTNU, 2006.

[Vio 07] I.A. Viorel, K. Hamemeyer, L. Strete, *"On the carter's factor calculation for slotted electric machines",* Advances in electrical and computer engineering, vol.7, number 2, 2007

Appendix 1: Geometries for radial flux PM machines

The geometric dimensions, for a machine with surface magnets are calculated from the input requirements and the magnetic and electric properties. Also volumes masses and prices are calculated.

Speed calculations:

$$\omega_m = 2 \cdot \pi \cdot n_m / 60$$
$$p = n_m / 2$$
$$\omega_e = p \cdot \omega_m$$
$$f_e = \omega_e / (2 \cdot \pi)$$

ω_m	[rad/s]	mechanical rotational speed
p		number of pole pairs
ω_e	[rad/s]	electric rotational speed
f_e	[Hz]	electric frequency

Geometrics:

$$\alpha_s = w_{si} / \left(\left(r_{si} + d_1 + d_2 \right) \cdot \theta_s \right)$$
$$\theta_m = \alpha_m \cdot \theta_p$$
$$\theta_p = (2 \cdot \pi) / N_m$$
$$\theta_s = (2 \cdot \pi) / N_s$$
$$\tau_c = coilspan \cdot \tau_s$$
$$\tau_m = r_{rb} \cdot \theta_m$$
$$\tau_p = r_{rb} \cdot \theta_p$$
$$\tau_s = r_{si} \cdot \theta_p$$
$$A_g = \tau_p \cdot L_{stk}$$
$$A_m = \tau_m \cdot L_{stk}$$
$$A_s = d_3 \cdot \left(\theta_s \cdot \left(r_{sb} - \frac{d_3}{2} \right) - \frac{w_{ti} + w_{tb}}{2} \right) + \frac{\left(d_2 \cdot \left(\theta_s \cdot \left(r_{si} + d_1 + d_2 \right) \right) - w_{ti} \right) + \left(d_2 \cdot \left(\theta_s \cdot \left(r_{si} + d_1 \right) \right) - w_t \right)}{2}$$
$$coilspan = \operatorname{int}\left(N_s / N_m \right)$$
$$d_1 = 0.125 \cdot w_{ti}$$
$$d_2 = 0.125 \cdot w_{ti}$$
$$d_3 = r_{sb} - r_{si} - d_1 - d_2$$
$$r_{cu} = \sqrt{(A_s \cdot k_{fill}) / (2 \cdot n_c \cdot \pi)}$$
$$r_{rb} = r_{ri} + w_{ry}$$
$$r_{ro} = r_{ri} + w_{ry} + l_m$$
$$r_{sb} = r_{so} - w_{sy}$$
$$r_{si} = r_{ro} + g$$

α_s		slot fraction
θ_m	[rad]	magnet angle
θ_p	[rad]	pole angle
θ_s	[rad]	slot angle
τ_c	[m]	coil pitch
τ_m	[m]	magnet pitch
τ_p	[m]	pole pitch
τ_s	[m]	slot pitch
A_g	[m^2]	gap area of one pole pitch
A_m	[m^2]	magnet area
A_s	[m^2]	slot area
coilspan		coilspan
d_1	[m]	width of shoetip (straight piece)
d_2	[m]	width of shoetip (skewed piece)
d_3	[m]	slot depth
r_{cu}	[m]	radius of copper conductors
r_{rb}	[m]	rotor yoke outer radius
r_{ro}	[m]	rotor outer radius
r_{sb}	[m]	stator yoke inner radius
r_{si}	[m]	stator inner radius

$$w_{ry} = \left(B_m \cdot \tau_m\right) / \left(2 \cdot B_{\max} \cdot k_{stk}\right)$$
$$= r_{ri} / \left(\frac{2 \cdot B_{\max} \cdot k_{stk}}{\hat{B}_g \cdot \theta_p \cdot k_{ml}} - 1\right)$$
$$w_s = \tau_s - w_t$$
$$w_{sb} = r_{sb} \cdot \theta_s - w_{tb}$$
$$w_{si} = \left(r_{sb} + d_1 + d_2\right) \cdot \theta_s - w_{ti}$$
$$w_{sy} = \left(\hat{B}_g \cdot \tau_p\right) / \left(2 \cdot B_{\max} \cdot k_{stk}\right)$$
$$w_t = \tau_m \quad , \qquad w_t = \tau_s - 0.0035$$
$$w_{tb} = w_{ti}$$

$$w_{ti} = \left(\hat{B}_g \cdot \tau_p \cdot N_m\right) / \left(B_{\max} \cdot N_s\right)$$

w_{ry}	[m]	rotor yoke width
w_s	[m]	slot top width
w_{sb}	[m]	slot outer width
w_{si}	[m]	slot inner width
w_{sy}	[m]	stator yoke width
w_t	[m]	tooth top width
w_{tb}	[m]	tooth outer width
w_{ti}	[m]	tooth inner width

The machine stack length l_{stk}[m] is calculated using the electric properties and the law of conservation of energy, which states:
Energy can neither be created nor destroyed.
Applying this for the three phase generator:

$$P_{out} + P_{loss,cu} = P_{in} - P_{loss,Fe} = 3 \cdot E_{ph} \cdot I_{ph} \cdot \cos\psi$$

Repeating the voltage equation:

$$E_{ph} = \frac{N_s}{N_{ph}} \cdot k_w \cdot \omega_m \cdot n_c \cdot l_{stk} \cdot r_{ro} \cdot \hat{B}_{g1} \cdot \sqrt{2}$$

From this the stack length follows:

$$l_{stk} = \frac{P_{in} - P_{loss,Fe} - P_{loss,ml}}{3 \cdot I_s \cdot \cos\psi \cdot \frac{2}{\sqrt{2}} \cdot \hat{B}_g \cdot r_{ro} \cdot \omega_m \cdot \frac{N_s}{N_{ph}} \cdot k_w}$$

For a machine from the inset magnet type (IMPM v-shape) the rotor dimensions are calculated differently. Figure A.1 shows a pole piece from a v-shape IMPM rotor, from which the dimensions can be calculated:

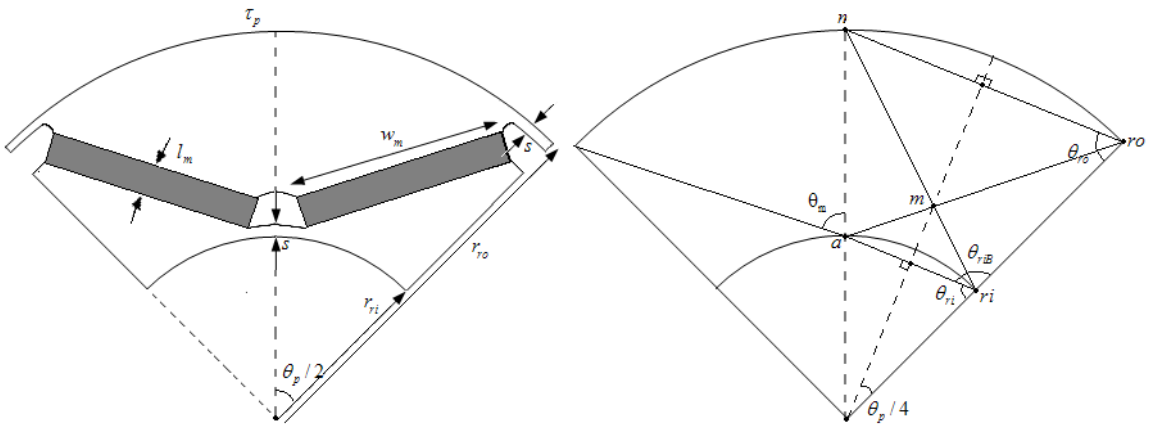

Figure A.1.: IMPM rotor pole piece

$$\theta_{ri} = (\pi/2) - (\theta_p/4)$$

$$l_{a-ri} = 2 \cdot r_{ri} \cdot \sin(\theta_p/4)$$

$$l_{a-ro} = \sqrt{{l_{a-ri}}^2 + (r_{ro} - r_{ri})^2 - 2 \cdot l_{a-ri} \cdot (r_{ro} - r_{ri}) \cdot \cos(\pi - \theta_{ri})}$$

$$l_{n-ro} = 2 \cdot r_{ro} \cdot \sin(\theta_p/4)$$

$$\theta_m = \cos^{-1}(((r_{ro} - r_{ri})^2 + {l_{a-ro}}^2 - {l_{n-ro}}^2)/(2 \cdot (r_{ro} - r_{ri}) \cdot l_{a-ro}))$$

$$w_m = l_{a-ro} - (2 \cdot l_m)$$

$$\alpha_c = (2 \cdot w_m)/\tau_s$$

θ_{ri}	[rad]	angle of point ri
l_{a-ri}	[m]	length between points a and ri
l_{a-ro}	[m]	length between points a and ro
θ_m	[rad]	angle of magnet skewness
w_m	[m]	magnet width
α_c		flux concentration factor

Machine volume calculations:

$$V_{s,sy} = \left(r_{so}{}^2 \cdot \pi - r_{sb}{}^2 \cdot \pi\right) \cdot L_{stk} \cdot k_{stk}$$

$$V_{s,teeth} = \left[\begin{array}{l} \left(\left(r_{sb} - \frac{d_3}{2}\right) \cdot \theta_s - \left(\frac{w_{sb} + w_{si}}{2}\right)\right) \cdot d_3 \\ + \left(\left(r_{si} + \frac{d_1}{2}\right) \cdot \theta_s - w_s\right) \cdot d_1 \\ + \left(\left(r_{si} + d_1 + \frac{d_2}{2}\right) \cdot \theta_s - \left(\frac{w_s + w_{si}}{2}\right)\right) \cdot d_2 \end{array}\right] \cdot N_s \cdot L_{stk} \cdot k_{stk}$$

$$V_{s,ry} = \left(r_{rb}{}^2 \cdot \pi - r_{ri}{}^2 \cdot \pi\right) \cdot L_{stk} \cdot k_{stk}$$

$$V_m = \left(r_{ro}{}^2 \cdot \pi - r_{rb}{}^2 \cdot \pi\right) \cdot L_{stk} \cdot \alpha_m$$

$$V_{cu} = \left(k_{fill} \cdot A_s \cdot Lstk + k_{fill} \cdot A_s \cdot \left(\frac{\pi \cdot \tau_c}{2}\right)\right) \cdot N_s$$

V_{cu}	$[m^3]$	volume of the copper
V_m	$[m^3]$	volume of the magnets
$V_{s,sy}$	$[m^3]$	steel volume of the stator yoke
$V_{s,teeth}$	$[m^3]$	steel volume of the stator teeth
$V_{s,ry}$	$[m^3]$	steel volume of the rotor yoke

Machine mass calculation:

$$m_s = \left(V_{s,sy} + V_{s,teeth} + V_{s,ry}\right) \cdot \rho_{steel}$$

$$m_m = V_m \cdot \rho_{magnet}$$

$$m_{cu} = V_{cu} \cdot \rho_{cu}$$

M_s	[kg]	steel mass
M_m	[kg]	magnet mass
M_{cu}	[kg]	copper mass

Price calculation:

$$p_s = m_s \cdot C_{steel}$$

$$p_m = m_m \cdot C_{magnet}$$

$$p_{cu} = m_{cu} \cdot C_{copper}$$

p_s	[euro]	steel price
p_m	[euro]	magnet price
p_{cu}	[euro]	copper price

Appendix 2: Maxwell's theory

Electro magnetic theory used for electrical machine modeling can be derived from the work of James Clerk Maxwell (13 June 1831 – 5 November 1879). An overview of Maxwell's theory can be found in almost every book on electrical machinery. But because of its importance and because many equations in this thesis are derived from the Maxwell equations, a brief overview of the Maxwell equations will be given in this appendix. Also the Lorentz Force equation will be described, since it describes the force due to the electromagnetic fields described in the Maxwell equations.

A.2.1. Maxwell equations

Electromagnetic behavior is described using the following quantities:

$\overline{E}$	[V/m]	Electric field stength vector
$\overline{H}$	[A/m]	Magnetic field strength vector
$\overline{J}$	[A/m^2]	Electric current density vector
$\overline{D}$	[C/m^2]	Electric flux density vector
$\overline{B}$	[T]	Magnetic flux density vector
$\overline{J^{ext}}$	[V/m]	External current density independant of the electromagnetic field

Maxwell Equations
The behavior of electromagnetic fields is described by the first two equations of Maxwell. Also called the first two laws of Maxwell. Equation A.2.1 respectively equation A.2.2. These equations can be written in integral form or in differential form.

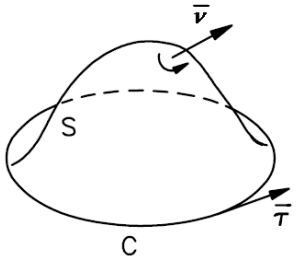

$$\begin{aligned} -\oint_c \overline{H}\cdot\overline{\tau}dl + \iint_S \left(\overline{J}+\partial_t\overline{D}\right)\cdot\nu dA &= -\iint_S \overline{J^{ext}}\cdot\nu dA \\ -\nabla\times\overline{H}+\overline{J}+\partial_t\overline{D} &= -J^{ext} \end{aligned} \qquad \text{(A.2.1)}$$

And

$$\begin{aligned} \oint_C \overline{E}\cdot\overline{\tau}dl + \iint_S \partial_t \overline{B}\cdot\nu dA &= 0 \\ \nabla\times\overline{E} + \partial_t \overline{B} &= 0 \end{aligned} \qquad \text{(A.2.2)}$$

Compatibility relations:

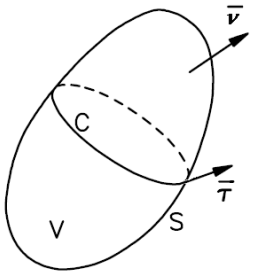

$$\begin{aligned} \oiint_S \left(\overline{J} + \partial_t \overline{D}\right)\cdot\overline{\nu}dA &= \iiint_V \rho dV \\ \nabla\cdot\overline{J} + \partial_t \nabla\cdot\overline{D} &= \rho \end{aligned} \qquad \text{(A.2.3)}$$

$$\begin{aligned} \oiint_S \partial_t \overline{B}\cdot\overline{\nu}dA &= 0 \\ \partial_t \nabla\cdot\overline{B} &= 0 \end{aligned} \qquad \text{(A.2.4)}$$

By applying a causality argument it can be shown that:

$$\nabla\cdot\overline{D} = \rho \qquad \text{(A.2.5)}$$

$$\nabla\cdot\overline{B} = 0 \qquad \text{(A.2.6)}$$

Constitutive relations:
The constitutive relations are given for linear isotropic material

$$\overline{J} = \sigma\cdot\overline{E} \qquad \text{(A.2.7)}$$

$$\overline{B} = \mu\cdot\overline{H} \qquad \text{(A.2.8)}$$

$$\overline{D} = \varepsilon\cdot\overline{E} \qquad \text{(A.2.9)}$$

Boundary conditions:
The boundary conditions between two materials are given by:

$$\nu\times\overline{H}^{(2)} - \nu\times\overline{H}^{(1)} = \overline{J_s} \qquad \text{(A.2.10)}$$

$$\nu \cdot \overline{B}^{(2)} - \nu \cdot \overline{B}^{(1)} = 0 \quad \text{(A.2.11)}$$

$$\nu \times \overline{E}^{(2)} - \nu \times \overline{E}^{(1)} = 0 \quad \text{(A.2.12)}$$

$$\nu \cdot \overline{D}^{(2)} - \nu \cdot \overline{D}^{(1)} = \rho_s \quad \text{(A.2.13)}$$

A.2.2. The Lorentz Force equation

The Lorentz force is the force on a point charge due to electromagnetic fields. It is given by equation A.2.14:

$$\overline{F} = q \cdot \left(\overline{E} + \nu \times \overline{B} \right) \quad \text{(A.2.14)}$$

Here $\overline{F}$ [N] is the force vector on an electric charge q[C] with velocity v[m/s]. From here the magnetic force on a current carrying wire can be derived as follow:

$$\overline{F} = q \cdot \left(\nu \times \overline{B} \right)$$

$$\nu = \frac{\partial l}{\partial t}$$

$$\partial F = \partial q \cdot \frac{\partial l}{\partial t} \cdot B$$

$$i = \frac{\partial q}{\partial t}$$

$$\overline{F} = i \cdot \overline{B} \cdot \int dl$$

If the wire is straight and exposed to a uniform magnetic field over length L[m], the derived integral becomes the well known law of force:

$$F = B \cdot i \cdot L \quad \text{(A.2.15)}$$

A.3. Winding factors

The most straight forward definition of a winding factor k_w is given by [Kir 05]. Where the winding factor is described by the ratio of the flux linkage of a winding to flux that would have been linked by a full-pitch concentrated winding with the same number of turns.

$$k_w = \frac{\lambda_{actual}}{\lambda_{concetrated,\, full-pitch}} \tag{A.3.1}$$

There are three parts considered, contributing to the winding factor:

$$k_w = k_p \cdot k_d \cdot k_{skew} \tag{A.3.2}$$

The pitch factor k_p:
If the number of poles and stator coils are unequal, the coil angle becomes shorter than the pole pitch angle θ_p[rad]. This is called a chorded or fractional pitch winding.
All concentrated coil winding configurations considered in this thesis, have coils wound around one tooth, therefore the coil pitch angle is the same as the slot pitch angle θ_s[rad].
Because of chorded windings, less flux will link the winding coils, compared to a full-pitch winding with the same number of coils and turns. The induced voltage will therefore have smaller amplitude. The pitch factor k_p takes this into account and is presented in equation A.3.4.

$$k_p = \sin\left(\frac{\pi \cdot \theta_s}{2 \cdot \theta_p}\right) \tag{A.3.4}$$

The distribution factor k_d:
When the coils of a winding are distributed over several slots and a fractional pitch concentrated coil winding is considered, the induced voltage in the coils can electrically be out of phase with each other. The amplitude of the induced winding voltage will therefore be smaller. The distribution factor k_d takes this into account and is presented in the following equation [Kir 05]:

$$k_d = \frac{\sin\left(\frac{m}{2} \cdot \left(1 - \frac{\theta_s}{\theta_p}\right) \cdot \pi\right)}{m \cdot \sin\left(\frac{\pi}{2} \cdot \left(1 - \frac{\theta_s}{\theta_p}\right)\right)} \tag{A.3.5}$$

$\left(1-\frac{\theta_s}{\theta_p}\right)\cdot\pi$ is the term indicating the electrical phase shift between coils of the same winding. And m is the number of coils in a winding. For fractional pitch windings with 9 coils around 9 teeth with 8 magnet poles m=3. For fractional pitch windings with 3 coils around three teeth with 2 magnet poles m=1, which means k_d becomes 1.

The skew factor:
The skew factor is applied when the magnets, and therefore the pole pitch angle is skewed in axial direction. Skewing is often applied to reduce harmonic components in the output voltage and to reduce cogging torque. For the developed generators in this thesis, the harmonics in the output voltage are of little concern. Torque ripple is already reduced by applying a fractional pitch winding. Therefore skewing of magnets is not advantageous for the generator of the prototype HPRE since it reduces the winding factor. Since skewing is not applied the skew factor k_{skew} becomes 1.

Appendix 4: Non linear modeling of the steel permeability

In the analytical models presented this thesis, the reluctances of the sheet steel $R_{m,y}$[A/Wb] and $R_{m,t}$[A/Wb] can be neglected during normal operation, because they are much smaller than the air gap reluctance $R_{m,g}$[A/Wb]. If the flux density in the steel is not very high this is a plausible assumption to make. Using this assumption makes calculating less complex, since no iterative processes are needed while using circuit theory to do the calculations.

However, the permeability of steel becomes very non linear if flux densities become higher. Within the electric machine there might be high local flux densities, due to armature reaction. Therefore modeling of reluctances and flux densities must be done while taking into account the non-linearity of the steel permeability. Modeling of the non-linearity is done by stating the steel permeability not as a constant, but as a non linear function of the flux density in the steel $\mu_{r,steel}(B_{steel})$. In this thesis the B-H characteristic and the permeability function are expressed as linearized functions, derived from the B-H characteristic of the steel manufacturer (Appendix 7), while taking into account the following assumption:

- The relative permeability of the steel has the same value as the relative permeability of air for flux densities above 2.2T:
  $\mu_{r,steel} = \mu_{r,0}=1$.

$$\mu_{r,steel}(B_{steel}) = \frac{B_{steel}}{\mu_0 \cdot H_{steel}}$$

$$= \begin{cases} 7462 & for \quad 0 \le B_{steel} < 0.9 \\ 17516 - B_{steel} \cdot 10920 & for \quad 0.9 \le B_{steel} < 1.3 \\ 28968 - B_{steel} \cdot 19100 & for \quad 1.3 \le B_{steel} < 1.4 \\ 17516 - B_{steel} \cdot 10920 & for \quad 1.4 \le B_{steel} < 1.5 \\ 11816 - B_{steel} \cdot 7120 & for \quad 1.5 \le B_{steel} < 1.6 \\ 3768 - B_{steel} \cdot 2090 & for \quad 1.6 \le B_{steel} < 1.7 \\ 1490 - B_{steel} \cdot 750 & for \quad 1.7 \le B_{steel} < 1.8 \\ 1292 - B_{steel} \cdot 640 & for \quad 1.8 \le B_{steel} < 1.9 \\ 551 - B_{steel} \cdot 250 & for \quad 1.9 \le B_{steel} < 2.2 \\ 1 & for \quad 2.2 \le B_{steel} \end{cases}$$

Figure A.2 is a plot of the linearized B-H steel characteristic of M270-35A steel. Figure… is a plot of the $\mu_{r,steel}$ - B_{steel} characteristic for M270-35A steel.

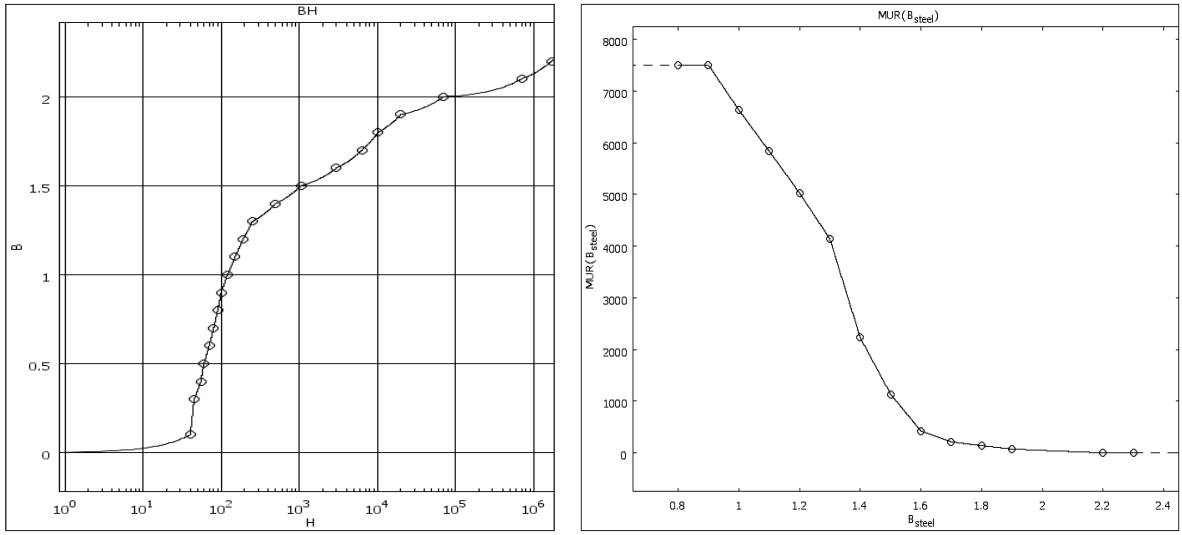

(a) ***(b)***

Figure A.2: Linearized function of the B-H characteristic (a) and the relative steel permeability (b)

Appendix 5: Inset mounted permanent magnet rotor design

An inset magnet permanent magnet (IMPM) rotor is designed according the following design criteria:

- The IMPM rotor design must have the same dimensions as the SMPM rotor.
- The IMPM rotor must produce the same effective air gap flux density B_g[T] in the generator as the SMPM rotor does.

The optimal SMPM rotor design can be made with a very small width. This makes it impossible to design an IMPM rotor of the same dimensions. In order to develop both the IMPM and SMPM rotor with the same dimensions, the SMPM rotor yoke width has been increased by 2mm. With use of the geometric calculations of appendix 1 an IMPM rotor with V-shape magnets has been designed, as is presented in figure A.3.

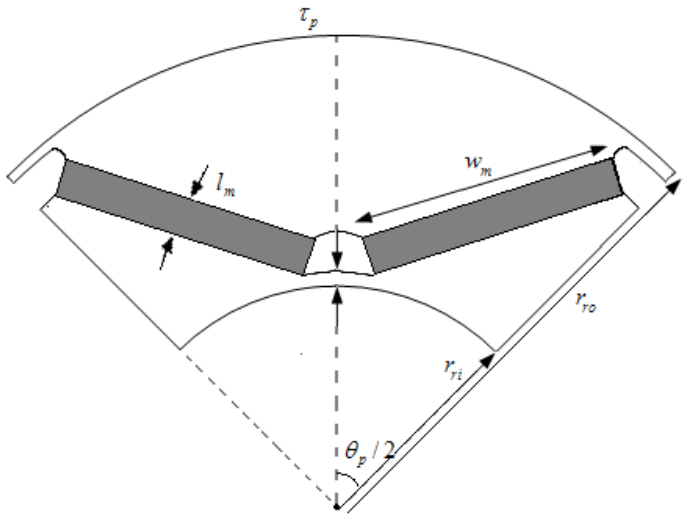

Figure A.3.: IMPM rotor pole piece

For the development of an IMPM rotor the strength of the rotor sheet steel is of importance. This is investigated using the Solidworks 10 computer software. A force is applied to every pole on the rotor. The applied force consists of the centrifugal forces F_c[N] due to the magnets and the magnetic forces F_m[N] due to the stator magnetic field and rotor magnetic field in radial direction.:

$$F_c = m \cdot \omega^2 \cdot r$$

$$m = 2 \cdot m_m$$

$$\omega = \omega_m$$

$$r = \frac{r_{ro} - r_{ri}}{2}$$

$$F_m = \frac{B^2 \cdot A}{2 \cdot \mu_0}$$

$$A = \tau_p \cdot l_{stk}$$

$$B = B_{ar,\max} + B_g$$

$$F_{tot} = F_c + F_m$$

Three inset magnet design variations are tested on strength properties. The calculation results are presented in figures A.4 to A.6:

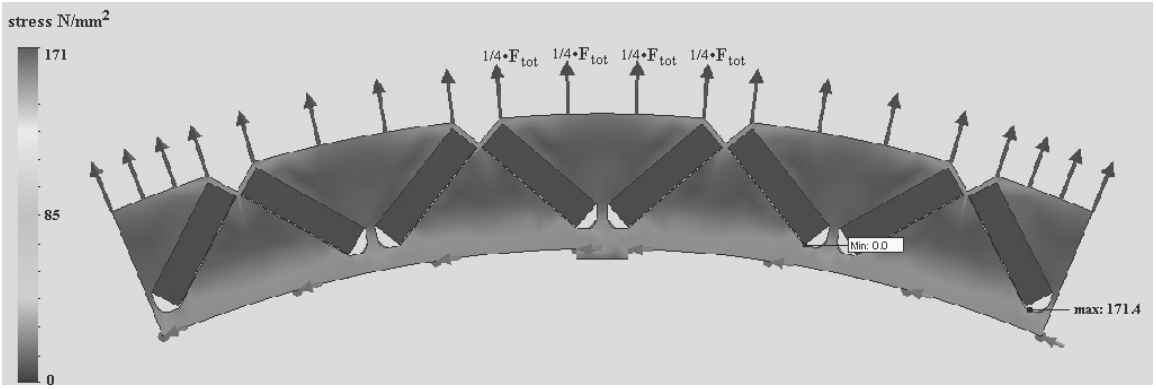

Figure A.4: Strength calculation of the IMPM rotor variation a

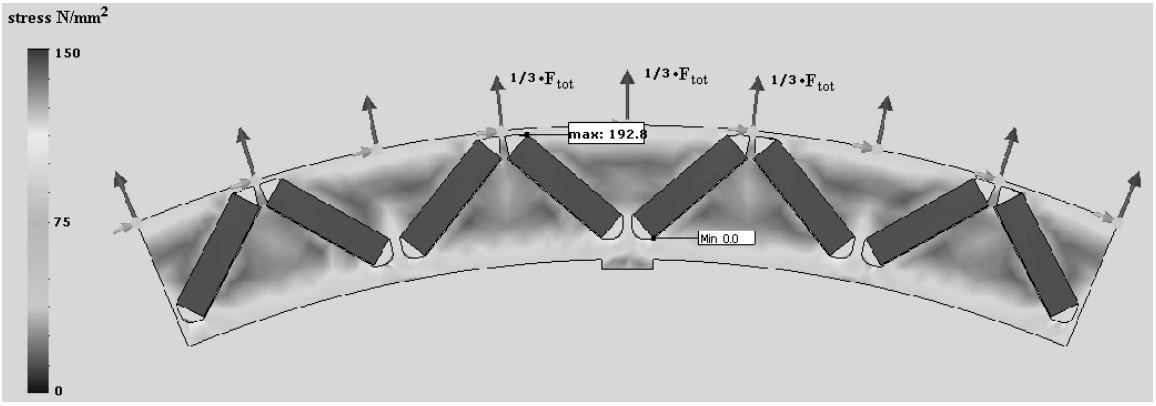

Figure A.5: Strength calculation of the IMPM rotor variation b

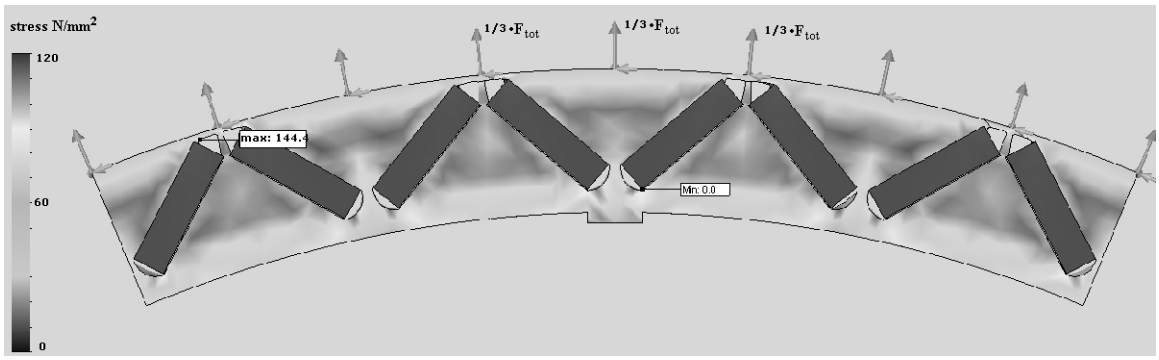

Figure A.6: Strength calculation of the IMPM rotor variation c

According to the strength calculations all three rotor design variations will hold. But variation b is stressed to its limit. (See appendix A.7.2. for the steel strength properties)
All three rotor design variations will be manufactured for the generator prototype series. In this way the computer calculations can be validated and the best construction can be determined.

Due to the magnetic short circuits in the rotor between magnet poles, an IMPM rotor will have extra magnet leakage. The magnet leakage is investigated in a FEM model. The magnetic field results for the IMPM-rotor for two different variations are presented in figure A.7.

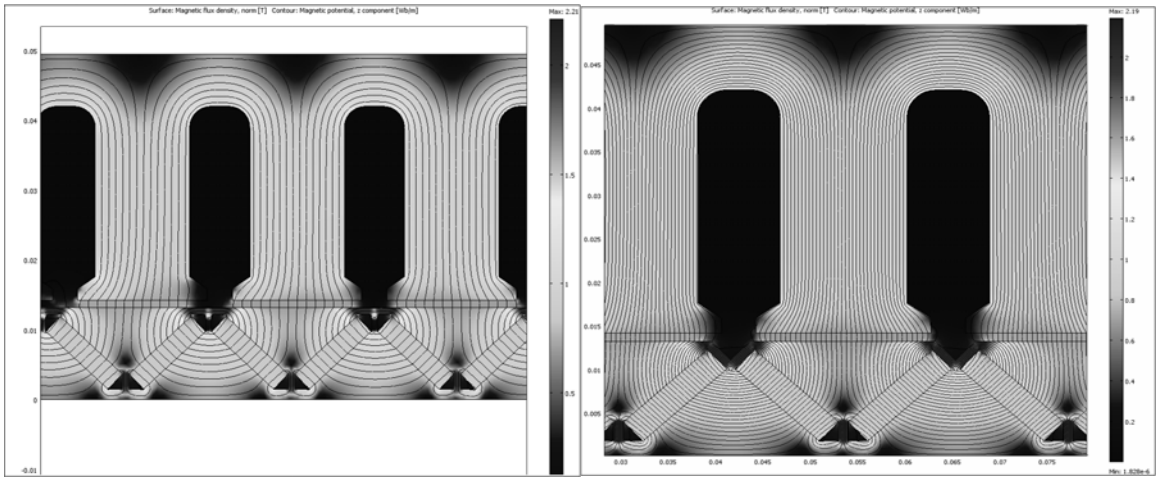

(a) Version b ***(b) version a***

Figure A.7: FEM calculation for the flux leakage in IMPM rotor constructions.

Due to the magnet leakage in the rotor, the flux density in the air gap decreases. In order to produce an equal flux density in the air gap as the SMPM rotor does, two options are possible:

- Change the magnet geometry.
- Use magnet material with higher remanent flux density values.

Since the magnet geometry is already at its limits, a stronger magnet material is chosen. To produce the same flux density values in the air gap, the magnet type N44SH is chosen for the IMPM rotor design. Characteristics of this magnet type can be found in appendix7.

Appendix 6: Generator design drawings

In this appendix the design drawings made with the Solidworks 10 computer software are presented. The following design drawings are considered:

Generator design drawing: ***(confidential information)***

- Generator exploded view.

Stator design drawings: ***(confidential information)***

- Stator with 36 teeth, including stator outer house.
- Stator with 48 teeth, including stator outer house.

Rotor design drawings: ***(confidential information)***

- Rotor inner can.
- SMPM rotor with 32 poles.
- IMPM rotor version a, with 32 poles.
- IMPM rotor version b, with 32 poles.
- IMPM rotor version c, with 32 poles.

Magnet drawings: ***(confidential information)***

- Arc shaped magnet for the SMPM rotor.
- Flat magnet for the IMPM rotor.

Coil winding drawings: ***(confidential information)***

- Winding arrangement for the 36 slots and 32 poles generator configuration.
- Winding arrangement for the 48 slots and 32 poles generator configuration.

Appendix 7: Used material specifications

This appendix presents an overview of the used material characteristics. The choice of material types is done in consultation with the manufacturer for the prototype generators: 'Combimac B.V.' and the supplier of magnet material 'Bakker magnetics'. The following materials are considered:

- Used magnet materials
- Used sheet steel.
- Insulation of the conductors. ***(confidential information)***

A.7.1. Magnet material characteristics

Magnetic properties of the used magnetic materials:

NEODYMIUM SINTERED

Grade	corrosion stable *1 specify as: grade+"/S"	Remanence Br mT		Normal coercivity Hcb kA/m		Intrinsic coercivity Hcj kA/m	Max. energy product BH(max) kJ/m3		Max. operating temp.
		min	typ	min	typ	min	min	typ	
N38 UH	38 UH/S	1220	1260	900	950	1989	279	303	180
N44 SH	44 SH/S	1330	1360	970	1020	1592	334	350	150

B-H characteristic of the N38UH magnet type used for the SMPM rotors:

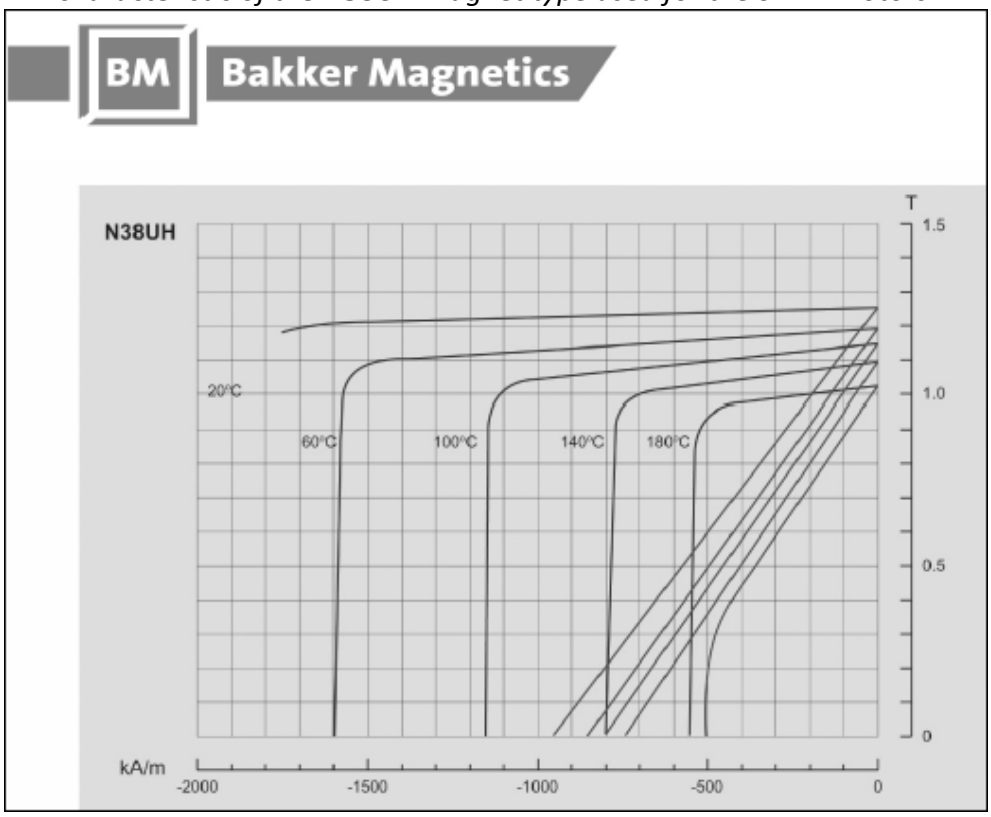

B-H characteristic of the N44SH magnet type used for the IMPM rotors.

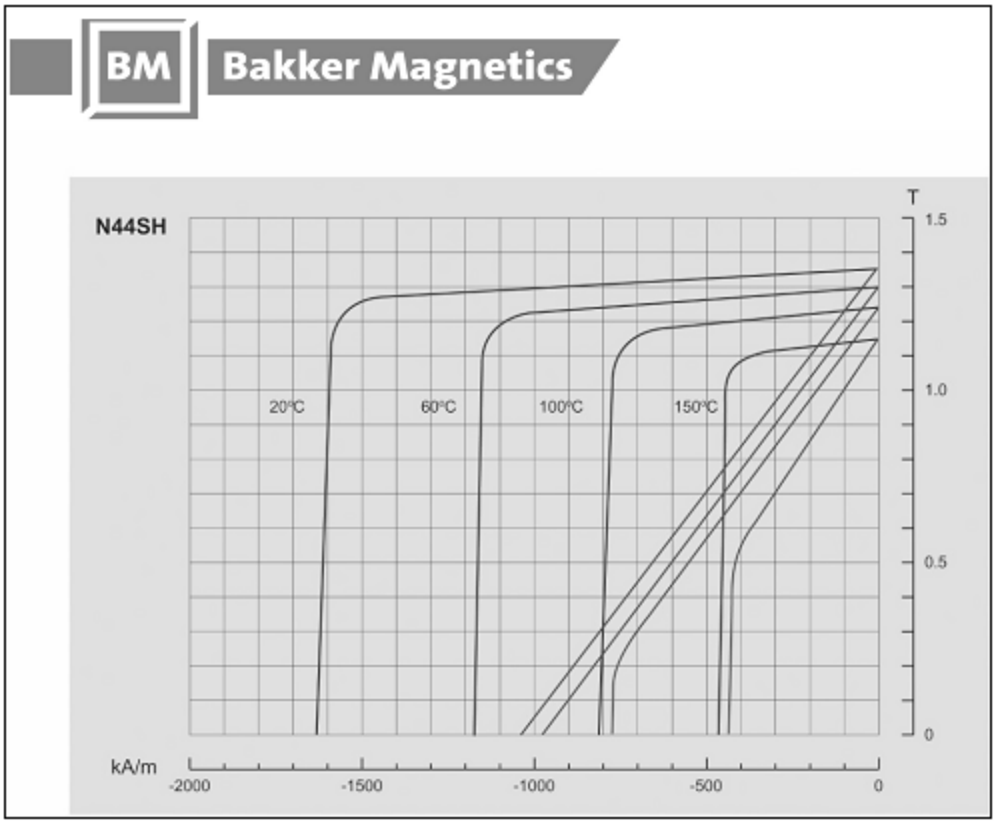

A.7.2. Sheet steel characteristics

The used sheet steel for the prototype generators is the M270-35A electrical steel. This steel is used in both the stator and the rotor. The characteristics and material properties for this steel type are presented below

B-H characteristic:

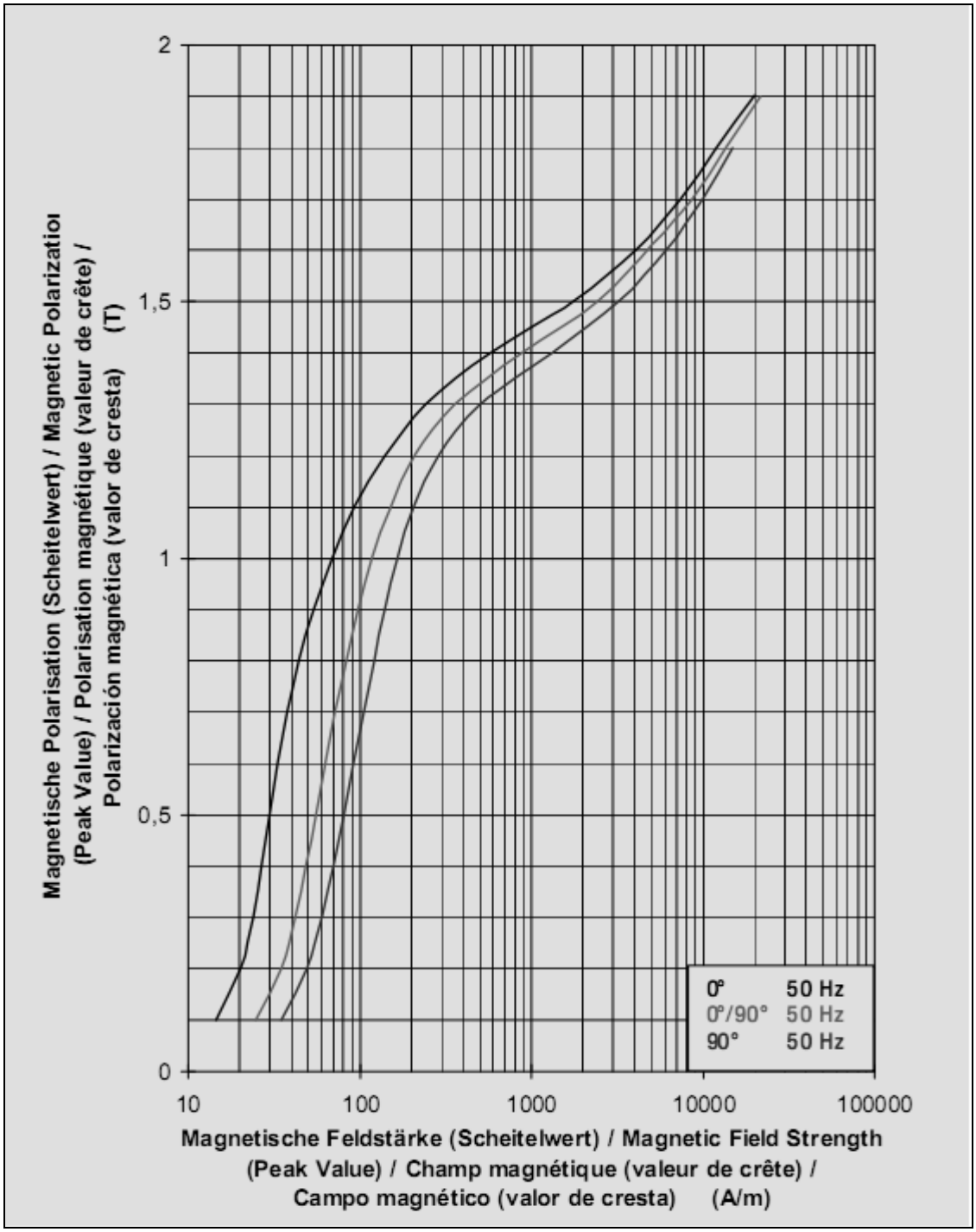

Specific loss $p_{loss,Fe}$[W/kg] *values:*

f = 50Hz								
J	H			μ_s	P_s			S_s
T	A/m				W/kg			VA/kg
	0°	90°	0°/90°	0°/90°	0°	90°	0°/90°	0°/90°
0,5	30	81	55	7185	0,24	0,39	0,31	0,57
0,6	33	92	63	7590	0,33	0,52	0,43	0,77
0,7	38	105	72	7760	0,43	0,67	0,55	1,00
0,8	44	121	83	7679	0,55	0,83	0,69	1,27
0,9	54	140	98	7342	0,68	1,00	0,84	1,62
1,0	**69**	**167**	**118**	**6728**	**0,83**	**1,19**	**1,01**	**2,06**
1,1	94	207	151	5806	1,01	1,39	1,21	2,70
1,2	140	285	210	4552	1,22	1,64	1,43	3,72
1,3	241	506	359	2885	1,48	1,96	1,71	5,98
1,4	577	1324	889	1254	1,79	2,36	2,02	13,80
1,5	**1767**	**3214**	**2437**	**491**	**2,11**	**2,69**	**2,34**	**40,95**
1,6	4045	6069	4717	271	2,42	2,93	2,67	88,43
1,7	7340	9880	8614	158	2,65	3,17	2,95	184,92
1,8	12026	15036	13557	107			3,21	317,86
1,9	19614	23058	21713	71				

f = 400Hz					f = 500Hz				
J	H	μ_s	P_s	S_s	J	H	μ_s	P_s	S_s
T	A/m		W/kg	VA/kg	T	A/m		W/kg	VA/kg
	0°/90°	0°/90°	0°/90°	0°/90°		0°/90°	0°/90°	0°/90°	0°/90°
0,2	44	3652	0,91	1,50	0,2	46	3456	1,25	1,95
0,3	56	4284	1,93	2,85	0,3	59	4024	2,67	3,79
0,4	66	4800	3,25	4,53	0,4	71	4482	4,49	6,05
0,5	76	5210	4,83	6,52	0,5	82	4842	6,73	8,77
0,6	87	5520	6,70	8,84	0,6	93	5108	9,29	11,90
0,7	97	5739	8,84	11,54	0,7	105	5284	12,30	15,60
0,8	108	5870	11,28	14,70	0,8	118	5378	15,75	19,92
0,9	121	5915	14,06	18,43	0,9	132	5410	20,02	25,35
1,0	**138**	**5785**	**17,49**	**23,30**	**1,0**	**150**	**5296**	**24,66**	**31,65**
1,1	161	5437	21,16	29,30	1,1	174	5030	30,02	39,78
1,2	214	4466	25,37	38,27	1,2	218	4385	36,06	51,32
1,3	354	2923	30,40	56,79	1,3	359	2883	43,35	74,95
1,4					1,4				
1,5					**1,5**				
1,6					1,6				

f = 1000Hz					f = 2000Hz				
J T	H A/m 0°/90°	μ_a 0°/90°	P_s W/kg 0°/90°	S_s VA/kg 0°/90°	J T	H A/m 0°/90°	μ_a 0°/90°	P_s W/kg 0°/90°	S_s VA/kg 0°/90°
0,2	58	2761	3,56	4,84	0,2	78	1027	10,46	12,96
0,3	76	3150	7,56	9,65	0,3	103	1544	21,77	25,96
0,4	92	3446	12,72	15,65	0,4	130	1837	37,45	43,50
0,5	109	3652	19,07	22,98	0,5	158	2021	56,95	65,49
0,6	129	3716	27,05	32,14	0,6	189	2104	81,22	92,84
0,7	148	3754	36,39	42,97	0,7				
0,8	170	3736	47,22	55,66	0,8				
0,9	195	3673	60,30	71,16	0,9				
1,0	**222**	**3581**	**75,51**	**89,58**	**1,0**				
1,1	253	3465	93,14	111,89	1,1				
1,2	287	3331	113,99	141,68	1,2				
1,3					1,3				
1,4					1,4				
1,5					**1,5**				
1,6					1,6				

Strength properties:

Festigkeit in Walzrichtung *Strength in rolling direction*	**Sortentypische Mittelwerte*** *Typical mean values**
Streckgrenze Re *Yield strength*	445 N/mm²
Zugfestigkeit Rm *Tensile strength*	567 N/mm²
Bruchdehnung in WR in % *Elongation in %*	17
Mikrohärte HV5 *Hardness HV5*	211